ROLE OF NONMUSCLE MYOSIN II ISOFORMS IN HEPATIC STELLATE CELL ACTIVATION

by

Cathy Castellon Moore

A dissertation submitted to the faculty of
The University of North Carolina at Charlotte
in partial fulfillment of the requirements for the
degree of Doctor of Philosophy in Biology

Charlotte

2009

Approved by:

_____
Dr. Laura W. Schrum, Advisor

_____
Dr. Iain H. McKillop

_____
Dr. Christopher M. Yengo

_____
Dr. Didier Dreau

_____
Dr. David Langford

ABSTRACT

CATHY CASTELLON MOORE. The role of nonmuscle myosin II isoforms in hepatic stellate cell activation. (Under the direction of DR. LAURA W. SCHRUM)

The hepatic stellate cell (HSC) plays a pivotal role in the development of hepatic fibrosis. Regulation of liver microcirculation is a complex system where blood flow is under systemic and sinusoidal control. Upon a fibrogenic stimulus, quiescent HSCs transdifferentiates into activated myofibroblast-like cell and exert a sustained contractile force, resulting in hyperconstricted vessels. Early phenotypic changes observed during the transdifferentiation process include cell stretching and elongation of cytoplasmic processes. These changes facilitate proliferation and migration of HSCs to the areas of injury where excess amounts of collagen are deposited altering normal liver architecture and leading to liver dysfunction. Under chronic liver injury, this wound healing response perpetuates and impairs blood flow through the liver resulting in portal hypertension, which is one of the main clinical manifestations of liver fibrosis. Nonmuscle myosin II (NMM II) has been shown to be involved in cellular contraction, proliferation and migration. Using a whole-cell contraction assay and a selective myosin II inhibitor, we have demonstrated that myosin II is essential for HSC contraction. Additionally, the expression of NMM II isoforms in activated HSCs was upregulated. To further explore the mechanism of regulation, we altered *in vitro* conditions to more closely depict the *in vivo* environment using a matrix stiffness assay. Under these conditions, a minimal increase in NMM II-A and II-B mRNA expression was detected, which suggests that mechanical properties of the liver may regulate NMM II isoforms in HSCs. siRNA mediated isoform knockdown had no effect on culture-activated HSC contraction and

proliferation but cell migration was inhibited by 25%. Overall, our results demonstrate that myosin II isoforms play a critical role in the development of portal hypertension and HSC migration; however, the specific isoform responsible for this hypercontractile response has yet to be identified. Supported by NIH Grant AA14891.

ACKNOWLEDGEMENTS

I am extremely grateful to my family, friends, and mentors who have helped me complete my educational goals. The past five years of my academic career have been cultivated by my graduate advisor Dr. Laura Schrum, whose strong commitment to teaching and mentoring both inside and outside of the academic setting has strengthened my character and desire to continue to work in the scientific community. She has motivated me throughout the past five years to be an independent scientist and I am forever grateful for her time and commitment to the successful completion of my academic career. I would also like to thank Cathy Culberson, Kasia Korneszczuk, Amel Kaara and Hong Xu for teaching me the basics of laboratory research and developing my surgical skills. I am also grateful to my peers in the Schrum laboratory: Kyle Thompson, Stephani Day, Alyssa Gulledge and Ashley Lakner, who have given me many hours of peer review and moral support. I also appreciate the guidance of my committee members Dr. Iain McKillop, Dr. Didier Dreau, Dr. David Langford and especially Dr. Christopher Yengo who had initiated the collaboration between biophysics and molecular biology of the hepatic stellate cell. And finally, words cannot begin to express the overwhelming appreciation I feel for my family; especially my parents who have always encouraged me to excel in my academic endeavors, and my loving husband, Chris, who has supported me both emotionally and financially throughout these past few years.

LIST OF FIGURES

LIST OF TABLES

LIST OF ABBREVIATIONS

HSC	Hepatic Stellate Cell
NMM II	Nonmuscle Myosin II
KC	Kupffer Cell
SEC	Sinusoidal Endothelial Cell
MMP	Matrix Metalloproteinase
TIMP	Tissue Inhibitor of Matrix Metalloproteinase
ET-1	Endothelin-1
ET_A	Endothelin A Receptor
ET_B	Endothelin B Receptor
HCV	Hepatitis C Virus
BDL	Bile Duct Ligation
YFP	Yellow Fluorescent Protein
FAK	Focal Adhesion Kinase
PI3K	Phosphoinositide 3-Kinase
TGF β	Transforming Growth Factor β
RBP	Retinol Binding Protein
DAPI	4’,6’-Diamidino-2-Phenylindole
MCP-1	Monocyte Chemotactic Peptide
MCSF	Macrophage Colony-Stimulating Factor
TLR	Toll-Like Receptor
LPS	Lipopolysaccharide
TGF β-R	Transforming Growth Factor β Receptor

EGF	Epidermal Growth Factor
IL-10	Interleukin-10
FGF	Fibroblast Growth Factor
INFγ	Interferon γ
NO	Nitric Oxide
NOS	Nitric Oxide Synthase
HPVG	Hepatic Portal Venous Gradient
iNOS	Inducible Nitric Oxide Synthase
PKG	Protein Kinase G
DEAN	Diethylamine NONOate
cAMP	Cyclic Adenosine 3', 5'-Monophosphate
MLCK	Myosin Light Chain Kinase
GTP	Guanosine Triphosphate
GAP	GTPase Activating Protein
GEF	Guanine Nucleotide Exchange Factor
GDI	Guanine Nucleotide Dissociation Inhibitors
ROCK	Rho Kinase
PDGF	Platelet-Derived Growth Factor
$p70^{S6K}$	Ribosimal S6 Kinase
ERK	Extracellular-Signal Regulated Kinase
MAPK	Mitogen-Activated Protein Kinase
JNK	c-Jun Nuclear Kinase
MLC	Myosin Light Chain

MHC	Myosin Heavy Chain
BDM	2,3-Butanedione Monoxime
BTS	N-Benzyl-P-Toluene Sulfonamide
V_{max}	Maximum Velocity
SM	Smooth Muscle
DMEM	Dulbecco's Modified Eagle Medium
FBS	Fetal Bovine Serum
HEPES	4-(2-Hydroxyethyl)-L-Piperazineethanesulfonic Acid
$NaHCO_3$	Sodium Bicarbonate
PBS	Phosphate Buffered Saline
EDTA	Ethylenediaminetetraccetic
DMSO	Dimethyl Sulphoxide
RT-PCR	Reverse Transcriptase Polymerase Chain Reaction
DNase	Deoxyribonuclease
SMEM	Spinner Modification Minimum Essential Medium
BSA	Bovine Serum Albumin
EGTA	Ethylene Glycol-Bis(2-Aminoethylether)-N',N',N'-Tetraacetic Acid
GBSS	Gey's Balanced Salt Solution
dNTP	Deoxynucleotide Triphosphate
TAE	Tris-acetate
LEV	Low Elution Volume
DEPC	Diethyl Pyrocarbonate

GAPDH	Glyceraldehyde 3 Phosphate Dehydrogenase
SMA	Smooth Muscle α-Actin
GFAP	Glial Fibrillary Acidic Protein
RIPA	Radioimmunoprecipitation Assay
SDS	Sodium Dodecyl Sulfate
ECL	Enhanced Chemiluminescence
TEMED	N,N,N',N'-Tetramethylethylenediamine
APS	Ammonium Persulfate
NaCl	Sodium Chloride
TBS	Tris Buffered Saline
TBST	TBS-Tween
PAGE	Polyacrylamide Gel Electrophoresis
sulfo-SANPAH	N-Sulfosuccinimidyl-6-(4'-azido-2'-nitrophenylamino) hexanoate
IACUC	Institutional Animal Care and Use Committee
ECM	Extracellular Matrix
H&E	Hematoxylin and Eosin
FRET	Fluorescence Resonance Energy Transfer

CHAPTER 1: INTRODUCTION

1.1 THE LIVER

1.1.1 Architecture and Vasculature

The liver is the largest internal organ and it is vital to survival. The primary cell type of the liver is the hepatocyte. The hepatocyte is responsible for cellular processes which include bile production, glucose storage and toxin removal [1]. The resident macrophages of the liver are the Kupffer cells (KCs), which reside within the specialized microvasculature of the liver, the sinusoid. The fenestrated cells lining the liver blood vessels are the sinusoidal endothelial cells (SECs), which are encircled by hepatic stellate cells (HSCs) (FIGURE 1.1). The HSC is a star-shaped cell that has several long extensions that protrude from the cell body and wrap around the sinusoids. Extracellular matrix components (ECM) comprised of collagen (type I, III, IV, and V), proteoglycans, glycoproteins and elastins provide scaffolding for liver architecture in the portal tracts, sinusoidal walls and central veins [2].

The functional unit of the liver is the hepatic lobule, which is a hexagonal arrangement of parenchymal cells extending to the central vein (FIGURE 1.2). The portal triad consists of a bile duct and a terminal branch of the hepatic artery and portal vein. The liver has a dual circulation; it receives 75% deoxygenated blood from the portal venous system, which delivers blood from the small intestines, stomach, pancreas, and spleen and 25% oxygen-rich blood through the hepatic arterial system to the sinusoids

[1]. The blood supply branches into the sinusoidal network within the liver to optimize filtration and nutrient transport to the parenchymal cells. The blood drains into the central vein of each lobule, which combines into the hepatic vein and empties into the vena cava.

Hepatocytes produce bile to aid in the digestion of lipids. The epithelial cells that line the hepatic bile duct are the cholangiocytes, which contribute to bile secretion by secreting water and producing bicarbonate to dilute the bile salts [1]. The bile canaliculus carries bile through hepatic ductiles to the common bile duct which drains into the gallbladder in humans. The gallbladder concentrates and releases bile in response to cholecystokinin stimulation in the duodenum in the opposite direction of blood flow [1]. The biliary network receives its blood supply through the peribiliary plexus which stems from the hepatic artery [3].

1.1.2 Chronic Liver Disease and Portal Hypertension

Chronic liver disease is the 12th leading cause of death in the United States as it accounts for nearly 30,000 deaths per year (CDC, National Center for Health Statistics, 2005). One of the primary forms of liver disease is fibrosis, which results from liver injuries such as chronic hepatitis, alcoholic-liver disease and obstructive gallbladder disease. The liver is responsible for xenobiotic and ethanol metabolism; as a result, toxic metabolites can cause acute injury to the hepatocytes. The parenchymal cells lose microvilli and apoptose; SECs reduce blood flow to the hepatocytes by closing fenestra and KCs become activated by reactive oxygen species which initiate an inflammatory response and ECM deposition of type I collagen by the HSCs (FIGURE 1.3) [4]. This ECM provides a scaffolding complex in which SECs migrate to the site of injury to form new vascular beds for regenerating hepatocytes [5]. However, if the insult is alleviated,

matrix metalloproteinase (MMPs), such as MMP-13, are secreted by the HSCs to restore the normal tissue structure [6].

Hepatic fibrosis results from normal wound-healing processes going awry and is the main cause of increased intrahepatic vascular resistance during liver injury [7]. When the injury is chronic, type I collagen deposition by HSCs occurs in excess of collagen break down by MMPs as a result of imbalance between fibrogenesis and fibrolysis [8]. Altered ECM architecture and mechanical distortion culminates in increased blood pressure in the portal venous system as blood must be diverted away from the liver [9]. In addition to occlusion and compression of the microvasculature, HSC hypercontractility contributes to increased resistance of the sinusoids leading to the clinical manifestation of portal hypertension which is characterized by both increased portal blood flow and augmented intrahepatic vascular resistance (FIGURE 1.4) [4, 7]. Consequences related to untreated portal hypertension are caused by the vasculature being shunted away from the liver.

HSCs regulate intrahepatic vascular resistance and blood flow at the sinusoidal level by encircling long cytoplasmic projections around sinusoids and the ability to upregulate contractile proteins such as smooth muscle α-actin, myosin II and endothelin A and B (ET_A and ET_B) receptors [10-12]. HSCs respond to vasoactive constrictors such as endothelin-1 (ET-1), which activates the contractile apparatus [10-13]. Kawada et al., demonstrated that HSCs contract on silicone rubber membranes when exposed to 10nM of ET-1 as early as 2 minutes after incubation [14]. Moreover, HSCs seeded on hydrated collagen gels decreased the disc diameter proportionally dependent on cell number and collagen concentration. *In vivo* studies confirmed these results by intravital microscopy of

the hepatic sinusoids [12]. Zhang et. al., demonstrated that ET-1-induced constriction coincided at the site of HSC fluorescence and concluded that HSC hypercontractility may contribute to portal hypertension. It has also been demonstrated that average force generated by ET-1-induced contraction of a single HSC was 14000 dyn/cm^2, which is greater than the sinusoidal pressure in cirrhotic rats [15]. Furthermore, a direct relationship between ET-1 mRNA receptors (ET_A and ET_B) and the degree of portal hypertension has been demonstrated in patients suffering from chronic liver injury [16, 17].

Alcohol abuse is a major cause of liver morbidity and mortality in the United States. Continued ethanol abuse culminates into four distinct disorders: alcoholic fatty liver disease (steatosis), hepatosteatosis (fatty liver and inflammation), fibrosis and cirrhosis. Five-year survival rates of these conditions vary between 25% and 60% [18]. While data suggest that alcoholic steatosis and hepatosteatosis can be reversible, the chronic progression of alcohol-induced fibrosis leads to irreversible cirrhosis in 10 to 15% of alcoholics [19]. The severity of alcoholic cirrhosis depends on the stage and activity of the disease, subsequent alcohol intake and the occurrence of complications such as renal insufficiency, esophageal varicies and ascites resulting from portal hypertension, hepatic encephalopathy, bacterial infections or hepatocellular carcinoma [7].

Chronic viral hepatitis is characterized by increased hepatocyte necrosis and inflammation of the portal triad caused by a viral load in excessive of 10^{12} cells/ day [20]. Hepatitis C (HCV) infection is the principal cause of nonalcoholic cirrhosis in the United States. Approximately 55-85% acute HCV cases progress into a chronic infection, while

only 5% of acute hepatitis B infections develop a chronic disease [21]. Excessive alcohol consumption accelerates the progression of cirrhosis in patients infected with HCV as compared to those who are not heavy consumers [22]. Additionally, HCV infected patients who abstained from alcohol consumption prolonged cirrhotic disease progression. Wiley et. al. showed that excessive alcohol consumption during interferon treatment impedes the patients' response to antiviral therapy because alcohol has adverse effects on the interferon-generated signaling pathway which modulates immune responses [21]. Although the molecular mechanisms which regulate HCV progression to cirrhotic liver disease in alcoholic patients is not well understood, it has been suggested that alcohol may increase viral replication and/ or rapid mutation of HCV and/or suppress the inflammatory response by inhibiting the proper function of dendritic cells.

Primary biliary cirrhosis is a progressive inflammatory disease of the liver that may be caused by a genetic predisposition to autoimmunity of the biliary network [23]. It is characterized by destruction of the interlobular bile ducts and the development of cirrhosis. Secondary biliary cirrhosis results from prolonged anatomical blockage of the extrahepatic biliary tree, which results in progressive hepatic injury. Liver injury induced by bile duct ligation (BDL) in experimental animals is a well-established method to investigate the pathogenesis of liver fibrosis [24]. The primary pathology of hepatic fibrosis induced by BDL is lesions surrounding the bile duct epithelium. The surgical maneuver of BDL obstructs the common bile duct and initiates proliferation of biliary cholangiocytes. Following rapid epithelial proliferation, sustained blockage of bile flow causes perpetual activation of HSCs in the periductal region, which promotes biliary fibrosis/cirrhosis.

Depending on the cause of hepatic injury, different disease types can lead to distinct zonal patterns of fibrotic expression (FIGURE 1.5) [25]. While viral hepatitis and primary biliary disease are periportal based (zone 1), alcoholic liver disease is pericentral based (zone 3) [26]. The location of initial scarring can be determined by an invasive liver biopsy, which can facilitate the diagnosis of disease progression. If properly treated, hepatic fibrosis can be a reversible process; however, chronic insult leads to the development of cirrhosis which results in nodule formation leading to altered hepatic function and obstructed portal blood flow [27].

As the disease progresses, complications may arise such as: jaundice, hepatic encephalopathy, and/ or portal hypertension. Jaundice is typically characterized by yellow discoloration of the skin and conjunctiva of the eyes due to the high levels of bilirubin present in the vasculature. Hepatic encephalopathy results from decreased clearance of ammonia by the liver, which directly affects the brain. Portal hypertension not only perpetuates insult to the hepatic tissue by depleting oxygen to the cells but also gives rise to esophageal varicies and ascites. If left untreated, variceal bleeding can lead to hemorrhage and death in a significant proportion of patients, as it accounts for 20-50% in-hospital mortality [28].

Esophageal varices and ascites may develop when the hepatic venous pressure gradient (HVPG) increases from a normal pressure of 3-6 mmHg to 10mmHg. Variceal bleeding may occur when the HVPG rises above 12 mmHg. Currently, the treatment regime for patients suffering with acute variceal bleeding is endoscopic ligation in conjunction with pharmacological therapy for 2-5 days [29]. Vasoactive agents, such as somatostatin or vasopressin, indirectly decrease flow to the portal system by inducing

splanchnic vasoconstriction. Octreotide, a synthetic analogue of somatostatin, is commonly used as an adjuvant therapy in the United States to control variceal bleeding; however, it has been suggested that octreotide's mechanism of action is associated with an increase in plasminogen activator protein [30]. Although the therapy decreases portal pressure, adverse effects associated with decreased blood clotting would be detrimental in the clinical setting of uncontrolled variceal bleeding. On the other hand, terlipressin, a vasopressin analogue, is most typically prescribed in European countries with the added benefit that it can be administered by intermittent intravenous injections rather than by continuous intravenous administration. Long-term treatment to manage uncontrolled bleeding may also include balloon tamponade, banding or sclerotherapy in conjunction with beta-blockers, which significantly reduce the risk of a first hemorrhage in patients with large varices and improves survival [31].

Besides removal of insult, liver transplantation remains the only effective treatment for end-stage liver disease; however, a huge gap remains between the number of people who need a liver transplant and the number of organs available. According to the 2008 U.S. Organ Procurement and Transplantation Network and the Scientific Registry of Transplant Recipients Annual Report, the number of patients awaiting a liver transplant at year-end peaked in 2001; however, a decrease of 3.8% was observed in deceased donor liver transplants in 2007 (FIGURE 1.6). This drop was due largely to decreases in donation, particularly by living donors. There were 423 (6.3%) fewer living donors in 2007 than in 2006. Similarly the number of organs recovered for transplant from deceased donors has also moderately declined (7,084 in 2006 vs. 7,029 in 2007). Although the gap between the number of candidates and recipients has been mildly

shrinking, there remains a critical for the development of treatments to prolong the life until a suitable organ is available. In addition, not all patients of end-stage liver disease are suitable candidates for liver transplantation. Generally, organs are transplanted to patients with the highest degree of survival. Patients positive for AIDS or HIV, with irreversible brain damage, multi-system failure that is not correctable by liver transplantation, malignancy outside the liver, infections outside the hepatobiliary system, active alcohol or substance abuse are not eligible. Therefore, treatment generally focuses on preventing progression and complications of the disease. Targeting portal hypertension may improve quality of life and prolong survival of patients awaiting transplantation by treating esophageal varicies and ascites and restoring proper hepatic microcirculation.

1.2 HEPATIC STELLATE CELLS

1.2.1 Embryonic Origin

The hepatic stellate cell (HSC) is a non-parenchymal cell type distributed homogenously throughout the perisinusodial space of Disse and comprises 15% of the liver [32]. The embryonic origin of HSCs has been inconclusive, however the majority of studies suggest HSCs may be derived from the endoderm or the septum transversum. Based on HSC expression of the transcription factor, Foxf1, in the developing and adult liver, a septum transversum-derived origin is implicated [33]. Additionally, Foxf1 +/- mice exhibited abnormal liver repair following injury due to decreased collagen production, reduced HSC activation and increased pericentral hepatic apoptosis. In support of an endoderm-derived origin, HSCs and hepatoblasts, which are undifferentiated progenitor cells originating from the ventral foregut endoderm, share a

common origin based on the expression cytokeratins in both cell types [34, 35]. These cells are present in the adult liver and can ultimately differentiate into hepatocytes and cholangiocytes [36].

Conversely, a neural crest-derived origin of HSCs has also been suggested based on the expression of a number of neural/neuroendocrine markers such as nerve growth factor, nestin, neural cell adhesion molecule, glial fibrillary acidic protein and cellular prion protein and based on their proximity to autonomic nerve endings [37]. However, the likelihood of neural crest origin of HSCs was refuted by a study using a transgenic mouse line expressing yellow fluorescent protein (YFP) in all neural crest cells and their derivatives [38]. While YFP was abundantly expressed in neural crest cells bifurcating from the neural tube and in all known neural crest-derived structures and cell populations, no detectable YFP expression was seen in the developing liver or in the HSC. This evidence further supports an embryonic origin derived from either the septum transversum or the endoderm.

1.2.2 Structure and Function in Normal and Injured Liver

In the normal quiescent state, HSCs project extensive cytoplasmic processes through the space of Disse and reach between hepatocytes and endothelial cells wrapping around neighboring sinusoids similar to tissue pericytes [39]. The expression of smooth muscle proteins and the strategic anatomical location of these cells suggest a functional role in maintenance of vascular tone much like a smooth muscle cell. The HSC is the main storage site of retinol in the liver (80-90%), similar to an adipocyte, with the remaining quantity being stored in hepatocytes awaiting release into the circulation to

maintain blood plasma levels of 2μM [40, 41]. HSCs also play a vital role in normal matrix maintenance and remodeling, similar to a fibroblast.

Upon a fibrogenic stimulus, the quiescent HSC transdifferentiates into an activated myofibroblast-like cell (FIGURE 1.7) [42]. Acute injury to the hepatocytes such as an increased viral load or chronic ethanol consumption initiates activation of the normal wound healing response. The metabolism of ethanol results in increased production of acetaldehyde and reactive oxygen species, which activates KCs subsequently stimulating release of cytokines and contributing significantly to HSC activation. HSCs proliferate, lose retinol droplets, increase expression of smooth muscle α-actin and secrete excess type I collagen for matrix repair [42-44]. Increased micro-projections from the myofibroblast allow for increased chemotactic signaling, which induces cellular migration to the site of injury [45]. Because of the anatomical location and increased contractile apparatus expression, it has been suggested that HSCs are capable of disrupting liver blood flow by hypercontracting, impeding microcirculation and contributing to portal hypertension [14, 46]. When the insult subsides, fibrosis resolves; however, if the injury is chronic, then the activated phenotype perpetuates and contributes to the progression of cirrhosis [6].

1.2.3 Extracellular Matrix Production and Degradation

In a healthy liver, HSCs produce ECM components for normal basement matrix remodeling including collagen (type I, III, IV, and VI), proteoglycans and glycoproteins [5, 47]. Type I, II, and V collagen is mainly confined to the portal tract and central vein wall, while type IV collagen along with laminin and entactin-nidogen form the basement membrane along the sinusoidal wall in the space of Disse [48]. In addition, HSCs

produce several types of MMPs (MMP-2, MMP-9, MMP-13, and stromelysin), which degrade ECM components [49-54]. In order to maintain basement membrane balance, HSCs produce tissue inhibitors of MMPs (TIMPs; TIMP-1and TIMP-2) [55]. Other distinct cell types also contribute to the production of collagens for hepatic architectural maintenance. Myofibroblast residing in the portal connective tissue, perivascular fibroblasts associated with the portal and central veins and periductular fibroblasts residing along the cholangiocytes of the bile duct all contributed to ECM maintenance [56]. Additionally, myofibroblast of bone marrow origin may contribute to the collagen accumulation within the liver [57]. Because ECM ultrastucture plays a role in the proper delivery of oxygen and nutrients across the fenestrated SECs, perisinusodial space of Disse and subsequently to the paraenchymal cells of the liver, it is important to understand the changes that occur during fibrosis.

In a fibrotic liver the balance of ECM composition is quantitatively increased (3-5 fold) [58]. Increased secretion of fibrillar collagens, specifically type I collagen, in the space of Disse, replaces the low density basement membrane with fibrous scar matrix (FIGURE 4) [59]. Type I collagen is synthesized by the coordinated expression of procollagen α1(I) and α2(I) mRNA [60]. Two pro-COL1A1 and one pro-COL1A2 polypeptide chains form the triple helix procollagen structure, which combine with other molecules to form larger collagen fibrils [60]. Both transcriptional and post-transcriptional modifications regulate collagen synthesis within the HSC [61]. At the transcriptional level, several repressor and enhancer elements, such as cytokine response elements, within the promoter of both subunits contain regulatory regions [62-64]. Additionally, DNA methylation of the first intron at different regulatory regions also

enhances transcription [60]. At the post-transcriptional level, it has been shown that not only does procollagen α_1(I) mRNA stability increase from 1.5 hours in quiescent HSCs to greater than 24 hours in activated HSCs, steady state levels also increase 60 to 70-fold [65]. Increased mRNA stability within the activated HSC is mediated by an RNA-binding protein on the 3'-untranslated region of the procollagen α_1(I) mRNA and through a stem-loop binding structure in the 5' end of the procollagen α1(I) mRNA [65]. Both increased type I collagen stability and secretion further contribute to scar matrix accumulation and thus impedes fibrotic resolution.

Increased matrix stiffness observed in liver fibrosis has been associated with perpetual HSC activation, which results in a shift of ECM components from a basal to a fibrillar matrix. Signaling from the ECM to the HSCs occurs through several specific cell membrane receptors such as integrins, discoidin domain receptors and dystroglycan [66-68]. Type I collagen stimulates cell adhesion by interacting with integrin α1β1 to stimulate focal adhesion kinase (FAK) phosphorylation, activation of phosphoinositide 3-kinase (PI3K), which leads to cellular migration [69, 70]. Additionally, MMPs are capable of cleaving ECM and cell surface molecules, which alter cell-matrix and cell-cell interactions, affecting biological function and growth factor release. Transforming growth factor β (TGFβ) can directly affect matrix stiffness by suppressing MMPs and activating TIMPs in HSCs[71]. Additionally, TGFβ may also signal through the Smad pathway directly altering matrix stiffness. HSCs isolated from mice overexpressing Smad3, a Smad family member, demonstrated an increase in stress fiber formation and focal adhesions following culture activation [72]. Although Smad3 overexpression did not increase smooth muscle α-actin expression (marker of HSC activation), it was shown

to be the determining factor in stress fiber organization, thus playing an important role in matrix rigidity of the fibrotic liver.

Culturing freshly isolated HSCs on uncoated plastic tissue culture dishes mimics the *in vivo* environment of liver fibrosis and activates quiescent HSCs. In cirrhotic patients, liver stiffness measurements range from 12.5 to 75.5 kPa [73]. Therefore, altering matrix stiffness regulates HSC activation [73]. The quiescent phenotype can be maintained in culture on a laminin-rich gel (Matrigel) that mimics the effects of a normal basement membrane. Additionally, HSCs are more fibrogenic when grown on type I collagen in response to TGFβ than on type IV collagen [74, 75]. Noninvasive strategies for the diagnosis of hepatic fibrosis have been measured by transient elastography (FibroScan) [76]. By using a mechanical pulse at the skin surface, FibroScan can measure the velocity of the wave, which directly correlates to liver stiffness, by ultrasound. The manifestation of matrix stiffness as a regulator of HSC activation strengthens the diagnostic potential of this screening method.

1.2.4 Retinol Production, Receptor Expression and Cytokine Secretion

In the liver, HSCs are responsible for retinoid metabolism, immunoregulation and the secretion of cytokines and growth factors. Most retinoid is stored in cytoplasmic vesicles in the form of retinyl esters [77]. Dietary vitamin A is esterified with long-chain fatty acids and packaged into chylomicrons for transport through lymphatic draining vessels from the intestines to the hepatocytes [40]. The retinyl esters are then hydrolyzed to retinol and transferred to HSCs mediated by retinol binding protein (RBP) [78]. The lipophillic compounds exhibit the characteristic blue autofluorescence of quiescent HSCs

when excited with a UV light and measured with a DAPI (4',6-diamidino-2-phenylindole) filter (~328nm λ) (FIGURE 1.8) [79].

In addition to retinoid production, HSCs also play a role in the complex interplay of the hepatic immune system. Activated HSCs produce chemokines such as monocyte chemotactic peptide (MCP)-1, macrophage colony-stimulating factor (MCSF), CCL21, RANTES and CCR5 to amplify the inflammatory response by inducing infiltration of mono- and polymorphonuclear leukocytes [80-82]. Similar to antigen presenting cells, HSCs also express toll-like receptor (TLRs) -4 and -2, which allow them to respond to both Gram-negative and -positive bacterial cell components such as lipopolysaccharide (LPS) and peptidoglcan, respectively [83, 84]. Subsequently, HSCs express the costimulatory molecules CD38 and CD40, which stimulate the secretion of proinflammatory molecules interleukin-6 and -8 (IL-6 and IL-8), respectively [85, 86].

IL-6 is a key cytokine in the hepatic acute injury response, which induces production of C-reactive protein, a key inflammatory marker. IL-6 has been shown to be critical in liver regeneration following transplantation [87], hepatoprotective in CCl_4 induced injury [88] and is required for wound healing in a hepatectomy model [89, 90]. However, in a fibrotic liver, the role of IL-6 is ambiguous, since IL-6 secretion contributes to the fibrotic progression [91, 92]. Additionally, IL-6 has been shown to up-regulate collagen production in many collagen-producing cell types, including activated HSCs [93-95]. Conversely, HSCs exhibit a dual role mediated by oxidative stress in a co-culture system with KCs [95]. Finally, activated HSCs produce IL-6 as well as respond to it [93, 96-98]. While IL-6 has been analyzed in multiple injury models, the role of IL-6 in HSC transdifferentiation has yet to be fully elucidated.

Although IL-6 is a potent fibrogenic cytokine, TGFβ has been described as the most potent fibrotic mediator of hepatic fibrosis. TLR-4 stimulates the secretion of latent TGFβ in response to acute injury. Three isoforms of TGFβ exist, with TGFβ1 being the most potent fibrogenic stimuli for HSCs and predominately acting in the immune response [99]. HSC activation upregualtes TGFβ-receptor (TGFβ-R) expression in HSCs, which stimulates retinol release, matrix deposition, contractility and chemotaxis mediated through Smad 2 and 3 [100-105]. Activated Smad 2 and 3 recruit Smad 4 to form a heterotrimeric complex that translocates to the nucleus and regulates gene transcription to stimulate the production and deposition of fibrillar EMC components such as type I and III collagen. HSCs also secrete TGFα and epidermal growth factor (EGF), which stimulates hepatocyte proliferation during regeneration, HSC mitosis, and creates an autocrine stimulus for perpetual HSC activation [101, 106-108]. Although HSCs are the main source of TGFβ secretion, KCs and platelets can also produce this cytokine [109].

In order to counteract the proinflammatory cytokines IL-6 and TGFβ, transcription factors in the activator protein-1 family, interleukin-10 signaling mediates the inhibition of type I collagen production and thus reduces inflammation [110, 111]. Other soluble factors such as fibroblast growth factor (FGF) and interferon γ (IFNγ) also reduce extracellular matrix deposition [112, 113]. Overall, the numerous cytokines and receptors HSCs secrete and express suggest a fundamental role in hepatic immunology.

1.2.5 Contraction

In the normal liver microcirculation autoregulation is delicately balanced by potent vasoactive modulators, such as nitric oxide (NO) and endothelin-1 (ET-1) [32,

114]. Several studies have shown that ET-1 levels are elevated in patients with cirrhotic livers, while levels of NO are decreased [115, 116].

NO, which is a potent vasodilator produced by SECs, is a gaseous compound biosynthesized endogenously from L-arginine and oxygen by nitric oxide synthase (NOS) and by reduction of inorganic nitrate. NO production is attributed to the activity of the inducible NOS isoform (iNOS) in HSCs [117]. NO binds guanylate cyclase, which increases cyclic guanosine monophosphate (cGMP) and activates protein kinase G (PKG) to regulate intracellular calcium in smooth muscle cells [118]. NO production inhibits calcium influx, which decreases contraction [119]. Exogenous NO has been shown to be capable of preventing ET-1 induced contraction as well as induce relaxation of pre-contracted gels [114]. In the normal liver, the NO donor diethylamine NONOate (DEAN) significantly increased cGMP production and reduced basal HSC contraction, while PKG chemical inhibition abolished the observed DEAN effects suggesting a cGMP-dependent/ PKG-dependent and -independent pathways [120]. These studies also demonstrated that cGMP/ PKG signaling is impaired in activated HSCs contributing to an imbalance of vasoactive modulators in the injured liver [120].

Endothelins are potent vasoactive substances synthesized by nonparenchymal cells of the liver, predominately in SECs in a prepro-form (200 amino acids) [121-123]. Three isoforms have been identified; ET-1, -2, and -3 [124]. Furin-like enzymes induce proteolytic processing of preproET to big endothelin (Big ETs; 38-41 amino acids). Big ETs are cleaved by endothelial converting enzymes at Trp-21-Cal/Il3-22 to yield the 21 amino acid mature peptide (ETs). ETs diffuse and bind to the guanine protein-coupled receptors ET_A and ET_B on neighboring cells or act in an autocrine manner [14, 125, 126].

ET-1 stimulation of ET_A receptors on smooth muscle cells lead to cellular contraction, while ET_B receptors display a similar affinity for all three ET isoforms and stimulate NO release. Presence of ET_A and ET_B receptors suggests that HSCs are capable of modulating vascular tone [121, 127]. Furthermore, *in vitro* results demonstrated that SECs release excessive ET-1, which has a stimulatory effect on HSC proliferation, αSMA expression and contraction of collagen lattices [14, 122]. This data was confirmed *in vivo* by showing that ET-1 induces significant sinusoidal constriction at the sites of HSCs but not at the sites of KCs or SECs [128]. Additionally, in a cirrhotic model, ET receptor density was increased on HSCs [129].

Simulation of ET_A receptors induces HSC contraction through both a calcium-dependent and independent medium (FIGURE 1.9) [127]. Similar to what is observed in smooth muscle cells, ET_A receptor binding increases the cyclic adenosine 3', 5'-monophosphate (cAMP) levels in HSCs [130]. Increased levels of calcium are generated by cAMP-induced activation of phospholipase C-β, cleavage of phosphatodyinositol 4,5-biophosphate and release of 1,4,5-triphosphate [122]. Influx of calcium activates calmodulin-dependent myosin light chain kinase (MLCK), which phosphorylates and subsequently stimulates the ATPase activity of myosin II and thus contractile force generation [131].

Conversely, previous results suggest that ET-1 predominately stimulates activation of calcium-independent pathways mediated through the RhoA signaling cascades [132]. RhoA is a small monomeric GTPase that is inactive in the GDP bound- and active in the GTP bound-state. GTPase activating proteins (GAPs), guanine nucleotide exchange factors (GEFs) and guanine nucleotide dissociation inhibitors

(GDIs) regulate the state of activation. While GEFs accelerate GTP hydrolysis, GAP and GDI increase GDP association and thus RhoA activation [133]. RhoA activation stimulates Rho kinase (ROCK), which inhibits myosin light chain (MLC)-phosphatase and directly phosphorylates MLC both resulting in enhanced phosphorylation of myosin II, stress fiber formation and cellular contraction.

By using a selective inhibitor for ROCK (Y-27632), it has been suggested that HSC contraction is predominately mediated through the RhoA pathway. Kawada et. al., demonstrated that HSCs cultured on collagen lattices in the presence of Y-27632 failed to contract when stimulated with ET-1 [134]. This study also showed that myosin II phosphorylation was decreased while αSMA expression remained stable indicating that ROCK inhibition directly impeded myosin II phosphorylation. Furthermore, ROCK inhibition, using Y-27632, decreased portal pressure *in vivo* and thus could potentially attenuate portal hypertension [134]. Treatment with Y-27632 also impeded progression of hepatic fibrosis as shown by decreased collagen accumulation and HSC activation, which has been shown to be mediated through the angiotensin II signaling pathway [135]. Therefore, distinguishing between ROCK-induced contractile properties and other fibrogenic responses requires a more selective inhibitor of HSC contraction.

A closer examination of the two distinct contractile pathways demonstrated that rearrangement of surrounding matrix, and thus gel contraction of collagen lattices seeded with myofibroblasts, was associated with rearrangement of central stress fibers induced by the Rho kinase-mediated signaling cascade, while the peripheral stress fiber system depended more on the calmodulin-dependent MLCK activity [136]. Although the calcium-independent pathway appears to predominate in HSC hypercontractility, these

findings suggest that the actomyosin-based cytoskeletal actions can be functionally diverse depending on the signaling cascade.

Collectively, an imbalance of vasoactive modulators leads to HSC hypercontractility and increases portal pressure by decreasing sinusoidal diameter. In addition to the change in production of vasoactive substances in the injured liver, the contractile machinery in activated HSCs is also upregulated, which confers an increase in contractile potential.

1.2.6 Proliferation and Migration

Activated HSCs not only contribute to the fibrotic condition through increased vascular resistance but also through expanding the cell number through proliferation. Platelet-derived growth factor (PDGF) is the most potent proliferative stimulus for HSCs and is mainly produced by KCs [4, 137, 138]. This cytokine exists either as a homodimer (PDGF-BB) or as a heterodimer (PDGF-AB), the dimers being connected through disulfide bonds. In order to enhance proliferation and regulate cell survival, PDGF-BB stimulates PDGF receptor expression and thus the PI3K-mediated signaling cascade, which leads to a multitude of downstream effects including Akt and ribosomal kinase S6 kinase ($p70^{S6K}$) activation (FIGURE 1.10) [139]. PI3K inhibitors, such as wortmannin and LY294002, have both been shown to reduce PDGF-dependent proliferation [69, 70]. Furthermore, wortmannin inhibition of PI3K also reduced PDGF-simulated activation of extracellular-signal regulated kinase (ERK) activity and c-fos mRNA levels, which is dependent of ERK activation, suggesting that cross- talk occurs between the PI3K and mitogen-activated protein kinase (MAPK) pathways in PDGF-stimulated HSCs [140]. PDGF stimulation can also directly activate MAPK pathway through the Ras-Rac-Raf

complex thereby activating c-Jun nuclear kinase (JNK) and ERK [141]. However, direct inhibition of p^{38} MAPK pathway by SB203580 increased HSC proliferation indicating a dual mechanism mediated by MAPK activation regulating HSC mitosis [142].

In addition, activation of $p70^{S6K}$ is also critical for HSC proliferation, collagen production and cell survival. The $p70^{S6K}$ chemical inhibitor, rapamycin, blocks PDGF-stimulated proliferation in culture-activated HSCs [137, 143]. Furthermore, rapamycin also reduces the α1 (I) collagen gene and collagen protein levels, indicating that $p70^{S6K}$ is positioned downstream of Akt in the PI3K signaling pathway. Finally, studies PDGF-stimulated cells increases FAK activity and genetically blocking this pathway inhibits PI3K activity and thus HSC proliferation [144].

Activated HSCs increase secretion of PDGF as wells as upregulate their tyrosine kinase receptor expression (PDGF receptor) during liver injury, which induces proliferation and stimulates cell migration [145, 146]. In addition to PDGF-BB, ET-1, TGFβ1 and/ or EGF have been associated with chemotactic HSC migration [45, 147, 148]. Based on exogenous ET-1expression, it has been shown that wound-induced migration of HSCs is associated with guanine receptor -mediated signaling of the actomyosin cytoskeleton (FIGURE 1.10) [148]. Additionally, HSC cytoplasmic projections facilitated the response of PDGF signaling and transduce this stimulant into mechanical forces that induce cell spreading at the leading edge, movement of the cell body towards the chemotactic signal and retraction of the trailing edge of the cell [45]. Thus endogenous ligand antagonists or receptor blockage to PDGF activity is a promising therapeutic approach to suppressing fibrogenesis.

1.3 MYOSIN

1.3.1 Structure and Function

Molecular motors play important cellular roles in actin-based motility, vesicle transportation, endocytosis, phagocytosis, stereocilia formation, cytokinesis and contraction. Myosins are a large super-family of molecular proteins found in eukaryotic tissues that bind actin filaments in order to generate force using ATP hydrolysis [149]., twenty-five different classes have been characterized based on amino acid sequences in their ATP-hydrolyzing motor domains. Myosins are comprised of three subdomains: the head region, which interacts with actin and binds ATP, the tail region, which anchors and positions the head region and the neck region, which binds either the MLCs or calmodulin (FIGURE 1.11). In many myosins, the tail region is capable of forming coil-coil complexes, which allows the molecules to form dimers. Analysis of different myosin structural cores demonstrates a strong conservation of the head regions' sequences but an enormous variability in the tail regions, while the neck regions maintain a conserved consensus sequence of IQXXXRGXXR, referred to as IQ motifs [150]. The number of IQ motifs in the neck regions ranges from zero to six in the different myosin classes. The differences in domain structure allow the different classes to perform specific cellular functions at the appropriate kinetics. Myosin V, which is an organelle transporter, has a much longer neck region than myosin II, and can traverses actin filaments by taking 30-40 nanometer steps with each cross-bridge cycle. In contrasts, myosin II takes 5-10 nanometers steps and functions as an assembly of motors to produce a contractile force in cells [150].

Myosin II also termed “conventional myosin” is responsible for generating contractile forces [151]. Myosin II molecules can be subdivided further into distinct classes based on different amino acid sequences in the motor domain: the sarcomeric myosin II from muscle cells (skeletal, cardiac and smooth), nonmuscle myosin II, and myosin II from lower eukaryotic species and fungi [149]. Human nonmuscle myosin II is weakly homologous (33%) to sarcomeric myosin, while they exhibit a higher homology as compared to smooth muscle myosins (72%) [152]. Generally, the hexameric myosin II protein, with a molecular weight of 171-244 kDa, consists of two identical heavy chains (MHCs) each with two associated MLCs [151]. The individual MHCs (head regions) consist of a catalytic motor domain, an α-helical neck region containing two IQ motifs and a coil-coil tail region [151]. The amino-terminal motor domain contains a nucleotide-binding region that is opposite a deep pocket that transverses the actin-binding domain [153]. Small conformational changes in the ATP binding region are coupled to large swings of the neck region [153]. The tail region forms antiparallel complexes, which polymerize hundreds of myosin molecules in thick filaments of skeletal muscle cells or as few as 28 myosins in nonmuscle cells [154]. The actin-associated proteins, troponin and tropomyosin, are the primary regulatory molecules of skeletal and cardiac muscle contraction; whereas, phosphorylation of the 20kDa MLC is the predominate regulator of nonmuscle and smooth muscle myosin [155, 156].

The activity of smooth muscle and NMM II has also been shown to be regulated through phosphorylation of the MHC by casein kinase II, small GTPases, such as Rho and Rac, and PKC [157-159]. While casein kinase II inhibits the assembly of the coiled-coil tail region of smooth muscle myosin in bovine aorta, Rac phosphorylation of the

MHC induces filament instability and promotes disassembly of actomyosin complexes [160]. Furthermore, insulin secretion in rat pancreatic islet cells can be activated by PKC-mediated phosphorylation of the MHC, independent of MLC phosphorylation [161].

In order to determine specific myosin II cellular functions, pharmacological agents have been used including, 2,3-butanedione monoxime (BDM), N-benzyl-p-toluene sulfonamide (BTS), Y-27632 (ROCK inhibitor) and blebbistatin [153, 162-164]. BDM inhibits myosin ATPase activity by blocking myosin II in a weak binding contraction after ATP binding [165]. BTS on the other hand blocks skeletal muscle myosin II by competitively interacting with the myosin II binding site on F-actin [166]. Y-27632 inhibits the Rho pathway by blocking the upstream stimulator of myosin II activity, ROCK. However inhibiting the Rho pathway blocks a wide range of cellular functions such as contraction, migration, apoptosis and proliferation via the MLC phosphorylation, LIM-kinase, Akt and the ERK pathway, respectively [167]. Therefore, using a chemical inhibitor, such as blebbistatin, which is more potent and selective than BDM or BTS, may prove to be beneficial in delineating the specific role of myosin II [168]. Blebbistatin is a reversible pharmacological inhibitor that preferentially binds to the ATPase intermediate with ADP and phosphate bound at the active site (myosin-ADP-P_i). Blebbistatin exerts its mechanism of inhibition by limiting phosphate release from the actomyosin complex, which prevents rigor of the myosin molecule and actin filament sliding. While studies have shown blebbistatin is an inhibitor of skeletal muscle and NMM II activity with minimal effects on smooth muscle myosin II, others have shown that blebbistatin is specific to smooth muscle myosin II [164, 169-171]. Chemical

inhibition of myosin II activity is useful in exploring the functional role of the molecular motor within the cell.

1.3.2 Smooth Muscle Myosin II

Although the structural cores of the myosin II classes are homologous, the minor amino acid alterations in the heavy and light chains alter kinetic and biochemical properties of the motor [172]. Smooth muscle myosins can be classified into two categories: tonic and phasic [173]. While tonic smooth muscle has the capacity to maintain force, force maintenance in phasic smooth muscle is less apparent. Generally, stimulation of smooth muscle results in an initial period of force activation followed by force maintenance. Both intracellular calcium and MLC phosphorylation increase rapidly during force activation before falling to a lower steady state level [174]. Similarly, the maximum velocity of muscle shortening (V_{max}) increases to a peak then falls to a lower level during force maintenance [174]. This state of force maintenance with low levels of calcium, MLC phosphorylation and V_{max} is referred to as the "latch state" [174, 175]. It has been suggested that the molecular basis for the latch state may be due to dephosphorylation of active cross-bridge cycling, dynamic cytoskeletal arrangements and the slow release of ADP from both phosphorylated and dephosphorylated smooth muscle myosin [176-178].

Four isoforms of smooth muscle myosin II are derived from one gene capable of alternative splicing; SM 1-A, SM 1-B, SM 2-A and SM 2-B [179-182]. The SM 1 isoforms contain a phosphorylation site for casein kinase II, suggesting a regulatory role for filament assembly and thus differences in contraction rates. Furthermore, a 7-amino acid insert in the loop-1 region at the 25/50kDA domain junction in the head of SM B

may be responsible for modulating actomyosin kinetics [183]. SM B knockdown in transgenic mice has been shown to result in a slower smooth muscle phenotype [184]. Additionally, two isoforms of the MLC are formed in smooth muscle: LC_{17a} and LC_{17b} [185]. While expression of LC_{17b} slows the actin activated ATPase, expression of LC_{17a} and SM B correlates to a faster smooth muscle phenotype.

1.3.3 Nonmuscle Myosin II

In nonmuscle cells, three isoforms of myosin II encoded by different genes have been identified in vertebrates, NMM II-A, II-B and II-C [186-188]. Each isoform has been mapped to different chromosomes. By genomic sequence analysis, the NMM II-A gene, MYH9, is mapped to 22q12.3-q11.2, while the NMM II-B gene, MYH10, is mapped to 17q13 [187]. The NMM II-C gene, MYH14, is mapped to chromosome 19q13.33 [189]. In the motor domain, the isoforms are 64-80% identical at the amino acid level. The distinct variations and enzymatic properties of each isoform are important in modulating the kinetic properties of the cell and allow for fine tuning of specific biological functions [190].

It has been shown that mutations in the MYH9 gene coincide with the autosomal dominant giant-platelet disorders May Hegglin anomaly (MIM 155100), Fechtner syndrome (MIM 153640), Epstein Syndrome (MIM 153650) and Sebastian syndrome (MIM 605249) [191]. Furthermore, the homozygous deletion of MYH10 in mice was lethal in embryos due to heart and brain defects, while mutations in MYH14 exhibited hearing loss as indicated by decreased auditory brainstem responses [192].

Higher organism tissues express relatively ubiquitous levels of all three isoforms; however, it has yet to be determined whether these proteins play redundant, overlapping

or distinct roles in performing various mechanical functions in the cell. While NMM II-A is only expressed in chicken intestinal epithelial cells and platelets, NMM II-B is predominately expressed in neuronal tissue [193, 194]. Both isoforms are distributed along stress fibers in a linear fashion and localization varies between different cell types [195]. Generally, NMM II-A co-localizes with actin filaments at the leading edge of cells, while II-B co-localizes to the cellular cortex [195]. The regional variations in the different myosins suggest that each isoform may be responsible for specific molecular functions within the cell that potentially correlate to the kinetics of each isoform.

Investigating the mechanochemical cycle of NMM II-A, II-B and II-C provided kinetic evidence that all three isoforms have slow ATPase activities as compared to other myosin II classes (NMM II-A: Vmax=1.2/s; K_{ATPase}=7.4μM; NMM II-B: Vmax=0.28/s; K_{ATPase}=12.7μM; NMM II-C: Vmax=0.55/s; K_{ATPase}=16.5μM;). NMM II-B has a higher ADP affinity than NMM II-A and spends the majority of its kinetic cycle bound to actin. With a lower ADP affinity, NMM II-A spends a smaller fraction of its kinetic cycle attached to actin [190]. The slower ADP release and long actin attachment time make NMM II-B an ideal candidate for long term force maintenance. Based on these calculations, one group determined that a transition between ADP states is the rate limiting step in the kinetic schematic [154]. Contrarily, others have shown that the phosphate release is the rate-limiting step [190]. The differing views explain the drastic differences in the reported duty ratios of NMM II B (23-40% compared to 82%) [154, 196]. Both groups agree that NMM II B molecule has a higher duty ratio than NMM II A (3.8-11%) [154, 196]. Therefore it can be concluded that NMM II-B may be involved in

maintaining tonic force, while the faster NMM II-A may be involved in the rapid tension generation [186].

1.3.4 Hepatic Stellate Cells and Myosin II

HSCs play a critical role in liver microcirculation and fibrosis; therefore, it is important to understand the molecular aspects governing HSC contractility, proliferation and migration in response to injury. HSCs express myosin II and actin and it has been suggested that this actomyosin complex regulates contraction much like it would in a smooth muscle cell [134, 136, 148, 197-200]. However in contrast to smooth muscle cells, HSCs favor a calcium-independent pathway mediated by RhoA [127, 198]. In order to characterize the role of myosin II in the HSC, pharmalogical agents, Y-27632 and blebbistatin, have been shown to inhibit myosin II phosphorylation [45, 134]. HSCs express a large number of early and late smooth muscle cell markers including smooth muscle (SM) α-actin, SM22α, desmin, SM myosin heavy chain, h1-calponin, h-caldesmon and myocardin. Therefore, the smooth muscle myosin II proteins may play a role in HSC contraction [201]. Since the HSC is a nonmuscle cell, it is also possible that HSCs express NMM II to modulate the contractile apparatus; however, the specific myosin II classes or isoforms have not been characterized nor been correlated to a specific biological function in the HSC.

1.4 HYPOTHESIS

We hypothesize that hypercontraction, migration and proliferation of activated hepatic stellate cells (HSCs) are modulated by specific nonmuscle myosin II (NMM II) isoforms. Since the HSCs play a critical role in regulating liver microcirculation and the wound healing response during liver injury, determining the expression profile and function of

each NMM II isoform and delineating the mechanism of isoform induced expression in the HSC may lead to the development of specific-targeted therapeutics to treat the complications of portal hypertension seen in liver injury.

Aims

1. To test if directly inhibiting myosin II activity with blebbistatin can modulate HSC contraction.
2. Determine the expression and cellular localization of the NMM II isoforms (II-A, II-B and II-C) in HSCs.
3. To test if gene knockdown of NMM II isoforms (II-A, II-B and II-C) can modulate contraction, migration and proliferation of HSCs.

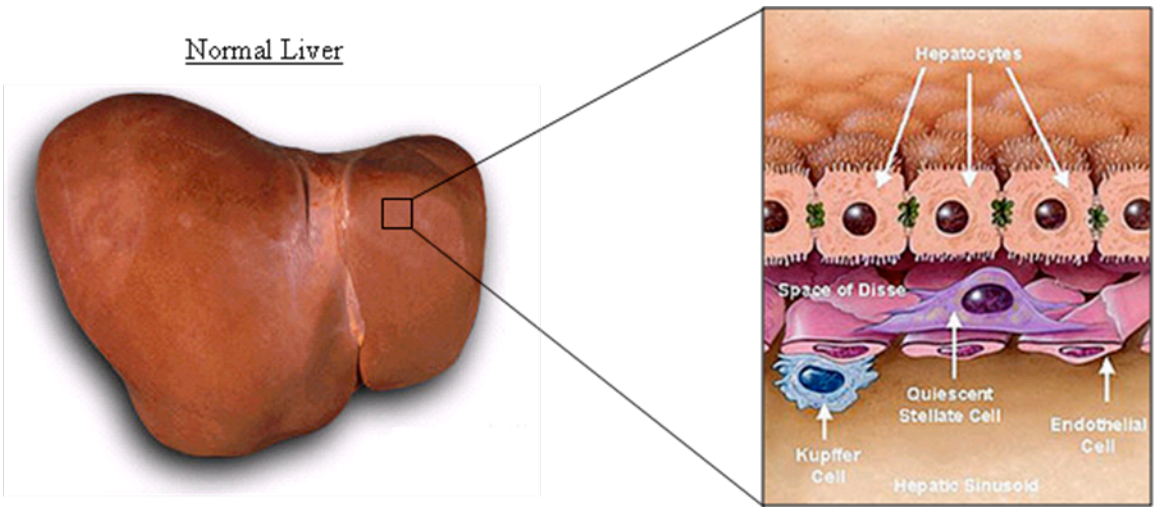

FIGURE 1.1: Schematic Drawing of Normal Liver Architecture. The liver is the largest internal organ; it is smooth in texture and bright red in color. The hepatocyte is the primary cell type of the liver and the SECs line the blood vessel wall. The HSCs reside in the Space of Disse and the Kupffer cells are the resident macrophages. (Adapted from Friedman SL 2000)

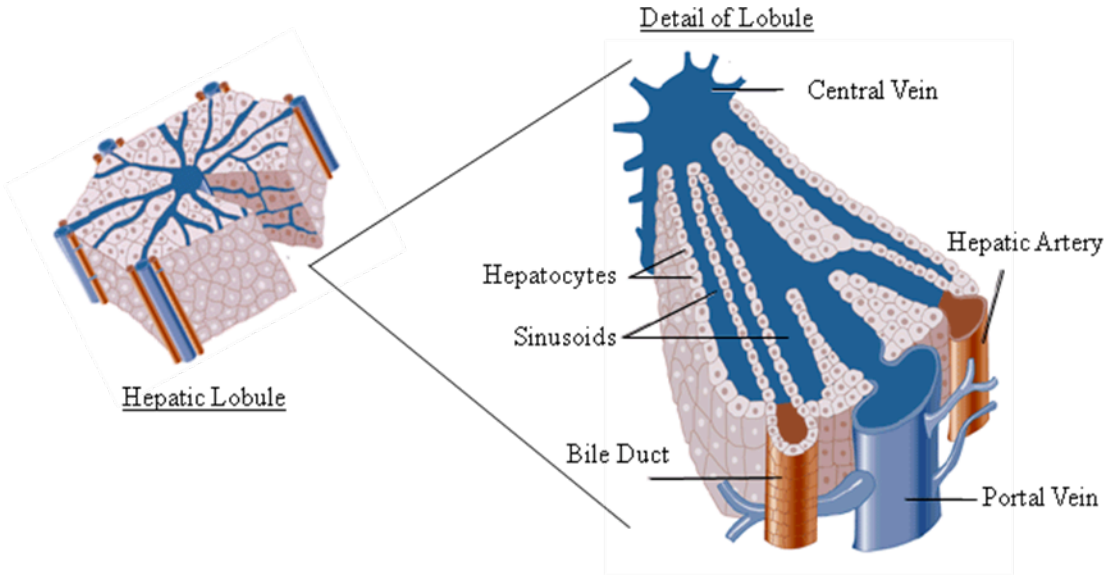

FIGURE 1.2: Schematic Drawing of Hepatic Lobule. The functional unit of the liver is the hepatic lobule. The liver receives 75% deoxygenated blood from the portal venous system and 25% oxygen rich blood from the hepatic arterial system. Hepatocytes optimize filtration, remove toxins from the microcirculation and excrete waste through the bile duct. Filtered blood drains through the central vein and exits the liver through the portal vein. (Adapted from Ross et al. 1995)

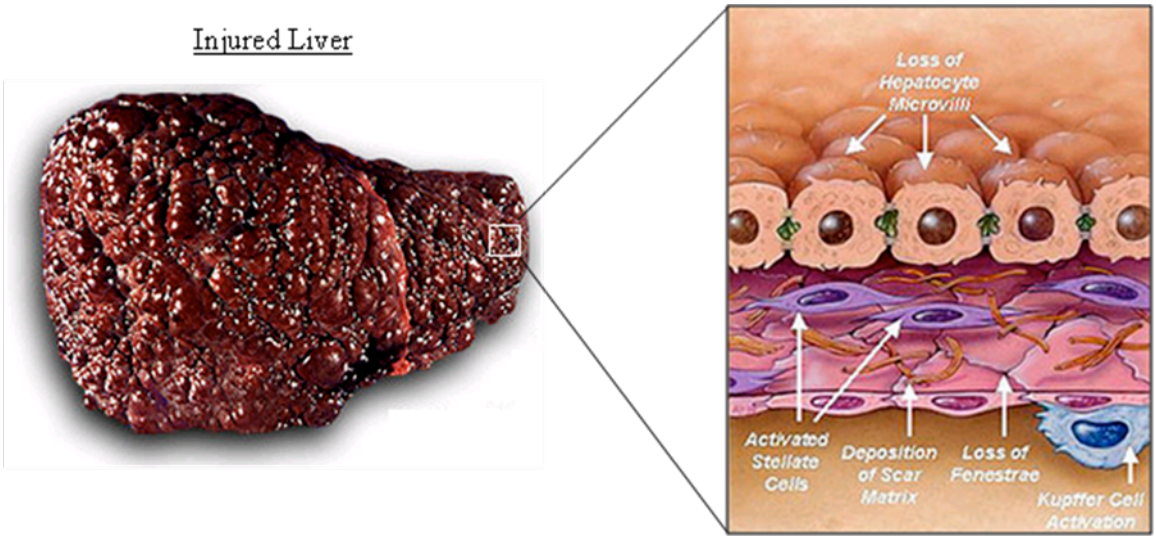

FIGURE 1.3: Schematic Drawing of Injured Liver. The injured liver is characterized by nodular formation and necrosis. Hepatocytes lose microvilli and Kupffer cells activate an inflammatory response. The SECs reduce blood filtration by closing fenestra and the HSCs excrete excessive collagen for matrix repair. (Adapted from Friedman SL 2000)

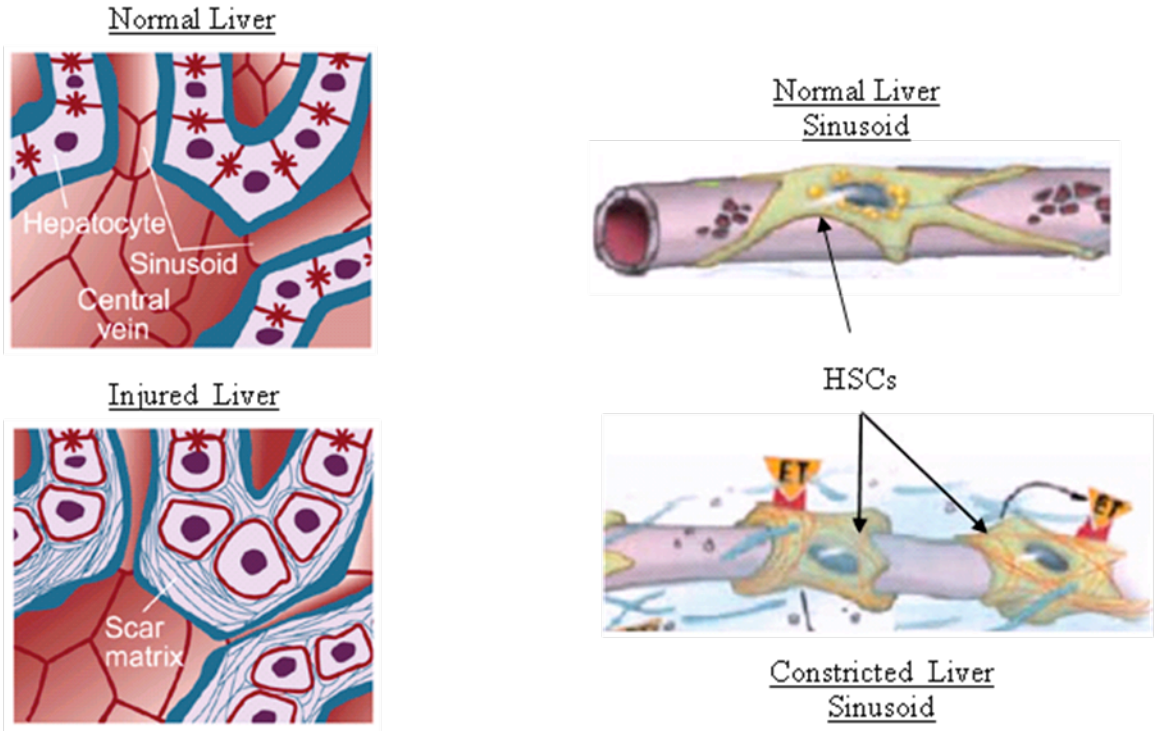

FIGURE 1.4: Schematic Drawing of Injured Liver Mechanical Distortion. Increased scar matrix deposition contributes to mechanical distortion of the hepatic microvasculature. Additionally, hypercontractility of the HSCs increases vascular resistance in the sinusoids further compounding the clinical manifestation of portal hypertension. (Adapted from Rockey et al. 2003)

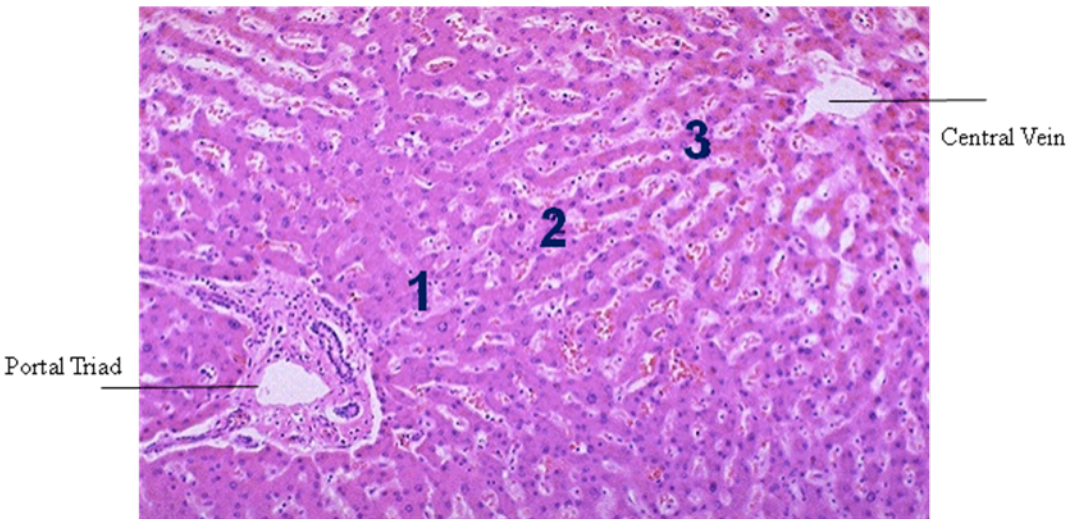

FIGURE 1.5: Hepatic Zonal Architecture. Functionally, the liver can be divided into three zones, based upon oxygen supply. Zone 1, the periportal triad region, is located around the portal tract where oxygenated blood from the hepatic artery enters. This region is susceptible to primary biliary disease. Zone 3, the pericentral region, is located around the central vein, where oxygen supply is low. This region is the most oxygen depleted and alcoholic liver fibrosis. (Adapted from The Internet Pathology Laboratory for Medical Education: The University of Utah Eccles Health Sciences Library)

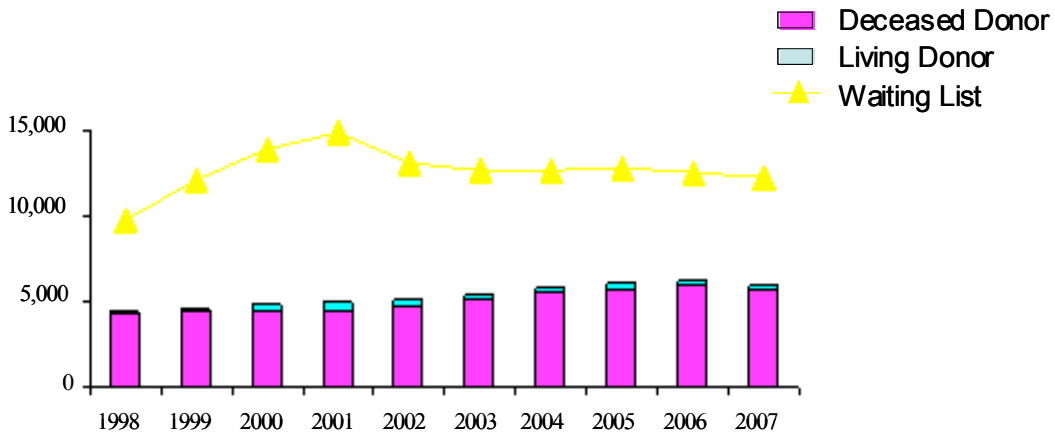

FIGURE 1.6: Liver Transplant Statistics (1998-2007). Number of liver transplantations and size of waiting list per year. In 2002, the number of patients awaiting liver transplantation peaked and the gap between the waiting list and liver transplantation has decreased. (2008 U.S. Organ Procurement and Transplantation Network and the Scientific Registry of Transplant Recipients Annual Report)

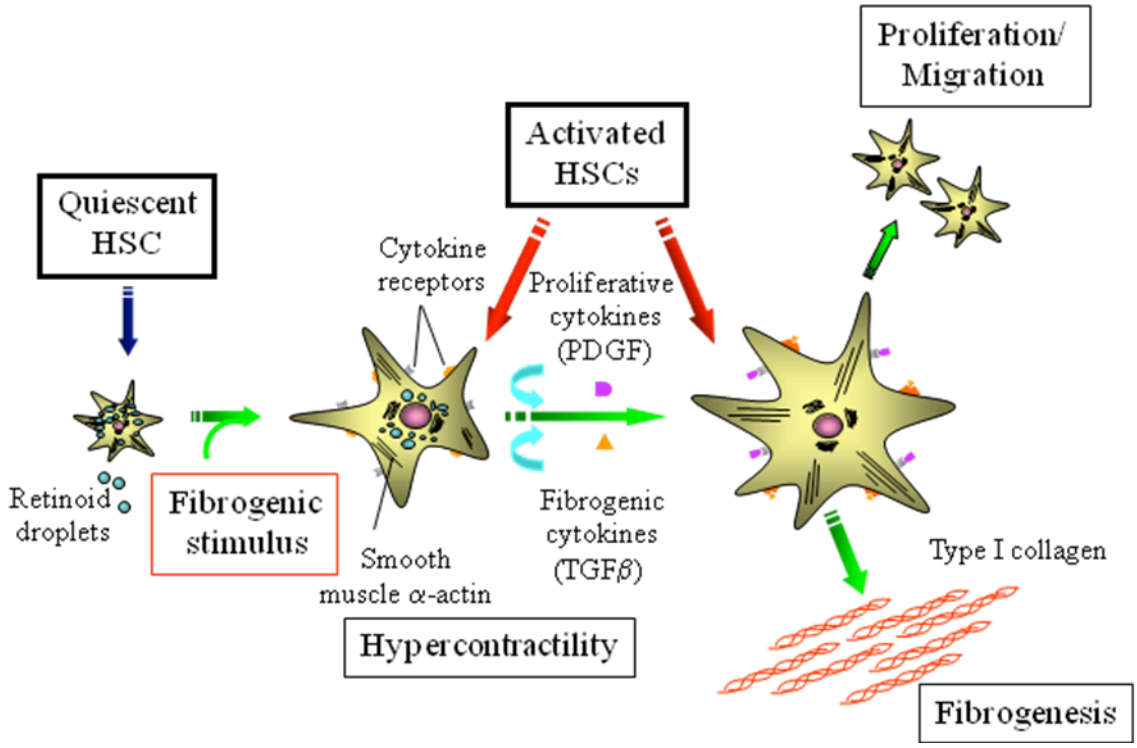

FIGURE 1.7: Schematic Drawing of HSC Transdifferentiation. Quiescent HSCs store vitamin A in the form of retinoid droplets. Upon exposure to a damaging stimulus, the HSC undergoes a phenotypic change from the quiescent state to the activated myofibroblast-like state. Activated HSCs migrate to the site of injury, proliferate vigorously, become hypercontractile, secrete collagen and produce numerous cytokines and growth factors, which provide an environment appropriate for tissue repair. (Adapted from Brenner 1999)

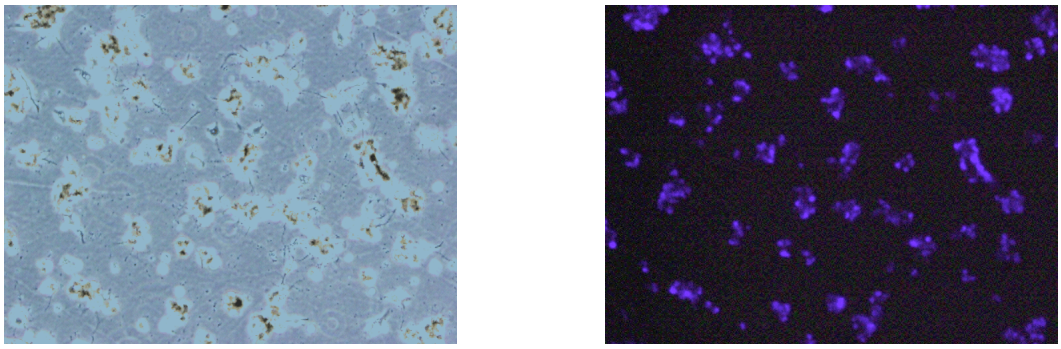

FIGURE 1.8: Representative Images of Quiescent HSCs *in vitro*. Quiescent HSCs are a star-like structure capable of modulating vascular tone. Lipophillic compounds exhibit characteristic blue autofluorescence measured with a DAPI (4',6-diamidino-2-phenylindole) filter (~328nm λ).

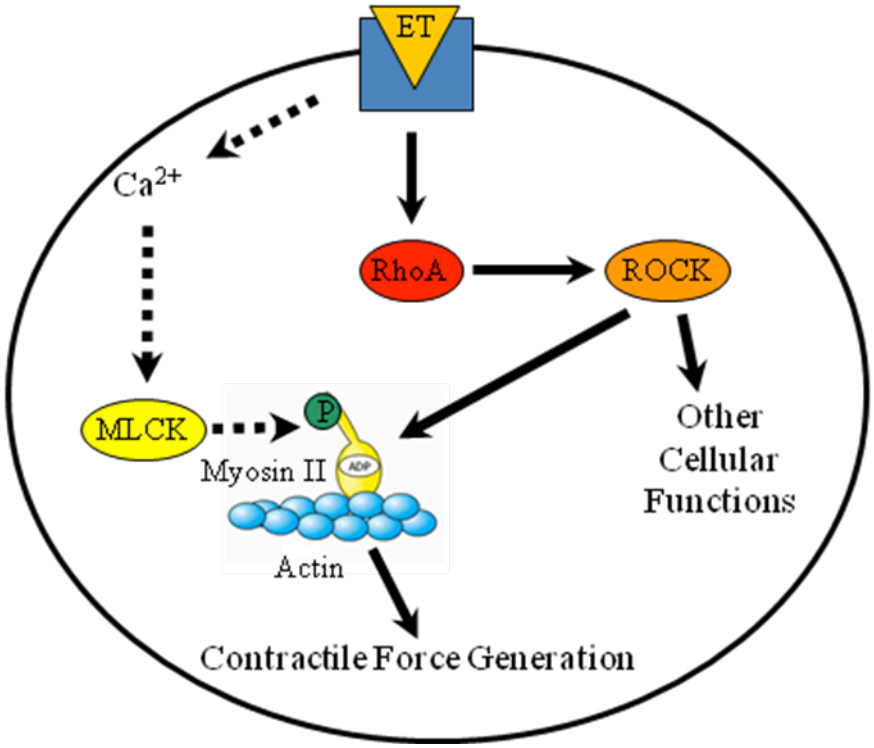

FIGURE 1.9: Schematic Drawing of ET-1-Induced Contraction in HSCs. ET-1 signals predominately through the ROCK signaling pathway resulting in phosphorylation and activation of myosin II promoting myosin II-generated contractile force in HSCs.

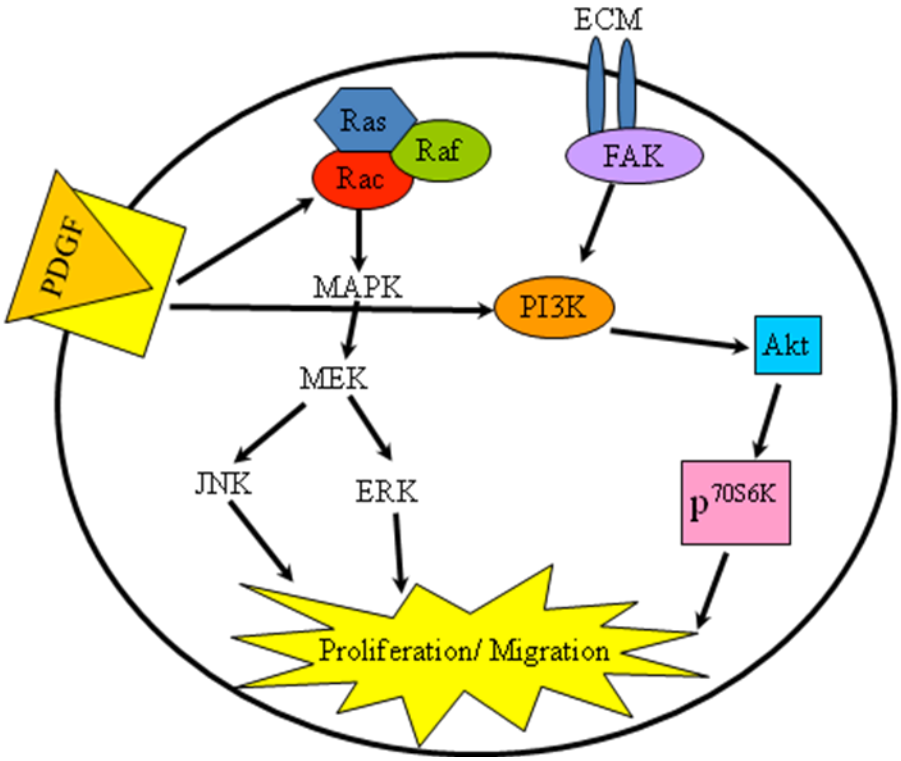

FIGURE 1.10: Schematic Drawing of HSC Proliferation/ Migration. Activation of several intracellular signaling pathways, including PDGF stimulation and FAK activation, lead to increased cell survival and proliferation of HSCs.

FIGURE 1.11: Schematic Drawing of Myosin II. The myosin II molecule is composed of two MHCs (green) and two pairs of MLCs (blue). The MHC consists of the C-terminal dimerized tail region, which polymerize hundreds of myosin molecules in thick filaments of skeletal muscle cells, or as few as 28 myosins in nonmuscle cells and the N-terminal catalytic head domain, which contains a nucleotide-binding region and attaches to the actin filament. Phosphorylation of the MLC in the neck region releases the myosin molecular and stimulates actin dissociation. (©2002 From Molecular Biology of the Cell, 4E by Alberts et al. Reproduced by permission of Garland Science/Taylor and Francis LLC.)

CHAPTER 2: GENERAL MATERIALS AND METHODS

2.1 CELL CULTURE

2.1.1 Materials

Dulbecco's Modified Eagle Medium (DMEM) was purchased from Sigma Aldrich (St. Louis, MO). Fetal bovine serum (FBS) was purchased from Atlanta Biologicals (Lawrenceville, GA). HEPES (4-(2-hydroxyethyl)-1-piperazineethanesulfonic acid) was purchased from EMD Chemicals Inc (Gibbstown, NJ). PSF (100 units penicillin/ml, 0.1 mg/ml streptomycin and 0.25 g/ml amphotericin B), L-Glutamine-200 mM, PSG (100 units penicillin/ml, 0.1 mg/ml streptomycin and 29.2 mg/ml L-Glutamine), sodium bicarbonate ($NaHCO_3$) and phosphate buffered saline (PBS) were all purchased from Meditech (Hendon, VA). Rat-1 fibroblasts were purchased from American Type Culture Collection (ATCC; Manassas, Virginia). The human hepatic stellate cell (HSC) line, LX-2, was provided by the laboratory of Dr. Scott Friedman (Mt. Sinai Medical Center; New York, NY). Trypan blue solution and trypsin-ethylenediaminetetraacetic acid (trypsin-EDTA; 0.25% (v/v)) were purchased from Invitrogen (Gibco; Carlsbad, CA). A bright line counting chamber/hemocytometer was purchased from Hausser Scientific (Horsham, PA). Polystyrene bottles with 0.22 μM and molecular grade dimethyl sulphoxide (DMSO) were purchased from Fisher Scientific (Pittsburg, PA).

Sterile tissue culture dishes and serological pipettes were purchased from Griener Bio-One Inc (Monroe, NC). Chamber slides were purchased from Lab-Tek (Rochester, NY). 5810R Centrifuge was purchased from Eppendorf (Olympus USA).

2.1.2 Media Preparation

All media was prepared under sterile conditions in a LABCONCO Purifier Class II Biosafety Cabinet. DMEM powder (13.4 g/l) was reconstituted in deionized water with 3.7 g/l $NaHCO_3$, 5.95 g HEPES, pH 7.35 and sterilized using polystyrene bottles with 0.22 μM filters. Primary HSCs and LX-2 cells were cultured on plastic tissue culture dishes (p60/p100) or chamber slides with DMEM supplemented with 10% FBS, 1X PSF and 2 mM glutamine. Rat-1 fibroblasts were cultured on plastic tissue culture dishes (p100) with DMEM supplemented with 10% FBS and 1X PSG. Growth media was exchanged every other day unless otherwise noted. Serum-free media lacked FBS supplementation. All cells were cultured in a 5% CO_2-95% air atmosphere at 37 ºC.

2.1.3 Cell Propagation

Cell lines were stored in cryovials submerged in liquid nitrogen. Vials were thawed in a 37ºC water bath and resuspended in culture media (10 ml). Cells were centrifuged at 500 *g* for 3 minutes. Media was aspirated and the pellet was resuspended in 10 ml media. Cells were placed on a tissue culture dish and grown to 90% confluency in a 5% CO_2-95% air atmosphere at 37ºC.

2.1.4 Cell Passaging and Splitting

Primary HSCs, Rat-1 fibroblasts and human LX-2 cells were passaged until confluent (HSCs; p100 (7 days), p60 (4 days)). The cells were washed 3X in PBS and

detached using 0.25% (v/v) trypsin-EDTA diluted in PBS for 7 minutes at 37ºC. The addition of culture media inhibited further trypsin digestion after cells were detached from tissue culture dishes. Cells were pelleted at 500 *g* for 5 minutes and resuspended in culture media. A split ratio of 1:4 was used for passaging HSCs in tissue culture dishes (p100); 1:2 was used for p60 tissue culture dishes. A split ratio of 1:10 was used for passaging Rat-1 fibroblasts on tissue culture dishes (p100). A split ratio of 1:2 was used for passaging human LX-2 cells on tissue culture dishes (p100).

2.1.5 Cell Storage

Cell lines cells were washed 3X in PBS, trypsinized for 5 minutes and pelleted at 500 *g* for 5 minutes and resuspended in cell freezing media (70% DMEM, 10% DMSO and 20% FBS). Suspensions were aliquoted at a concentration of 1 x 10^6 cells/ml into cryovials. The vials were stored at -80ºC overnight and submerged into liquid nitrogen for long term storage.

2.2 PRIMARY CELL ISOLATION

2.2.1 Materials

Primary Isolation General Materials: Male Sprague-Dawley rats (190-200g; hepatocyte isolation and >650g; hepatic stellate cell (HSC) isolation) were purchased from Charles River Laboratory Inc (Wilmington, MA) and housed in the University Vivarium. 5810R Centrifuge was purchased from Eppendorf (Olympus USA). Polystyrene bottles with 0.22 µM filters and Nalgene 50ml conical tube filter units were purchased from Fisher Scientific (Pittsburg, PA). Tissue culture dishes (p60 and p100) and conical tubes (15 and 50 ml) were purchased from BD Biosciences (San Diego, CA).

PSF (100 units penicillin/ml, 0.1 mg/ml streptomycin and 0.25 μg/ml amphotericin B) was purchased from Meditech (Hendon, VA). Deoxyribonuclease I (DNase) and Type I collagenase were purchased from Sigma Aldrich (St. Louis, MO). DNase (10 mg/ml) was reconstituted in deionized water and sterilized using syringe filters (0.45 μM) purchased from Corning Inc (Corning, NY).

Primary HSC Isolation Protocols: Multiple strategies were employed to isolate a pure (95%) population of primary HSCs. The protocol was altered three times to optimize cell number and to eliminate fungal/bacterial contamination. Pronase was purchased from Roche Applied Sciences (Chicago, IL).

Protocol A: Spinner Modification Minimum Essential Medium (SMEM) was purchased from Sigma Aldrich (St. Louis, MO). Gey's Balanced Salt Solution (GBSS) was freshly prepared with salts/glucose purchased from Fisher Scientific (Pittsburg, PA; TABLE 2.1A), pH 7.35 and sterile filtered.

GBSS	g/l
NaCl	8
KCl	0.4
KH_2PO_4	0.05
NaH_2PO_4	0.15
$MgCl_2$-$6H_2O$	0.21
$MgSO_4$-7 H_2O	0.07
$CaCl_2$	0.23
Glucose	2

TABLE 2.0A: GBSS Buffer Protocol A. GBSS buffer was freshly prepared each week for HSC isolation. Salts were reconstituted in 4 liters of deionized water, pH 7.35 and sterile filtered.

Pronase and collagenase were reconstituted in pre-warmed GBSS (46ºC). Density gradients were prepared from Larcoll (Sigma Aldrich) reconstituted in freshly prepared BSG-BSA solution (1.22 mg/ml Na_2HPO_4, 0.169 mg/ml NaH_2PO_4, 7.2 mg/ml NaCl, 0.373 mg/ml KCl, 0.116 mg/ml $MgCl_2$, 2 mg/ml glucose, and 30 mg/ml Bovine Serum Albumin (BSA)), pH 7.35 and sterile filtered. Portable refractometer was purchased from Fisher Scientific. Optima L-90K UltraCentrifuge and Ultra-clear centrifuge tubes (9/16 x 3 ¼ in) were purchased from Beckman Coulter Inc (Fullerton, CA).

Protocol B: SC-1, SC-2, GBSS/A and GBSS/B solutions were freshly prepared with salts purchased from Fisher Scientific (TABLE 2.1B), pH 7.35 and sterile filtered. Ethylene glycol-bis(2-aminoethylether)-*N,N,N′,N′*-tetraacetic acid (EGTA) was purchased from Sigma Aldrich.

g/l	SC-1	SC-2	GBSS/A	GBSS/B
NaCl	80	80	(-)	80
KCl	4	4	3.7	3.7
NaH_2PO_4	0.88	0.88	(-)	(-)
Na_2HPO_4	1.2	1.2	0.59	0.59
HEPES	23.8	23.8	(-)	(-)
$NaHCO_3$	3.5	3.5	(-)	(-)
EGTA	1.9	(-)	(-)	(-)
Glucose	9	(-)	9.91	9.91
$CaCl_2$	(-)	5.6	2.25	2.25
$MgCl_2$-$6H_2O$	(-)	(-)	2.1	2.1
$MgSO_4$-7 H_2O	(-)	(-)	0.7	0.7
K_2HPO_4	(-)	(-)	0.3	0.3

TABLE 2.1B: Isolation Buffers Protocol B. Isolation buffers were freshly prepared each week for HSC isolation. Salts were reconstituted in 4 liters of deionized water, pH 7.35 and sterile filtered.

Pronase and collagenase were reconstituted in pre-warmed SC-2 (37ºC). Density gradients were prepared from Histodenz (Sigma Aldrich) reconstituted in GBSS/A (290 mg/ml) and sterile filtered.

Protocol C: Buffer A solution and GBSS were freshly prepared with salts purchased from EMD Chemicals Inc (Gibbstown, NJ), EGTA purchased from Sigma Aldrich and glucose purchased from Fisher Scientific (TABLE 2.1C), pH 7.35 and sterile filtered.

g/l	Buffer A	GBSS
NaCl	6.7	7
KCl	0.37	0.37
NaH_2PO_4	(-)	0.15
HEPES	5.95	5.95
$NaHCO_3$	(-)	2.27
EGTA	0.2	(-)
Glucose	(-)	1
$CaCl_2$	(-)	0.22
$MgCl_2$-$6H_2O$	(-)	0.21
$MgSO_4$-7 H_2O	(-)	0.07
KH_2PO_4	0.136	0.03

TABLE 2.1C: Isolation buffers were freshly prepared each week for HSC isolation (Protocol C). Salts were reconstituted in 4 liters of deionized water, pH 7.35 and sterile filtered.

Pronase and collagenase were reconstituted in pre-warmed GBSS (42.5ºC). Density gradients were prepared from Optiprep (Axis-Shield; Oslo, Norway) reconstituted in GBSS and sterile filtered: 66.7 ml OptiPrep (60%) stock solution + 33.3 ml GBSS= 40% (v/v) OptiPrep working solution.

Primary Hepatocyte Isolation Protocol: Buffer A, Buffer B and Buffer C solutions were freshly prepared with salts purchased from EMD Chemicals Inc, BSA purchased from and EGTA purchased from Sigma Aldrich (TABLE 2.2), pH 7.35 and sterile filtered.

g/l	Buffer A	Buffer B	Buffer C
NaCl	6.7	6.7	6.7
KCl	0.37	0.37	0.37
KH_2PO_4	0.136	0.136	0.136
HEPES	5.95	5.95	5.95
EGTA	1.9	(-)	(-)
BSA	(-)	(-)	6
$CaCl_2$	(-)	0.0184	0.0368

TABLE 2.2: Isolation buffers were freshly prepared for hepatocyte isolations. Salts were reconstituted in 1 liter of deionized water, pH 7.35 and sterile filtered.

Collagenase was resuspended in pre-warmed Buffer B and Buffer C (42.5ºC).

2.2.2 Hepatic Stellate Cell Isolation

Primary Isolation General Methods: In all procedures retired breeder male Sprague-Dawley rats were used under appropriate anesthesia and aseptic conditions. Breathing pattern and conscious level were used to monitor animal's anesthesia. Prior to the procedure, all surgical instruments were sterilized by autoclaving. The skin was shaved and disinfected with Betadine and 75% (v/v) ethanol. A midline laparotomy on the rat abdomen was performed, and the hepatic portal vein and vena cava were dissected out. Heparin (500U) was injected into the vena cava to alleviate red blood cell clotting and permit perfusion of liver. The portal vein was cannulated with SURFLO I.V. catheter proximal to bifurcation, attached with 3-0 (USP) silk suture, and the descending aorta was

immediately cut to allow exsanguination. Cell purity was measured by morphology and autofluorescence.

Protocol A: Density gradients (ρ=1.045 and 1.035) were prepared using 20% (w/v) Larcoll in BSG-BSA solution and sterile filtered. Approximately, 1.045(ρ)=42.9 ml 20% Larcoll solution + 57.1 ml BSG-BSA; 1.035(ρ)=29.1 ml 20% Larcoll solution + 70.9 ml BSG-BSA. A portable refractometer was used to determine accurate density readings (1.045: refractometer reading=8.1; 1.035: refractometer reading=5.5) Perfusion, pronase, collagenase, agitation and washing buffers were also prepared prior to surgery (TABLE 2.3A).

	Perfusion	Pronase	Collagenase	Agitation	Washing
SMEM	200 ml	(-)	(-)	(-)	(-)
GBSS	(-)	100 ml	200 ml	100 ml	200 ml
Pronase	(-)	0.4 %b.w.	(-)	(-)	(-)
Collagenase	(-)	(-)	25-30 mg	(-)	(-)
DNase	(-)	(-)	(-)	100 µl	200 µl
PSF	2 ml	1 ml	2 ml	1 ml	2 ml

TABLE 2.3A: Isolation buffers were freshly prepared for each HSC isolation with SMEM and GBSS (TABLE 2.1A). Collagenase buffer was sterile filtered.

Retired breeder male Sprague-Dawley rats (>650 g) were injected with sodium pentobarbital (50 mg/kg) subcutaneously and pre-warmed buffers pumped through the liver at a rate of 15 ml/min. The liver was initially perfused with perfusion buffer for 10 minutes and then switched to pronase buffer. After collagenase digestion, the liver was excised, placed in tissue culture dish, minced and washed in a 500 ml beaker with agitation buffer. The solution was agitated at 120 RPM for 10 minutes in 37 ºC water bath. In the

tissue culture hood, two conical tubes (50 ml) were overlaid with sterile gauze filters. The liver homogenate was filtered into the tubes and centrifuged for 2 minutes at 50 *g* at 25ºC. The pellet was washed 2X. The pellet was resuspended and centrifuged for 7 minutes at 700 *g* at 25ºC. The density gradients were prepared in UltraClear tubes (1.035/1.045; 2.5 ml each). The pellet was resuspended in washing buffer and layered on top of density gradient (7 ml/tube). The tubes were placed in the Optima L-90K UltraCentrifuge and centrifuged for 35 minutes at 22,000 RPM at 20ºC with break set to 800 RPM. A distinct HSC layer and HSC/Kupffer cell (KC) layer were transferred to two conical centrifuge tubes (50 ml) and washed (FIGURE 2.1). The suspension was centrifuged for 7 minutes at 700 *g* at 25ºC. The pellet was resuspended in 1 ml HSC media and 20 µl of the cell suspension was diluted (10X) and counted with a hemocytometer. Cell viability was measured by the total number of trypan blue stained (dead) vs. live cells: (Total number) x (viability) = Total number of live cells/ml. For quiescent HSCs, only the pure layer was used for experiments. For culture-activated HSCs, the pure layer was combined with HSC/KC layer ($3x10^6$ cells/p100) to optimize cells number. The culture media does not support KC viability. On average, 10-12 $x10^6$ cells were obtained using this protocol.

Protocol B: Due to ultracentrifuge scheduling conflicts and economic benefits, our lab developed a new protocol for HSC isolation that did not require the use of the Optima L-90K UltraCentrifuge. To increase cell numbers per isolation we also optimized the buffers used and perfusion apparatus. Changes to Protocol A included decreasing pronase and increasing collagenase concentration, changing anesthetic method, buffer solutions and density gradients. Density gradient was prepared using Histodenz solution and sterilized

using 0.22 µM filter. Perfusion, pronase, collagenase, agitation and washing buffers were also prepared prior to surgery (TABLE 2.3B).

	Perfusion	Pronase	Collagenase	Agitation	Washing
SC-1	200 ml	(-)	(-)	(-)	(-)
SC-2	(-)	120 ml	250 ml	120 ml	(-)
GBSS/B	(-)	(-)	(-)	(-)	200 ml
Pronase	(-)	80 mg	(-)	(-)	(-)
Collagenase	(-)	(-)	80 mg	(-)	(-)
DNase	(-)	(-)	(-)	100 µl	200 µl
PSF	2 ml	1 ml	2 ml	1 ml	2 ml

TABLE 2.3B: Isolation buffers were freshly prepared for each HSC isolation with Buffer A and GBSS (TABLE 2.1B). Collagenase buffer was sterile filtered.

Retired breeder male Sprague-Dawley rats (>650 g) were anesthetized using isoflurane inhalation (2-5%) and liver perfused as previously described. In the tissue culture hood, four conical tubes (50 ml) were capped with nylon mesh sheets (120 µM). The liver homogenate was filtered into the tubes and centrifuged for 8 minutes at 500 *g* at 4ºC. The pellet was washed (washing buffer) and re-centrifuged. The pellet was resuspended in washing buffer (34 ml/ tube) and combined with Histodenz solution (14 ml/ tube). The liver homogenate/density gradient mixture (12 ml/tube) was transferred to 15 ml conical tubes and washing buffer (1 ml) was layered onto the solution. The tubes were placed in the Eppendorf 5810R Centrifuge and spun for 17 minutes at 2500 RPM at 4ºC with no break. A distinct HSC layer was visible and transferred to a conical centrifuge tube (50 ml) and washed (FIGURE 2.2). The suspension was centrifuged for 7 minutes at 700 *g* at 4ºC. Cells were counted and viability measured as previously described. On average, 15-20 $x10^6$ cells were obtained using this protocol.

Protocol C: After five months of contamination and low cellular yield, our lab changed the protocol used for HSC isolation. Changes to Protocol A included altering the buffer and density gradient solutions. Density gradients were prepared using 40% (w/v) Optiprep solution and sterile filtered. Perfusion, pronase, collagenase, agitation and washing buffers were also prepared prior to surgery (TABLE 2.3C).

	Perfusion	Pronase	Collagenase	Agitation	Washing
Buffer A	250 ml	(-)	(-)	(-)	(-)
GBSS	(-)	100 ml	200 ml	125 ml	200 ml
Pronase	(-)	80 mg	(-)	(-)	(-)
Collagenase	(-)	(-)	25-30 mg	(-)	(-)
DNase	(-)	(-)	(-)	125 µl	200 µl
PSF	2.5 ml	1 ml	2 ml	1 ml	2 ml

TABLE 2.3C: Isolation buffers were freshly prepared for each HSC isolation with Buffer A and GBSS (TABLE 2.1C). Collagenase buffer was sterile filtered.

Retired breeder male Sprague-Dawley rats (>650 g) were anesthetized using isoflurane inhalation (2-5%) and liver perfused as previously described. In the tissue culture hood, four conical tubes (50 ml) were capped with sterile gauze. The liver homogenate was filtered into the tubes and centrifuged for 7 minutes at 700 *g* at 4ºC. The pellet was washed and re-centrifuged for 7 minutes at 700 *g* at 4ºC. The pellet was resuspended in washing buffer (37.8 ml/tube) and combined with 40% Optiprep solution (10.2 ml/tube). The liver homogenate/density gradient mixture (12 ml/tube) was transferred to 15 ml conical tubes and washing buffer (2 ml) was layered onto the solution. The tubes were centrifuged for 17 minutes at 1400 *g* at 4ºC with no break. A distinct HSC layer was visible (similar to Protocol B), transferred to a conical tube (50 ml) and washed. The

suspension was centrifuged for 7 minutes at 700 *g* at 4ºC. Cells were counted and viability measured as previously described. On average, 20-30 x10^6 cells were obtained using this protocol.

2.2.3 Hepatocyte Isolation

The HSC isolation method (Protocol C) was used to isolated hepatocytes with minor revisions. In all procedures retired breeder male Sprague-Dawley rats (190-200 g) were used and surgeries performed as described for HSC isolation. Changes to Protocol C included omitting of the pronase solution and changing the perfusion and collagenase buffer. Perfusion, collagenase and agitation/washing buffer were all prepared prior to surgery (TABLE 2.4).

	Perfusion	Collagenase	Agitation/ Washing
Buffer A	250 ml	(-)	(-)
Buffer B	(-)	200 ml	(-)
Buffer C	(-)	(-)	500 ml
Collagenase	(-)	30 mg	(-)
DNase	(-)	(-)	500 µl
PSF	2.5 ml	2 ml	5 ml

TABLE 2.4: Isolation buffers were freshly prepared for each hepatocyte isolation with Buffer A/B/C (TABLE 2.2). Collagenase buffer was sterile filtered.

In the tissue culture hood, four conical tubes (50 ml) were capped with sterile mesh filter (150 µm pore diameter). The liver homogenate was filtered into the tubes and centrifuged for 3 minutes at 50 *g* at 25ºC. The pellet was washed and re-centrifuged for 3 minutes at 50 *g* at 25ºC. Cells were counted and viability measured as previously described.

2.3 ANIMAL MODEL OF LIVER FIBROSIS

2.3.1 Materials

Male Sprague-Dawley rats (350-450 g) were purchased from Charles River Laboratory Inc (Wilmington, MA) and housed in the University Vivarium. Black 3-0 (USP) silk and nylon sutures were purchased from LOOK Surgical Specialties Corporation (Reading, PA). TissuePrep paraffin based embedding media, xylene, HistoPrep tissue capsules and Superfrost plus microscope slides were purchased from Fisher Scientific (Pittsburgh, PA). 10% (w/v) formalin solution was purchased from Sigma Aldrich (St Louis, MO). Phosphate buffered saline (PBS) was purchased from Meditech (Hendon, VA). Hematoxylin and eosin were purchased from EMD Chemicals Inc (Gibbstown, NJ). HM 315 rotary microtome was purchased from Richard-Allan Scientific (Kalamazoo, MI). ATP1 automatic tissue processor was purchased from Triangle Biomedical Sciences Inc. (Durham, NC). Hematoxylin and eosin staining was visualized with an Olympus IX71 microscope and Fluoview FV500 version 4.3 image processing software (Olympus USA).

2.3.2 Bile Duct Ligation Surgery

Animal model of bile duct ligation (BDL) induced-fibrosis: 30 minutes prior to procedure, animals were injected with buprenophrine (0.05 mg/kg) subcutaneously. Prior to the procedure, all the surgical instruments were sterilized by autoclaving. Under isoflurane anesthesia (2-5% by inhalation), the skin was shaved and disinfected with Betadine and 75% ethanol. Breathing pattern and conscious level were used to monitor animal's depth of anesthesia. A midline laparotomy on the rat abdomen was performed and the hepatic bile duct identified, double-ligated with silk suture and transected. The abdomen was closed by continuous pattern using absorbable sutures approved by the

attending veterinarian. The skin was closed using non-absorbable sutures in an interrupted pattern. Sham operations were performed in the same manner except without BDL. The animals were injected with buprenophrine every 8-12 hours for the first 48 hours or until animal was alert, active and eating a minimum of two pellets of chow per day. Animals were followed for 14 days and sacrificed by exsanguination under anesthesia for tissue sample processing.

2.3.3 Tissue Preparation

Liver tissue samples were harvested and fixed in formalin solution overnight at room temperature. Formalin solution was replaced with 50% (v/v) ethanol for 1 hour followed by final storage in 50 ml conical tube of 70% (v/v) ethanol. Cells were dehydrated in ascending ethanol gradient (50%, 70%, 80%, 95% and 100%) for 10 minutes each and blocked in paraffin in an automatic tissue processor. 5 μM sections were cut using HM 315 rotary microtome and adhered onto positively charged glass slides. Sections were dried at 37ºC on a slide warmer and stored at room temperature.

2.3.4 Hematoxylin and Eosin Staining

Slides were incubated at 65^{o}C for 1 hour, submerged in xylene for 5 minutes and rehydrated using descending ethanol gradient (100%, 90%, 80%, 70%, and 60%) for 10 minutes each with a final wash in PBS for 5 minutes. Slides were incubated in hematoxylin solution for 5 minutes and rinsed in tap water before staining with eosin solution for 10 seconds. After eosin staining, slides were dehydrated into descending grades of ethanol (100%, 95%, 80%, 70% and 50%) followed by xylene incubation for 10 seconds. Slides were mounted and coverslipped using Permount mounting media.

Images were captured with IX71 microscope and Fluoview FV500 version 4.3 image processing software.

2.4 CONTRACTION ASSAY

2.4.1 Materials

Rat tail type I collagen, prepared in 0.02N Acetic Acid (3.65-4.5 mg/ml), was purchased from BD Biosciences (Bedford, MA). Dulbecco's Modified Eagle Medium (DMEM) purchased from Sigma Aldrich (St. Louis, MO), HEPES (4-(2-hydroxyethyl)-1-piperazineethanesulfonic acid) purchased from EMD Chemicals Inc (Gibbstown, NJ) and sodium bicarbonate purchased from Fisher Scientific (Pittsburgh, PA) were reconstituted into a 10X solution. Acetic acid and molecular grade dimethyl sulphoxide (DMSO) were purchased from Fisher Scientific. Sterile 24-well tissue culture plates were purchased from Griener Bio-One Inc (Monroe, NC). Bovine serum albumin (BSA) purchased from Roche Applied Sciences (Chicago, IL) was reconstituted in phosphate buffered saline (PBS) purchased from Meditech (Hendon, VA). Endothelin-1 (ET-1) was purchased from American Peptide (Sunnyvale, CA) and reconstituted in sterile deionized water. Blebbistatin was purchased from Calbiochem (San Diego, CA) and reconstituted in DMSO. BioSpectrum AC Imagining System and ImageMaster program purchased from UVP Inc (Upland, CA) was used to measure changes in collagen lattice diameter over time.

2.4.2 Collagen Lattice Preparation

Collagen lattices were prepared as previously described with minor modifications [14, 32]. 24-well tissue culture plates were incubated with 0.1% (w/v) BSA and washed

3X for 5 minutes with PBS. A combination of 8 parts type I collagen, 1 part 0.2 M HEPES and 1 part 10X DMEM (optimal collagen concentration experimentally determined to be 3.65 mg/ml) was mixed at room temperature. The mixture (optimal volume experimentally determined to be 300 µl) was aliquoted onto each well of a 24-well plate and allowed to congeal for 1 hour at 37°C.

2.4.3 Hepatic Stellate Cell Seeding

Primary HSCs (5 x 10^6 cells/p60) were cultured to confluency (3 days) and incubated in serum-free DMEM overnight. Day 4 culture-activated HSCs were trypsinized and seeded onto the congealed collagen lattice (optimal cell number experimentally determined to be 300,000 cells/well diluted in 300 µl serum-free DMEM) and allowed to recover overnight in a 5% CO_2-95% air atmosphere at 37°C.

2.4.4 LX-2 Cell Seeding

LX-2 cells were grown to confluency and incubated in serum-free DMEM overnight. LX-2 cells were trypsinized and seeded onto the congealed collagen lattice (300,000 cells/well) and allowed to recover overnight in a 5% CO_2-95% air atmosphere at 37°C.

2.4.5 Chemical Treatment

ET-1 Treatment: Serial dilutions of ET-1 (0.1 pM-100 nM; logarithmic increments) were prepared and incubated with HSC-seeded collagen lattices. Serum-free DMEM served as negative control. Collagen discs were dislodged from wells with a 10 µl pipette tip. LX-2 cells were treated with an experimentally determined ET-1 concentration (1 nM). Images were captured with UVP BioSpectrum AC Imagining System at indicated

time points and the PTI ImageMaster program was used to measure changes in collagen diameter after 24 hours.

Blebbistatin Treatment: Wells were pre-treated with increasing doses of the blebbistatin active enantiomer or inactive enantiomer (5-25 μM; 5 μM increments) for 30 minutes. Collagen discs were dislodged from wells with a 10 μl pipette tip and empirically determined ET-1 concentration (1 nM) was incubated with pre-treated cells to induce contraction. Serum-free DMEM served as positive control for ET-1 induced contraction. Images were captured with UVP BioSpectrum AC Imagining System at indicated time points and the PTI ImageMaster program was used to measure changes in collagen diameter over time.

2.5 PREPARATION OF RNA and cDNA

2.5.1 Materials

Diethyl pyrocarbonate (DEPC)-treated water and agarose were purchased from EMD Chemicals Inc (Gibbstown, NJ). TRIzol reagent, SuperScript III Reverse Transcription System, random primers (3 μg/μl) and deoxynucleotide triphosphates (dNTPSs; reconstituted in DEPC-treated water; 20 nM) were purchased from Invitrogen (Carlsbad, CA). Chloroform, isopropanol and ethidium bromide were purchased from Fisher Scientific Inc (Pittsburg, PA). Maxwell 16 Total RNA Purification Kit, RQ1 RNase-Free DNase Kit, Impromptu II Reverse Transcription System, 100 bp DNA ladder and blue/orange 6X loading dye were purchased from Promega Corporation (Madison, WI). Chloroform and isopropanol were purchased from Fisher Scientific. Sodium acetate solution (3 M) and Tris-acetate (TAE) buffer were purchased from Meditech (Hendon, VA). Microcentrifuge tubes were purchased from Griener Bio-One

Inc (Monroe, NC). 5415R Centrifuge was purchased from Eppendorf (Olympus USA). Gene Spectrophotometer (MiraiBio; San Francisco, CA) and NanoDrop (Fisher Scientific Inc) were used to quantitate RNA and cDNA concentrations.

2.5.2 RNA Isolation

Total RNA from tissue (30 mg), Rat-1 fibroblasts, quiescent and culture-activated hepatic stellate cells (HSCs) were isolated using the TRIZOL method according to the manufacturer's directions. Cells (2-5 x 10^6) were lysed in 1 ml of reagent and transferred to 1.5 ml micro-centrifuge tubes. Samples were incubated with 200 µl chloroform, vortexed and incubated at room temperature for 10 minutes to allow complete dissociation of nucleoprotein complexes. Samples were centrifuged at max speed (12,000 *g*) at 4^{o}C for 10 minutes. Following centrifugation, the mixture separated into a lower red, phenol/chloroform phase, a buffy white interphase and a clear upper aqueous phase. The aqueous phase was either transferred to a new 1.5 ml micro-centrifuge tube or Well #1 of the Maxwell 16 Total RNA Purification Kit. Samples transferred to new 1.5 ml micro-centrifuge tubes were incubated with 500 µl isopropanol to precipitate the RNA. Samples were centrifuged at max speed at 4^{o}C for 10 minutes. The pellet was washed with 75% (v/v) ethanol and centrifuged at max speed. Final RNA was dissolved in 12-20 µl DEPC-treated water, quantified with the Gene Spectrophotometer or the NanoDrop and stored at -80°C. Alternatively, samples transferred to Well # 1 of the Maxwell 16 Total RNA Purification Kit were run on the LEV (low elution volume) program (Version 3.31) and dissolved in 50 µl DEPC-treated water. RNA samples were diluted with 6X loading dye and run with 100 bp ladder on a 2% (w/v) agarose gel (dissolved in TAE buffer) stained with ethidium bromide to determine RNA integrity and purity.

2.5.3 cDNA Preparation

RNA samples were DNase treated and reverse transcribed with Impromptu II or Superscript III according to the manufacture's directions. Approximately 5-10 μg RNA was incubated with 1 μl of 10X RQ1 DNase buffer (400 mM Tris-HCl [pH 8.0 at 25°C], 100 mM $MgSO_4$, 10 mM $CaCl_2$) and 1 μl of RQ1 DNase at 37°C. Stop Buffer (20 mM EGTA [pH 8.0 at 25°C]) was added after 30 minutes. Samples were incubated at 75°C for 5 minutes, cooled to room temperature and combined with master mix from each protocol (TABLE 2.5).

Impromptu II Protocol	SuperScript III Protocol
4 μl 5X Buffer	4 μl 5X Buffer
2.5 μl $MgCl_2$	1 μl 0.1 M DTT
1 μl dNTPs	1 μl dNTPs
1μl Random Primers	1μl Random Primers
1 μl Reverse Transcriptase	1 μl Reverse Transcriptase

TABLE 2.5: Master mix for cDNA transcription using Impromptu II or SuperScript II protocol.

Samples were incubated at 37°C for 90 minutes and the reverse transcriptase heat inactivated at 80°C for 5 minutes. To precipitate the cDNA, samples were incubated with 2 μl sodium acetate and 300 μl 100% (w/v) ethanol. The mixture was incubated at -80°C overnight and centrifuged at max speed. Final cDNA pellet was dissolved in 50 μl DEPC-treated water, quantified with the Gene Spectrophotometer or the NanoDrop and stored at -80°C.

2.6 REVERSE TRANSCRIPTION-PCR AND REAL TIME PCR

2.6.1 Materials

Diethyl pyrocarbonate (DEPC)-treated water and agarose were purchased from EMD Chemicals Inc (Gibbstown, NJ). GoTaq Green Master Mix was purchased from Promega Corporation (Madison, WI). SYBR green 2X reaction mixture and capillary tubes were purchased from Roche Applied Sciences (Chicago, IL). TAE buffer was purchased from Meditech. Techne TC-512 (Techne Inc; Burlington, NJ) and Roche LightCycler 2.0 Instrument (Roche Applied Sciences) were used to amplify cDNA templates. Using the published GenBank sequence for Glyceraldehyde 3-phosphate dehydrogenase (Gapdh; NM_017008), smooth muscle α-actin (Acta2; NM_031004), glial acidic fibrillary protein (Gfap; NM_017009.2), nonmuscle myosin II-A (MYH9; NM_022410), II-B (MYH10; NM_031520) and II-C (MYH14; NM_028021), primers were generated with the OLIGO 6 program (TABLE 2.6) and purchased from Integrated DNA Technologies (Coralville, IA).

Gene	Forward (5'→3')	Reverse (3'→5')	Size (bp)
Glyceraldehyde 3 Phosphate Dehydrogenase (Gapdh)	ATCCCGCTAACATACCCTGG	ACTGTGGTCATGAGCCCTTC	292
Smooth Muscle α-Actin (Acta)	CATCAGGAACCTCGAGAAGC	TCGGATACTTCAGGGTCAGG	247
Glial Acidic Fibrillary Protein (Gfap)	AGAAAACCGCATCACCATTC	TTGGGCCTAGCAAACAAGAC	264
Nonmuscle Myosin II A (Myh9)	CCCTGCTAGATGAGGAGTGC	TGTTCTTCATCAGCCACTCG	189
Nonmuscle Myosin II B (Myh10)	GGCACTGGAGGAACTCTCTG	CTTCTTCCAGCAGGGTTGAG	287
Nonmuscle Myosin II C (Myh14)	GCTGCTCAAGGACCATTACC	GTACCAGCTTGCCAGAGAGG	275

TABLE 2.6: Primers were generated using OLIGO 6 program and used in RT-PCR and RealTime PCR analyses.

2.6.2 Reverse Transcription-PCR

The RT-PCR amplification reaction combined 1 μg cDNA with 25 μl GoTaq Green Master Mix, 20 μl DEPC-treated water, and 0.5 μg of each primer. PCR was performed with the Techne TC-512, using standard protocol: 52 to 57°C annealing step, for 20-45 cycles. Amplified products were resolved by electrophoresis in 2% (w/v) agarose gels and visualized by UV illumination.

2.6.3 RealTime-PCR

RealTime PCR amplification reactions were performed using the Roche LightCycler 2.0 instrument. The reaction combined 1 μl of cDNA, 5 μl SYBR green 2X reaction mixture, 1 μl of each primer (5 μM), and 2 μl DEPC-treated water in a 20 μl capillary tubes. All samples underwent 40 cycles at the determined annealing temperature. A reference pair of PCR products was generated in order to quantitate the message in the samples. The sample products were electrophoresied on a 2% (w/v) agarose gel to ensure a distinct product.

Data was reported as cross-point, the point at, which the SYBR green fluorescence was detected above the background [202]. Minor modifications were made by subtracting the cross-point from the largest adjusted cross-point (ΔCP) in the gene set and normalized to total cDNA concentration.

2.7 PREPARATION OF PROTEIN LYSATES

2.7.1 Materials

Radioimmunoprecipitation assay (RIPA) buffer (1X lysis buffer, PMSF, protease inhibitor cocktail and sodium orthovanadate) was purchased from Santa Cruz Biotechnology Inc (Santa Cruz, CA). Tris-base was purchased from BioSpectra Inc

(Stroudsburg, PA). F-actin (105-120 μM) stock was freshly prepared by in Dr. Chris Yengo's laboratory (University of North Carolina at Charlotte). Bradford protein assay was purchased from Pierce Biotechnology (Rockford, IL). Bovine serum albumin (BSA) was purchased from Roche Applied Sciences (Chicago, IL). Sodium dodecyl sulfate (SDS), bromophenol blue, glycerol and 2-mercaptoethanol (BME) were purchased from Fisher Scientific (Pittsburg, PA). Laemmli buffer (2X; 4% (w/v) SDS, 20% (w/v) glycerol, 10% (w/v) 2-mercaptoethanol, 0.004% (w/v) bromphenol blue, 0.125 M Tris-HCl) was prepared in deionized water. Semi-microcuvettes were purchased from BioRad Laboratories (Hercules, CA). Sonfier 150 homogenizer was purchased from Branson Ultrasonic Corporation (Danbury, CT). Optima TLX120 Ultracentrifuge and DU640 scanning spectrophotometer were purchased from Beckman Coulter Inc (Fullerton, CA). 5415R Centrifuge was purchased from Eppendorf (Olympus USA).

2.7.2 Bradford Protein Assay

Protein concentrations were determined using the Bradford method. Protein standards (0-12 μg/ml) were prepared using BSA (1 mg/ml) diluted in RIPA buffer. Standards and lysates were assayed using DU640 scanning spectrophotometer. Working protein assay solution was prepared by diluting Bradford reagent in deionized water (1:5; 1 ml/sample) and solution added to semi-microcuvettes (both standards and lysates). Absorbance at 595 nM was measured with the spectrophotometer. Absorbance for each standard was corrected for mean zero standard absorbance and plotted against protein concentration (mg/ml). The resulting standard curve was used to determine protein concentration of unknown samples.

2.7.3 Preparation of Cell Lysates for Protein Analysis

Quiescent and culture-activated hepatic stellate cells (HSCs) and Rat-1 fibroblasts were sonicated in RIPA buffer at 4°C. Subsequently, lysates were centrifuged at 16,000 *g* for 5 minutes at 4°C and the supernatant subjected to precipitation by F-actin selection. Protein concentrations were measured by the Bradford method (Section 2.7.2). For pull-down experiments, the quiescent samples were diluted to 1 μg/μl of protein in RIPA buffer, while the remaining samples were diluted to 0.5 μg/μl and incubated with 10 μM F-actin stock at 4°C for 30 minutes. The complex was centrifuged at 320,000 *g* in an Optima TLX120 Ultracentrifuge for 30 minutes at 4°C. The pellet was resuspended in 50 μl of 2X Laemmli buffer and stored at -80°C overnight.

2.7.4 Preparation of Tissue Lysates for Protein Analysis

Tissues were resected and immediately snap frozen in liquid nitrogen. To extract whole cell lysates, approximately 30 mg of tissue was placed in 1 ml RIPA buffer and homogenized in an ice bucket using the Sonifier 150 (level 5) 3-5 seconds and centrifuged at 16,000 *g* for 5 minutes at 4ºC. The resulting supernatant was collected, briefly resonicated and stored at -80ºC. Protein concentrations were measured by the Bradford method (Section 2.7.2).

2.8 WESTERN BLOTTING

2.8.1 Materials

Enhanced chemiluminescence (ECL) detection kit and CL-XPosure X-ray film were purchased from Pierce Biotechnology (Rockford, IL). Tris-base was purchased from BioSpectra Inc (Stroudsburg, PA). Acrylamide solution (Acrylamide: Bis, 29:1

acrylamide/N,N'-ethylenebisacrylamide) and TEMED (N,N,N',N'-Tetramethylethylenediamine) were purchased from EMD Chemicals Inc (Gibbstown, NJ). Ponceau S solution was purchased from Sigma Aldrich (St. Louis, MO). Sodium dodecyl sulfate (SDS), ammonium persulfate (APS; 10% (w/v) solution reconstituted in deionized water), Tween-20, sodium chloride (NaCl) and 2-mercaptoethanol (BME) were all purchased from Fisher Scientific (Pittsburg, PA). Glycine and Tris-HCl were purchased from VWR International (West Chester, PA). Mini-Protean 3 electrophoresis system, preformed combs, glass plates and Mini Trans-Blot were purchased from BioRad Laboratories (Hercules, CA). Protran nitrocellulose membranes and filter paper were purchased from Whatman (Dassel, Germany). Mix N' Drink, non-fat dry milk, was purchased from SACO Foods, Inc (Middleton, WI). See Blue Plus II pre-stained protein size marker was purchased from Invitrogen (Carlsbad, CA). X-ray film was developed using AFP Imaging Mini-Medical/90 Film Developer (Elmsford, NY) and densitometry performed using the Quantity One software (BioRad Laboratories). Electrophoresis running buffer (25 mM Tris-base, 0.2 M glycine and 3.5 mM SDS), transfer buffer (25 mM Tris-base, 0.2 M glycine, 20% (v/v) methanol) and Tris-buffered saline (TBS; 25 mM Tris-HCl, 144 mM NaCl, pH 8) were freshly prepared every two to three months. Tween TBS (TBST) was prepared using TBS with 0.2% v/v Tween-20. Blocking solution was prepared using non-fat dry milk (5% w/v) reconstituted in TBST. AC Imagining System was purchased from UVP BioSpectrum (Upland, CA).

2.8.2 Preparation of Western Blot Gels

SDS- polyacrylamide gel electrophoresis (PAGE) gels (8%; 0.75 mm) were freshly prepared using the Mini-Protean 3 electrophoresis system. The lower (separating) gel contained acrylamide solution, 4X Tris/SDS (1.5 M Tris-base, 14 mM SDS pH 8.8), APS solution and TEMED. The upper (stacking) gel contained acrylamide solution, 4X Tris/SDS (0.5 M Tris-base, 14 mM SDS, pH 6.8), APS solution and TEMED (TABLE 2.7).

Reagent	Stacking Gel	Separating Gel
Water	3.05 ml	4.10 ml
Acrylamide	0.65 ml	3.33 ml
4XTris/SDS pH 6.8	1.25 ml	(-)
4XTris/SDS pH 8.8	(-)	2.5 ml
APS	50 µl	100 µl
TEMED	4.5 µl	6.5 µl

TABLE 2.7: 8% SDS-PAGE gel was prepared by layering stacking gel on top of separating gel in glass plates separated by 0.75mm spacers.

Wells for protein loading were created in the upper gel using preformed combs. Gels were stored at 4ºC for up to one week.

2.8.3 Methods

Pull-down protein samples (10-20 µg) were boiled for 10 min and resolved on an 8% SDS-PAGE gel. To determine correct protein size, a prestained marker (10 µl) was used. Proteins were resolved on 8% SDS-PAGE gels using the Mini-Protean 3 electrophoresis system and running buffer. Proteins were transferred to nitrocellulose membrane in a Mini-Trans Blot Module using electrophoresis transfer buffer. Ponceau S solution was applied to membrane and image was captured with AC Imagining System in

order to assess equal protein loading and transfer. Membranes were incubated with blocking solution for 1 hour at room temperature with rocking. Membranes were washed 3X with TBST at room temperature for 5 minutes and incubated overnight at 4°C with primary antibody in blocking solution (1:1000). The membranes were washed 3X with TBST and incubated for 2 hours with appropriate secondary horseradish peroxidase-conjugated antibody diluted 1:2500 or 1:5000 in blocking solution at room temperature with mild agitation. Membranes were washed 3X with TBST. Bound enzymes were detected with ECL solution and exposed to X-ray film. Film was processed using an AFP Film Developer. Densitometric quantification of Western blot signal intensity was performed using a Quantity One densitometric analysis program and corrected for equal protein loading.

2.9 IMMUNOFLUORESCENCE

2.9.1 Materials

Citrosolv clearing agent, Permount mounting media, 22 x 60 microscope cover glass, Triton X, citric acid, sodium citrate and sodium borohydrate were purchased from Fisher Scientific (Pittsburgh, PA). Phosphate buffered saline (PBS) was purchased from Meditech (Hendon, VA). Paraformaldehyde and 10% (w/v) formalin solution were purchased from Sigma Aldrich (St Louis, MO). 4% (w/v) paraformaldehyde solution was prepared by reconstituting paraformaldehyde into PBS. Prolong gold anti-fade mounting solution, rhodamine-phalloidin, AlexaFluro secondary antibodies and 4',6-diamidino-2-phenylindole (DAPI) were purchased from Invitrogen (Molecular Probes; Carlsbad, CA). Donkey and goat serum were purchased from Zymed Laboratories (San Francisco, CA).

Bovine serum albumin (BSA) was purchased from Roche Applied Sciences (Chicago, IL). ICC blocking solution (0.2% (v/v) serum and 0.1% (w/v) BSA) and IHC blocking solution (5% (v/v) normal goat or donkey serum, 0.3% (w/v)BSA and 0.1% (w/v) Triton X) were prepared in PBS. Antibodies to NMM II-A, II-B were purchased from Covance (Princeton, New Jersey) and NMM II-C was provided by Dr. Robert Adelstein (NIH/NHLBI). All NMM II antibodies were rabbit-anti-rat. Anti-human smooth muscle α-actin (αSMA) antibody was purchased from Dako Corporation (Glostrup, Denmark). Anti-glial acidic fibrillary protein (GFAP) antibodies were purchased from Santa Cruz (Santa Cruz, CA) and Abgent (San Diego, CA). Immunofluorescence was visualized with an Olympus IX71 fluorescence microscope and Fluoview FV500 version 4.3 image processing software (Olympus USA).

2.9.2 Cell Preparation

Hepatic stellate cells (HSCs) and Rat-1 fibroblasts were cultured on chamber slides for indicated number of days. Prior to immunocytochemistry, cells were washed 3X with PBS (to remove non-adherent cells) and fixed in 4% (w/v) paraformaldehyde solution for 30 minutes at -20^{o}C. Cells were washed with PBS 3X (10 minutes each) and stored at -80^{o}C overnight.

2.9.3 Immunohistochemistry

Tissues were prepared as previously described (Section 2.3.3). Slides were incubated at 65^{o}C for 1 hour, de-paraffinized with Citrosolv and rehydrated using descending ethanol gradient (100%, 90%, 80%, 70%, and 60%) for 10 minutes each with a final wash in deionized water. Cross-linked proteins were exposed using heat-induced

epitope retrieval and proteolytic enzyme digestion. The slides were incubated with citrate buffer (10 mM: 0.1 M citric acid, 0.1 M sodium citrate) in food steamer for 30 minutes then cooled to room temperature for 20 minutes. The slides were washed in deionized water and incubated on ice with sodium borohydrate (10 mg/ml in PBS) 3X for 15 minutes. The slides were then washed and incubated with IHC blocking solution for 1 hour at room temperature. The slides were washed and incubated overnight at 4^{o}C using rabbit polyclonal NMM II-A, II-B or II-C. GFAP and αSMA primary antibodies were used to detect quiescent and activated HSCs, respectively. Duplicate slides were incubated with PBS only and served as negative controls. The slides were washed 3X and incubated at room temperature for 1 hour with the appropriate fluorescent secondary antibodies: AlexaFluro 488 anti-rabbit and AlexaFluro 594 anti-mouse. After three washes, the slides were incubated with DAPI for 5 minutes, washed again (3X; 5 minutes each), mounted with ProLong Gold anti-fade reagent, affixed with cover glass and stored at 4°C. Florescent staining was visualized using the Olympus IX71. Lung tissue served as positive controls for anti-NMM II isoform detection.

2.9.4 Immunocytochemistry

Slides were thawed, washed with PBS and incubated with ICC blocking solution for 1 hour at room temperature. Slides were incubated overnight at 4^{o}C using rabbit polyclonal NMM II-A, II-B and II-C. Duplicate slides were incubated with PBS only and served as negative controls. The secondary antibody was AlexaFluro 488 goat anti-rabbit. The slides were then incubated for 15 minutes with rhodamine-phalloidin for F-actin detection, washed and incubated with DAPI for 5 minutes (2.5 μg/ml). The slides were washed and mounted using ProLong Gold antifade reagent. Fluorescent staining was

visualized using the Olympus IX71. Rat-1 fibroblasts served as positive controls for anti-NMM II isoform detection.

2.10 MATRIX STIFFNESS ASSAY

2.10.1 Materials

Glass plates were purchased from BioRad Laboratories (Hercules, CA). Acrylamide, bis-acrylamide and ammonium persulfate (APS) purchased from Fisher Scientific (Pittsburg, PA) were reconstituted in deionized water. Molecular grade dimethyl sulphoxide (DMSO) was also purchased from Fisher Scientific. HEPES (4-(2-hydroxyethyl)-1-piperazineethanesulfonic acid) solution (1 M) and phosphate buffered saline (PBS) was purchased from Meditech (Hendon, VA). TEMED (N,N,N',N'-Tetramethylethylenediamine) was purchased from EMD Chemicals Inc (Gibbstown, NJ). N-Sulfosuccinimidyl-6-(4'-azido-2'-nitrophenylamino) hexanoate (sulfo-SANPAH) purchased from Pierce Biotechnology (Rockford, IL) was reconstituted in DMSO (100 μg/μl). Working sulfo-SANPAH solution (0.5mM) was prepared by diluting 30 μl stock, 600 μl HEPES (50mM) and 11.34 ml deionized water. Rat tail type I collagen prepared in 0.02N Acetic Acid (3.65-4.5 mg/ml) was purchased from BD Biosciences (Bedford, MA). Gel punch (½" diameter stainless steel) was purchased from McMaster-Carr (Robbinsville, NJ). Syringe filters (0.45. μM) were purchased from Corning Inc (Corning, NY).

2.10.2 Preparation of Polyacrylamide Substrates

Collagen-coated polyacrylamide gels were prepared as previously described with minor modifications [203]. Glass plates, 0.75mm spacers, forceps and gel punch were

washed, rinsed with deionized water and allowed to air dry on a rack in laminar flow hood for 20 minutes. Once dried, materials were sterilized by UV illumination for 30 minutes. Gels were prepared with 10% (w/v) acrylamide, 0.03 or 0.26% (w/v) bis-acrylamide, 1% (w/v) 1M HEPES, APS, TEMED and syringe filtered. The mixture was poured between glass plates separated by 0.75mm spacers. Solutions were polymerized for 30 minutes, and gel discs were manually punched from the polymerized material using gel punch and placed into 24-well tissue culture plates. Sulfo-SANPAH solution (0.5 mM) was added to each well and photoactivated for 10 minutes with UV illumination (2X). The gel surface was rinsed with 50 mM HEPES 3X to remove excess reagent. Acrylamide gels were coated with collagen (0.2 mg/ml solution) overnight at 4^{o}C. Gels were washed with 50 mM HEPES (1X) and PBS (3X).

2.10.3 Methods

Primary hepatic stellate cells (3 x 10^{6} cells/p60) were culture-activated to confluency for 4 days, trypsinized and seeded onto freshly prepared polyacrylamide gels of varying degrees of matrix stiffness (4.6 and 21.6 kPa, reported by Pelham et .al.). After 24 hours of altered matrix stiffness exposure, cells were lysed with TRizol, RNA extracted and converted to cDNA as described (Section 2.5). Alterations in mRNA expression of NMM II isoforms were detected using RealTime PCR as described (Section 2.6).

2.11 siRNA-MEDIATED INHIBTION

Multiple transfection strategies were used to down-regulate glyceraldehyde 3-phosphate dehydrogenase (GAPDH) and nonmuscle myosin II (NMM II) expression in

the LX-2 cell line and primary hepatic stellate cells (HSCs). Transfectam and Tfx-20/50 reagents were unsuccessful in the down-regulation of GAPDH. Lipofectamine Reagent successfully transfected GAPDH and NMM II siRNA into primary HSCs.

2.11.1 Materials

GAPDH, NMM II and scramble siRNA were purchased from Ambion/Applied Biosystems (Austin, TX) and reconstituted with nuclease free water (TABLE 2.8). Trypsin-ethylenediaminetetraacetic acid (trypsin-EDTA; 0.25% (w/v)) and OptiMEM I Reduced Serum were purchased from Invitrogen (Gibco; Carlsbad, CA). Sodium chloride (NaCl) purchased from Fisher Scientific (Pittsburg, PA) was freshly prepared (150 mM solution) using syringe filters (0.45 μM) purchased from Corning Inc (Corning, NY).

Gene	Sense	Anti-Sense	Duplex #
NMM II-A (Myh9)	GUGUGGUCAUUAAUCCUUAtt CACCUUACUCCAUUCCGAAtt	UAAGGAUUAAUGACCACACag UUCGGAAUGGAGUUAGGUGtg	s130643 s228824*
NMM II-B (Myh10)	GGGAUGAAGUGAUCAAGCAtt CAACUAUGCAUCAACUACAtt	UGCUUGAUCACUUCAUCCCgg UGUAGUUGAUGCAUAGUUGtt	s135203* s135204
NMM II-C (Myh14)	GCAUGCUUCAGGAUCGUGAtt GGAAGAUCGUGAACGGUAtt	UCACGAUCCUGAAGCAUGCtg UACCCGUUCACGAUCUUCCac	s158958 s158959

TABLE 2.8: Multiple siRNA duplexes were chemically synthesized and tested in transfection reactions. *Indicates successful down-regulation.

2.11.4 Methods

Freshly isolated HSCs were seeded at 2 x 10^6 cells on p60 tissue culture dishes, incubated with DMEM supplemented with 10% (v/v) FBS and subsequently transfected on day 3 of culture-activation with siRNAs for NMM II isoforms (II-A, II-B and II-C) and GAPDH using Lipofectamine reagent. Briefly, in a 5 ml polystyrene tube (solution A), increasing amounts of NMM II isoforms (final concentration 10-100 nM; 25 nM increments) and 100 nM GAPDH and scramble siRNA were incubated with 600 μl

OptiMEM and vortexed. In a separate 5 ml tube (solution B), 10-20 μl Lipofectamine reagent was incubated with 600 μl OptiMEM and vortexed. Solutions A and B were immediately combined, vortexed and incubated for 30 minutes at room temperature. Cells were washed 3X with OptiMEM and incubated with 1.5 ml OptiMEM. The siRNA mixtures (1 ml) were then added to tissue culture dishes for 8 hours. At the end of the transfection incubation period, 2.5 ml of fresh media was added to the wells and incubated for 48 hours prior to analysis of mRNA and protein expression, contraction, migration and proliferation.

2.12 FUNCTIONAL STUDIES

2.12.1 Materials

Endothelin-1 (ET-1), which was purchased from American Peptide (Sunnyvale, CA) was reconstituted in sterile deionized water. A bright line counting chamber hemocytometer was purchased from Hausser Scientific (Horsham, PA). 5415R Centrifuge was purchased from Eppendorf (Olympus USA). Trypan blue solution was purchased from Invitrogen (Carlsbad, CA). IX71 fluorescence microscope and Fluoview FV500 version 4.3 image processing software were purchased from Olympus (Olympus USA).

2.12.1 Methods

Freshly isolated HSCs were seeded at 2 x 10^6 cells on p60 tissue culture dishes, incubated with DMEM supplemented with 10% FBS and subsequently transfected with siRNA on day 3 of culture-activation (Section 2.12.4).

For contraction assay, collagen lattices were prepared as previously described (Section 2.4.2). Day 4 culture-activated/transfected HSCs were trypsinized and seeded

onto the congealed collagen lattice and allowed to recover overnight. Collagen discs were dislodged from wells with a 10 µl pipette tip. Transfected cells were treated with experimentally determined ET-1 concentration (1 nM; Section 2.4.5). Images were captured with UVP BioSpectrum AC Imagining System (Upland, CA) at indicated time points and the PTI ImageMaster program was used to measure changes in collagen diameter over time.

For migration assay, a sterile pipette tip was dragged through the cell sheet, creating a cleared zone 48 hours after transfection. Images were immediately taken of the scrape in four locations per dish using the Olympus IX71 microscope. 24 hours later, images were taken in the exact same locations. To assess the number of migrating cells, the PTI ImageMaster program was used to measure changes in the distance traveled into the 'damaged area' (cleared zone) after 24 hours.

For proliferation assay, cells were trypsinized 48 hours after transfection, centrifuged at 500 *g* for 5 minutes to pellet, resuspended in media and counted on a hemocytometer. Trypan blue exclusion analyses were performed to determine viability.

2.13 ASSURANCES

All animal procedures were performed under the guidelines set by the Institutional Animal Care and Use Committee (IACUC) at University of North Carolina at Charlotte and are in accordance with those set by the National Institutes of Health.

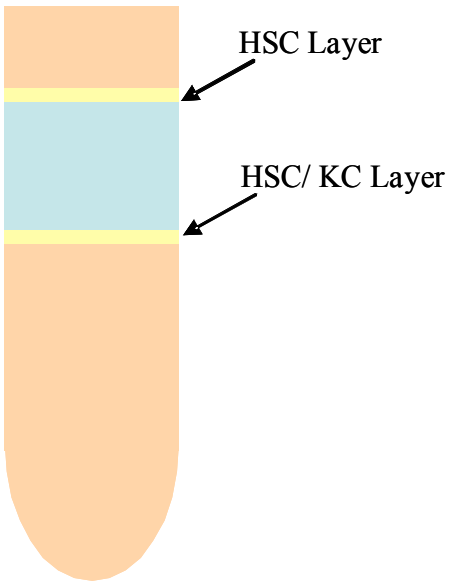

FIGURE 2.1: Schematic Drawing of Centrifuged HSC Layers (Protocol A). Freshly isolated rat HSCs separate into two distinct buffy coat layers (yellow) in Larcoll gradient.

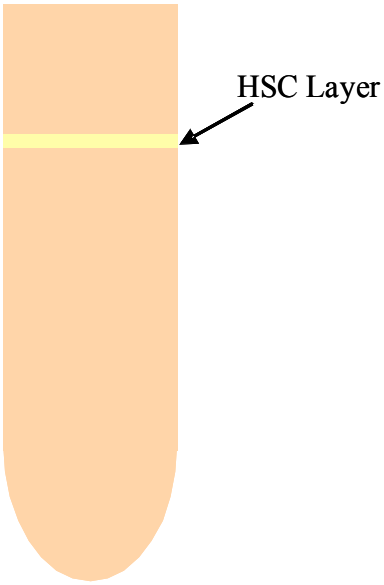

FIGURE 2.2: Schematic Drawing of Centrifuged HSC Layer (Protocol B and C). Freshly isolated rat HSCs separate into one distinct buffy coat layer in Histodenz and OptiPrep gradient.

CHAPTER 3: IDENTIFICATION AND INHIBITION OF NONMUSCLE II MYOSIN ISOFORMS IN THE HEPATIC STELLATE CELL

3.1 INTRODUCTION

The hepatic stellate cell (HSC) is a nonparenchymal cell type located in the perisinusodial space of Disse between the hepatocytes and endothelial cells and comprises 15% of the hepatic cell population [32]. In the normal quiescent state, HSCs project long cytoplasmic processes through the space of Disse and reach between hepatocytes and sinusoidal endothelial cells (SECs) wrapping around neighboring sinusoids [39]. HSCs function to store vitamin A, produce collagen for extracellular matrix remodeling and regulate hepatic microcirculation by modulating sinusoidal diameter [15, 204-206]. In diseased liver states, such as steatohepatitis, fibrosis, cirrhosis, or hepatocellular carcinoma, damaging stimuli phenotypically transdifferentiate the quiescent HSCs to activated myofibroblast-like cells [43]. Additionally, activated HSCs proliferate vigorously, loses vitamin A droplets, increase the expression of smooth muscle α-actin (αSMA) and disrupt liver microcirculation by hypercontracting and impeding blood flow [43, 44]. Increased secretion of type I collagen changes the surrounding matrix, which contributes to sinusoidal constriction and perpetuates HSC activation leading to the clinical manifestation of fibrosis.

In the normal liver autoregulation of microcirculation is delicately balanced by vasomodulators, such as endothelin-1 (ET-1) and nitric oxide [32, 114]. ET-1 is a potent vasoconstrictor synthesized by endothelial cells and several studies have shown that ET-1

levels are elevated in patients with cirrhotic livers [115, 116, 123]. In response to injury, SECs release excessive ET-1, which binds ET_A receptors on the HSC and stimulates, through calcium-dependent and -independent mechanisms, contractile force generation [125, 127]. Portal hypertension results from occlusion and compression of the sinusoidal vascular tone, which is directly mediated by increased myosin II activity in the activated HSC.

Myosins are a super-family of molecular proteins that bind actin to generate force using ATP hydrolysis. Specifically, myosin II is responsible for the generation of contractile forces in cells [151]. Myosin II was first identified and characterized in skeletal muscles; however, related classes of myosin II have been identified in smooth, cardiac and nonmuscle cells [149]. The hexameric molecular motor consists of two identical heavy chains (MHC) and two pairs of light chains (MLC) [151]. The individual MHCs (head regions) consist of a catalytic motor domain, a neck region and a coil-coil tail region [151]. The MHC contains a nucleotide-binding region and attaches to the actin filament [153]. The tail region forms antiparallel complexes, which polymerize hundreds of myosin molecules in thick filaments of skeletal muscle cells, or as few as 28 myosins in nonmuscle cells [154]. A contractile force is generated to facilitate contraction, migration and proliferation within the cell when the ensemble of motors interact with the actin filaments [207].

Upon ET-1 binding to its receptor in smooth muscle cells, increases in intracellular levels of calcium are generated by cyclic adenosine 3', 5'-monophosphate-induced mechanism. Activation of phospholipase C-β leads to cleavage of phosphatodyinositol 4,5-biophosphate and the release of 1,4,5-triphosphate [122]. Influx

of calcium activates calmodulin-dependent MLC kinase (MLCK), which results in increased phosphorylation of MLC [130, 131]. Much like smooth muscle cells, HSCs have also been shown to signal through calcium-dependent mechanisms. Chemically blocking ET-1-induced activation of MLCK, with the pharmacological inhibitor ML-7, decreases MLC phosphorylation in HSCs and thus indicates that contraction is calcium-dependent [127, 136]. However, it has also been shown that HSC contraction favors a calcium-independent pathway, specifically the Rho/ Rho kinase pathway [136, 198].

By using a selective inhibitor for Rho kinase (ROCK; Y-27632), studies have shown that HSC contraction is predominately mediated through the RhoA pathway [134]. In this pathway, increased phosphorylation of myosin II occurs through inhibition of the myosin phosphatase as well as through direct phosphorylation of MLC by ROCK leading to stress fiber formation and cellular contraction. Treatment with a ROCK inhibitor not only impedes ET-1 induced contraction of activated HSCs, but it also inhibits the progression of hepatic fibrosis as evident by decreased collagen accumulation and perpetual HSC activation. However, this fibrogenic response has also been shown to be mediated through the angiotensin II signaling pathway [134, 135]. Therefore, distinguishing between ROCK-induced contractile properties and other cellular responses mediated through ROCK requires a more selective and direct inhibition of HSC contraction.

Blebbistatin is a potent, selective and reversible pharmacological inhibitor of myosin II ATPase activity; however, tissue specificity of the drug is not well understood. Blebbistatin preferentially binds to the ATPase intermediate of the myosin II molecule, which inhibits phosphate release and thus actin dissociation and activated ATPase

activity [134, 170]. While studies have shown blebbistatin is an inhibitor of skeletal and nonmuscle myosin II activity, with minimal effects on smooth muscle myosin II, others have suggested that blebbistatin is specific to nonmuscle myosin II (NMM II) [164, 169-171]. Direct chemical inhibition of myosin II activity, rather than blocking upstream signaling events, is important in determining the functional role of the motor protein within the cell.

Although the structural cores of the myosin II classes are homologous, the minor amino acid alterations in the heavy and light chains alter kinetic and biochemical properties of the motor [172]. Specifically in nonmuscle cells, three isoforms of myosin II encoded by different genes have been identified in multiple tissues, NMM II-A, II-B and II-C [186]. The distinct enzymatic properties of each isoform allow for fine tuning of mechanical properties and are important in modulating the functional role of each isoform in the cell [190]. It has previously been shown that NMM II plays a role in many highly dynamic and transient cellular processes including cytokinesis, cell motility and cell polarity in many eukaryotic cells [149].

The structure and kinetics of NMM II isoforms may be useful in understanding the contractile properties of the HSC. HSCs express both myosin II and actin proteins; however, the particular class of myosin II has not been identified in HSCs. Thus, since HSCs are nonmuscle cells, we chose to investigate NMM II expression and localization of the three different NMM II isoforms in quiescent and activated HSCs.

One of the key phenotypic responses of the HSC that occurs during liver damage is changes in the extracellular matrix (ECM) of the liver. ECM remodeling leads to disruption of the liver architecture and thus accelerates HSC activation. This perpetual

activation of the HSC has been attributed to the ECM components such as type I collagen that increases matrix rigidity. Therefore, since HSCs can respond to changes in ECM, studies were performed to alter matrix stiffness to investigate changes in ECM as a possible mechanism for NMM II isoform regulation. Finally, this study selectively inhibited myosin II activity in the HSCs using blebbistatin, which allows us to closely scrutinize the specific role of myosin II in HSC contraction.

3.2 RESULTS

3.2.1 Blebbistatin inhibits basal- and vasoconstrictor-induced contraction of HSCs

HSC transdifferentiation is a key element in the development of portal hypertension. Understanding specific molecular components that are upregulated in this process requires identification of myosin II classes in quiescent, and early- and late-activated HSCs. As seen in fibrotic conditions, increased collagen type I deposition increases the matrix rigidity of the liver; therefore culturing freshly isolated HSCs on plastic tissue culture dishes mimics this *in vivo* environment. Culture-activated HSCs lose retinol esters, spread out and increase expression of αSMA; all of which are characteristic of activated HSCs (FIGURE 3.1). Using this *in vitro* model provides a method to measure the daily genetic and morphological changes in the process of HSC transdifferentiation.

To validate our *in vitro* HSC collagen contraction assay, we showed that culture-activated HSCs were contractile and responsive to the vasoconstrictor, ET-1 (Section 2.4.2). Collagen lattices prepared using an 8:1:1 rat tail type I collagen: 0.02 N Acetic Acid (3.65-4.5 mg/ml): 0.2 M HEPES: 10X DMEM solution. Day 4 culture-activated HSCs were trypsinized and seeded onto collagen lattices. Cells were serum starved for 24

hours and subsequently treated with increasing doses of ET-1 to determine optimal vasoconstriction concentrations (0; 0.1 pM - 100 nM; logarithmic increments). HSCs have previously been shown to be the most responsive to ET-1 on day 5 and the proteins (αSMA, myosin II and ET_A and ET_B receptors) responsible for contraction are not expressed in abundance until day 5, thus we chose this day of culture-activation [208]. In addition, other investigators routinely use day 5 for HSC contraction studies [32, 209]. The optimal volume and concentration of type I collagen in the collagen lattices and cell number was determined to be 300µl of 3.65 mg/ml collagen solution and 300,000 cells/ 1.88 cm^2 well. The optimal concentration of ET-1 after 24 hours was determined to be 1nM, as this concentration significantly decreased the collagen lattice diameter to 28.5% of the original collagen diameter, while higher doses of ET-1 did not result in further contraction (FIGURE 3.2).

Myosin II activity regulates cell morphology and HSC contraction; however, this hypothesis had not been tested with a selective inhibitor of myosin II activity, all previous studies manipulated upstream effectors of myosin II activity. Therefore, we tested the effects blebbistatin had on HSC morphology and contraction. Day 4 culture-activated HSCs were seeded on collagen lattices and serum starved overnight (FIGURE 3.3). The wells were then pretreated with blebbistatin for 30 minutes and treated with the optimal ET-1 dose (1 nM). Consistent with previous findings, day 5 HSCs were contractile and exhibited a star-like shape when seeded onto a collagen lattice (FIGURE 3.3A). ET-1 treatment caused HSC hyperconstriction and changed the phenotype into a stretched polygon morphology reaching across the collagen lattice (FIGURE 3.3B). As expected, pre-treatment with blebbistatin (50 µM) inhibited ET-1 induced

hyperconstriction of the cell morphology (FIGURE 3.3C), while vehicle treatment pre-treatment permitted ET-1 induced hyperconstriction of the HSCs (FIGURE 3.3D).

In addition, we also tested the effects of blebbistatin on basal- and ET-1-induced HSC contraction of collagen lattices. HSCs were pretreated with increasing doses of blebbistatin (0-25 μM; 5 μM increments) for 30 minutes followed by ET-1 (1 nM) treatment. As the HSCs contracted, the collagen lattice decreased in circumference. The cells pretreated with higher doses of blebbistatin (15-25 μM), abolished basal- and ET-1 induced contraction, while lower doses of blebbistatin (5 and 10 μM) significantly inhibited ET-1 induced contraction (FIGURE 3.4; light grey bars).

Additionally, we demonstrated that 5μM blebbistatin treatment decreased the rate of HSC contraction 36% as compared to the vehicle (vehicle pre-treatment contraction rate= 0.0577 cm^2/hour; blebbistatin pre-treatment contraction rate= 0.0208 cm^2/hour) after 24 hours (FIGURE 3.5). Overall, by using the selective pharmacological agent, blebbistatin, our results demonstrated that myosin II activity maintained HSC cellular morphology, completely abrogated its contractile properties and modulated the rate of contraction.

3.2.2 NMM II isoform expression in HSCs

Our initial study with blebbistatin confirmed that myosin II is present in the HSC and directly responsible for contraction; however there are multiple classes of myosin II: the sarcomeric myosins from skeletal, cardiac muscle and smooth muscle cells, nonmuscle myosins, and the myosin II from lower eukaryotic species and fungi [149]. Since HSCs are nonmuscle cells, we chose to focus on the nonmuscle myosins but

keeping in mind that the identification of other myosin II family members, such as smooth muscle myosins, may also be important and may warrant further investigation.

To demonstrate that specific NMM II isoforms are expressed by HSCs, freshly isolated cells (quiescent), day 1 and day 14 culture-activated HSCs were measured by reverse transcriptase PCR (RT-PCR) and RealTime PCR to visualize and quantify mRNA expression, respectively (Section 2.6.2 and 2.6.3). Primers were designed using OLIGO 6 program and validated using lung control as a positive control (FIGURE 3.6). As determined by RT-PCR, mRNA expression of all three isoforms was detected and visualized on an agarose gel (FIGURE 3.7). HSCs were freshly isolated (quiescent) from rat livers as described in Section 2.2.2 and culture-activated HSCs (day 1 and 14) were harvested from tissue culture dishes as described in Section 2.1.4. RNA was generated from HSCs as previously described in Section 2.5.2 and reverse transcribed to cDNA with SuperScript III Reverse Transcription System. The housekeeping gene, GAPDH, was initially used as a method of myosin II isoform normalization; however, our studies indicated that this method was not appropriate due to variations in expression of this gene over days in culture-activation (FIGURE 3.8). Other standard housekeeping genes, including β-actin and HPRT were also tested for normalization of NMM II isoform expression. These genes were also not suitable for mRNA normalization since there were wide variations in mRNA expression based on total cDNA content (FIGURE). Therefore, total cDNA, as determined by NanoDrop concentration measurements, was used for normalization to quantitate changes in gene expression.

Using RT-PCR, *in vitro* data revealed mRNA expression of all three isoforms in quiescent and culture-activated HSCs (day 1 and 14). Strong mRNA expression of NMM

II-A was detected at 28 cycles; while expression of NMM II-B and II-C was detected at 34 and 42 cycles, respectively (FIGURE 3.7A). Using RealTime PCR to quantify mRNA expression of NMM II isoforms normalized to total cDNA concentrations, NMM II-A and II-B were significantly increased by culture-activation, whereas expression of NMM II-C was variable (FIGURE 3.7B). Interestingly, mRNA expression of NMM II-B increased 2.8-fold over culture-activation, whereas NMM II-A expression only increased 1.4-fold suggesting that NMM II-B maybe play and important role in the later stages of HSC transdifferentiation.

To determine if mRNA expression correlated with protein expression, whole cell extracts were harvested from HSCs and subjected to precipitation by F-actin selection as previously described in Section 2.7.2. Using Western blots to analyze protein expression of NMM II isoforms (Section 2.8.3), our studies indicated no detectable expression of all three isoforms in quiescent cells, which was unexpected since mRNA expression was present (FIGURE 3.9; NMM II isoform 1:1000 antibody dilution). To confirm these results, the concentration of quiescent samples was doubled and reanalyzed; although Ponceau S staining verified total protein loading of quiescent samples increased twofold, expression of all three isoforms still was undetected in quiescent samples. All three isoforms were present after initiation of HSC activation (day 1), but showed relatively weak expression as compared to the protein expression in fully activated cells (day 14). As shown in FIGURE 3.9, there was a strong increase in protein amounts for all three isoforms at fully activated HSCs (day 14), NMM II-A and II-B showing significant increases. Since NMM II-A and II-B have been shown to play individual roles in migration and contraction, it is possible that they perform different roles in the activated

HSC as well, providing separate targets for different cellular functions. Although the function of NMM II-C has not been identified, it too increased with culture-activation, suggesting yet another contributor to cellular function.

NMM II-A and II-B are distributed along stress fibers, in a linear or interspersed fashion within lamellipodia and co-localize around the nucleus [195]. The NMM II-A isoform preferentially co-localizes with actin filaments in the leading edge of cells, while II-B co-localizes in the trailing edge [195]. In order to visualize the protein expression of each isoform, culture-activated HSCs were sparsely seeded onto plastic chamber slides and immunocytochemistry was performed (Section 2.9.4). As determined by immunofluorescence, protein expression of three isoforms was detected in culture-activated cells (FIGURE 3.10; NMM II 1:500 antibody dilution). Initial activation of HSCs at day 1 produced weak expression, whereas full activation at day 14 showed strong but variable expression. At day 14, expression of NMM II-A and II-B was co-localized to actin stress fibers, while expression of NMM II-C was dispersed.

In order to determine if NMM II expression is upregulated in liver fibrosis, bile duct ligation (BDL) induced liver injury was performed as described in Section 2.3.2. Fibrosis induced by BDL typically generates lesions surrounding the bile duct epithelium and gives rise to uncontrolled proliferating cholangiocytes, which results in hepatic injury [24]. HSCs respond to stimulation and become activated. Sham operations were performed in the same manner, except without BDL. Our results, as determined by Sirus red staining (performed by Carolinas Medical Center Department of Surgery) and hematoxylin and eosin (H&E; Section 2.3.4) staining, are consistent with previous findings of liver injury induced by BDL (FIGURE 3.11). While Sirus red staining

indicated increased levels of collagen deposition in fibrotic liver tissue, H&E staining confirmed uncontrolled proliferation of the biliary epithelium.

As seen in culture-activation, mRNA expression levels of αSMA in HSCs are increased 2,000-fold (FIGURE 3.12A), thus this protein is typically used as a classic marker of liver fibrosis. We have also shown that glial fibrillary acidic protein (GFAP) mRNA expression is upregulated in quiescent HSCs; therefore, we expected that protein expression should be increased in normal liver tissue (FIGURE 3.12B). We used immunofluorescence to detect these protein markers in normal and injured liver tissues (FIGURE 3.12C). Expression of αSMA was evident in the smooth muscle cells surrounding the central vein exclusively, while expression in the injured tissue was intercalated between hepatocytes, where HSCs normally reside. Unexpectedly, expression of GFAP was undetected by immunofluorescence in both normal and injured liver tissue (data not shown). We used multiple antibodies from different companies and various tissues; however, we were unable to use this protein marker for fluorescent quiescent HSC detection.

In order to determine if NMM II expression was upregulated in liver fibrosis, we used fluorescent immunohistochemistry to co-localize isoform expression with αSMA positive cells (activated HSCs) in injured liver tissue (FIGURE 3.13). Only NMM II-A and II-B protein expression was minimally detected in normal liver tissue, while NMM II-B was the only isoform found to co-localize with activated HSCs in injured liver tissue.

3.2.4 Substrate stiffness modulates NMM II isoform expression of HSCs

Previous studies have shown that HSC transdifferentiation is dependent on matrix stiffness (Wells). In cirrhotic patients, liver stiffness measurements range from 12.5 to 75.5 kPa [76]; therefore we generated polyacrylamide substrates coated with a thin layer of type I collagen to mimic this *in vivo* environment. To test the effects of changes in mechanical rigidity on NMM II isoform expression, we seeded day 5 culture-activated HSCs on 'normal' and 'fibrotic' substrates (4.6 and 21.6 kPa) and allowed the cells to incubate overnight. As assessed morphologically, culture-activated HSCs seeded onto 'normal' substrate reverted to their quiescent phenotype, while cells seeded onto 'fibrotic' substrate maintained myofibroblastic projections characteristic of the activated phenotype (FIGURE 3.14A). Using RT-PCR analysis, we demonstrated that expression of both NMM II-A and II-B were downregulated in cells plated on softer substrate supports (FIGURE 3.14B). While expression of NMM II-A was decreased moderately, NMM II-B expression was significantly decreased 21%, indicating a regulatory role for matrix stiffness on isoform expression (FIGURE 3.14C).

3.3 DISCUSSION

HSCs play several important roles in facilitating the hepatic immune response. Quiescent HSCs in a healthy liver maintain normal hepatic microcirculation by wrapping around liver sinusoids and contract and dilate in response to local vasoactive modulators, notably ET-1 and nitric oxide. However, during acute injury, HSCs hyperconstrict blood vessels, allowing for architectural stabilization and reduced toxin influx. HSCs also undergo a transdifferentiation process from the quiescent state to an activated myofibroblast-like cell. The activated cells divide and migrate to the site of injury where

they secrete fibrillar collagen. If the injury persists , the HSC's wound healing responses never resolves and excessive collagen accumulates and blood vessels constriction is sustained. By modulating collagen biosynthesis, it has been suggested that fibrosis is partially reversible [6]. However, complete resolution of excessive collagen deposition in a cirrhotic liver with restoration of normal hepatic microcirculation may not be possible. Current treatment for fibrosis and cirrhosis focuses on portal hypertension and its complications; however, these treatments do not have an effect on the pathophysiological mechanisms that lead to portal hypertension. Thus, effective vasodilating drugs directed towards HSC contractility may be beneficial.

In order to establish an effective treatment regime directed at HSC hypercontractility, migration and proliferation, an in depth understanding of the intracellular components and pathways is necessary; however, no studies to date have identified these specific proteins and pathways. Prolonged exposure to a fibrogenic insult has been shown to increase myosin II protein expression in HSCs, which is necessary for contractility [209]. By inhibiting ROCK, an upstream effector of myosin II activity, HSC contraction is prevented; however, blocking the upstream Rho pathway also interferes with a wide range of cellular functions including contraction, migration, apoptosis and proliferation by targeting LIM kinase, Akt and the ERK pathways, respectively, which all phosphorylate MLC [167]. No studies have examined direct inhibition of myosin II on contraction. In this study we used a myosin II inhibitor, blebbistatin, which is a cell-permeable specific pharmacological inhibitor of myosin II ATPase activity, to block HSC contraction. Blebbistatin has previously been used to inhibit protrusion-mediated lamella formation and chemotactic migration of HSCs [45]. While the IC_{50} values of blebbistatin

range from 0.5 to 5 μM for myosin II isoforms, smooth muscle myosin II is weakly inhibited with an IC_{50} value of 80 μM. Our studies demonstrated that blebbistatin inhibits ET-1-induced contraction with an IC_{50} value of 5 μM, which is consistent with previous findings [210]. Blocking myosin II activity subsequently inhibited both basal- and ET-1-induced contraction of the HSCs, demonstrating for the first time that that myosin II plays a direct role in HSC contraction.

Tissue and isoform specificity of blebbistatin is not well understood. While some studies describe that the pharmacological inhibitor can block skeletal muscle and NMM II activity with minimal effects on smooth muscle myosin II, others have shown that blebbistatin is specific to smooth muscle myosin II; therefore, it is possible that smooth muscle and nonmuscle myosin II may contribute to HSC contraction [164, 169-171]. Since HSCs are nonmuscle cells, we chose to examine the expression of NMM II isoforms in the process of HSC transdifferentiation.

Protein and mRNA expression of all three NMM II isoforms were detected in culture-activated cells. Interestingly, protein expression of all isoforms was undetectable in quiescent cells, while mRNA expression was detected. The process of HSC transdifferentiation is a key element in liver fibrosis and understanding the expression of NMM II isoforms in early (day 1) and late (day 14) HSC culture-activation provides possible insights into their particular cellular functions. Since NMM II-A and II-B contribute to cellular migration and contraction, it is possible that these isoforms perform different roles in the progression of HSC transdifferentiation as well. Although the function of NMM II-C has not been identified, it too increases with culture-activation, suggesting yet another contributor to cellular functioning.

In order to associate isoform expression with a particular cellular function we determined isoform location. Using immunofluorescense, we showed that NMM, II-A and II-B co-localized to actin stress fibers suggesting that these molecules are functionally active. Strong expression of NMM II-A in the periphery of activated HSCs may be important in migration of HSCs, while strong NMM II-B expression in the cellular cortex may indicate an important role for this isoform in controlling the hypercontraction of the HSC during injury. Expression of NMM II-C however was not clearly distinguishable, indicating that isoform may be in too low of quantities to be detected by this technique or may possibly be an artifact of the assay. *In vivo* studies only demonstrated upregulation of NMM II-B isoform expression in activated HSCs. Although this data remains inconclusive, it is possible that fluorescent technique employed was unable to delineate between expressions of the other isoforms in surrounding cells. We expect that future studies measuring the genetic inhibition of each NMM II isoforms will delineate the functional roles of the isoforms in culture-activated HSCs. These studies are described in the following chapter.

Activated HSC increase synthesis and deposition of type I collagen accompanied with changes in matrix metalloproteinases and its inhibitors. This overall accumulation of type I collagen increases the matrix stiffness of the basement membrane. It has been suggested that increased matrix rigidity is associated with perpetual HSC activation [72]. However, it is not clear if increased static pressure of hepatic sinusoids itself influences the functional transformation of HSCs. Early symptoms of chronic liver disease are often presented with clinical features attributable to portal hypertension. A recent study demonstrated that increased static pressure and ethanol exposure can modulate HSC

activation *in vitro* [211]. The results suggest that increased matrix stiffness accompanied by sinusoidal static pressure will result in the continual activation of the HSC. Thus, we tested the relative contribution of matrix stiffness on isoform modulation. Our results indicated that mechanical properties of the liver can alter NMM II isoform expression providing insight to the mechanism of HSC-induced sinusoidal constriction.

Overall these studies show that myosin II is the primary molecular motor responsible for HSC contraction by using the selective inhibitor of the NMM II ATPase intermediate of the myosin II molecule, blebbistatin. Additionally, we determined the expression and localization of NMM II isoforms in quiescent and activated HSCs and based on cellular location, our data suggest that II-A could participate in the initial force generation necessary for migration, while II-B may participate in sustained hypercontraction. Finally, we have shown that NMM II isoform expression may be modulated through mechanical properties, such as matrix stiffness.

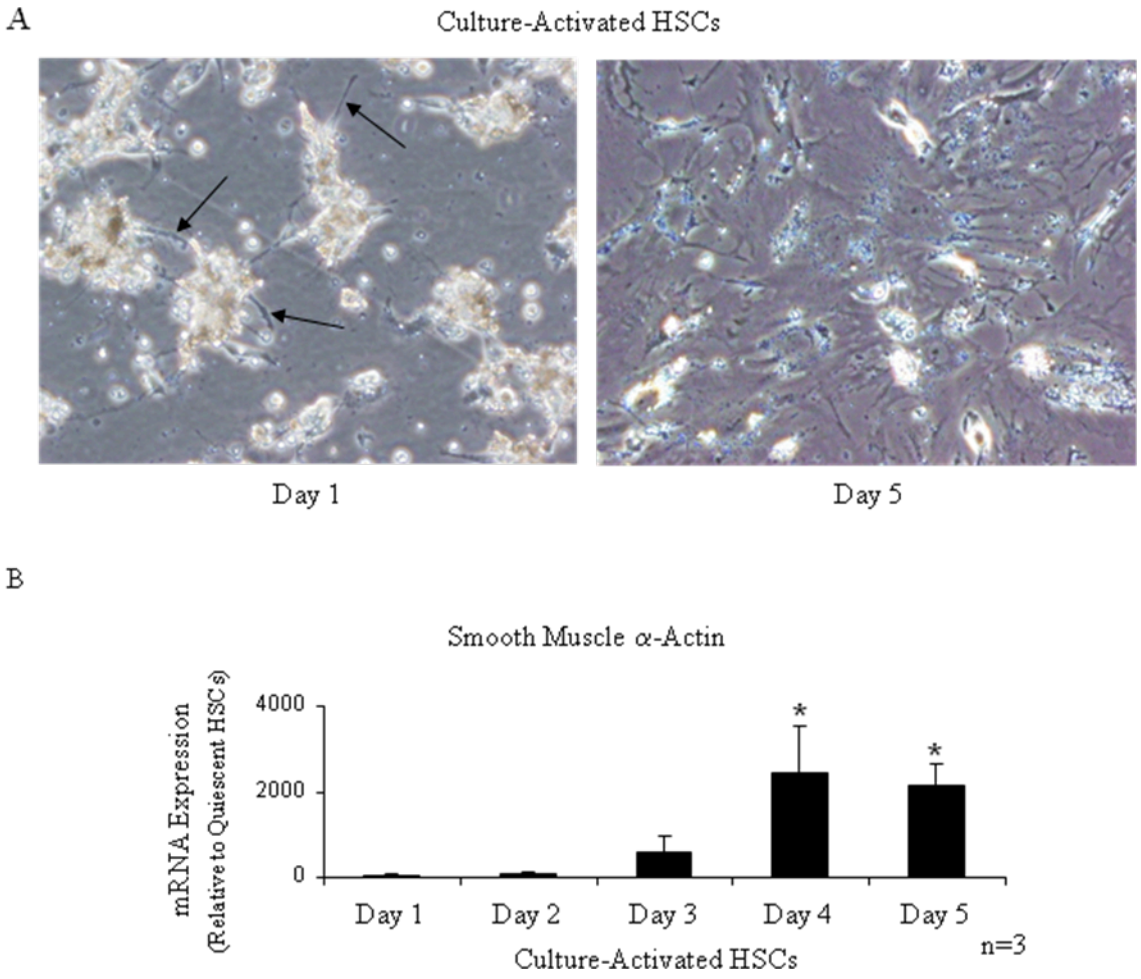

FIGURE 3.1: Culture-activated HSCs Transdifferentiate into α-SMA Expressing Myofibroblasts. HSCs plated onto plastic tissue culture dishes proliferate vigorously, lose retinol esters and increase mRNA expression of smooth muscle a-actin. (A) On day 1 of culture-activation, retinol esters (white) are present in abundant quantity. By day 5 of culture activation, retinol esters and cytoplasmic projections (black arrows) have depleted. (B) Over days in culture, activated HSCs increase mRNA expression of smooth muscle α-actin approximately 2000-fold as measured by RealTime PCR (*$p<0.05$ compared to Day 1.)

A

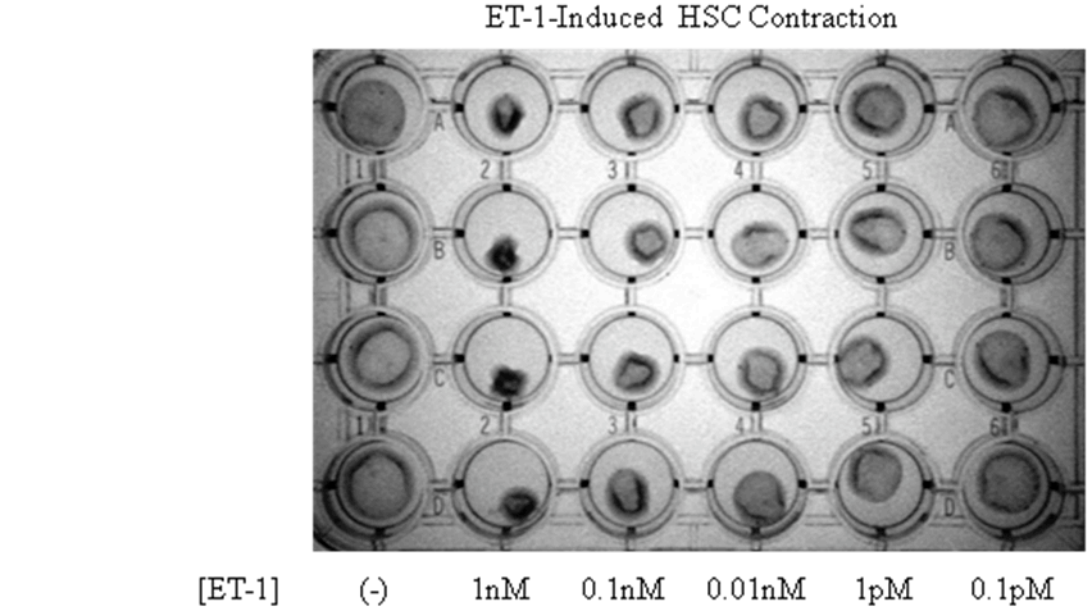

B

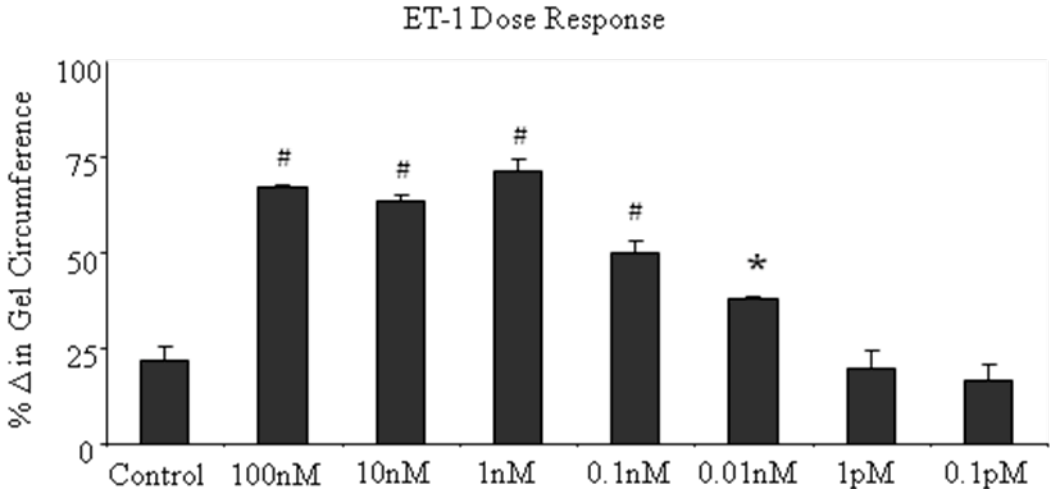

FIGURE 3.2: ET-1 Treatment Induces HSC Contraction of Collagen Lattices. Optimal ET-1 concentration was determined using increasing doses of the peptide. (A) Representative collagen contraction assay. (B) Quantification of ET-1-induced HSC collagen contraction. Day 5 culture-activated HSCs were seeded onto the lattices and treated with increasing doses of ET-1. Day 5 HSCs, contracted the collagen lattice (control or basal) and increasing doses of ET-1 amplified the contraction. Percent change in gel circumference peaked at 71.5% with 1nM ET-1 treatment. PCR (*$p<0.05$; #$p<0.001$ compared to Control.)

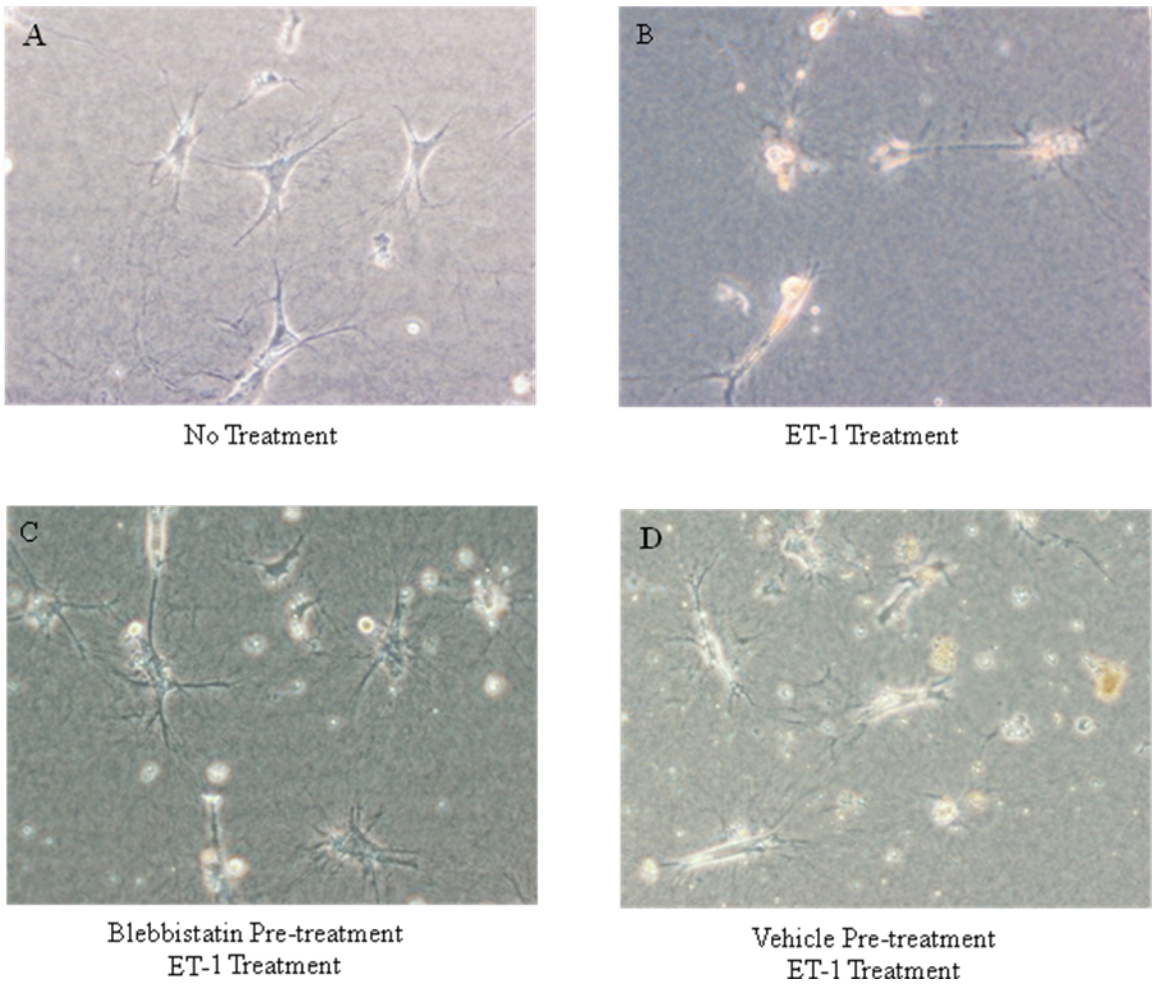

FIGURE 3.3: Blebbistatin Inhibited ET-1-Induced Changes in HSC Morphology. HSCs seeded onto a collagen lattice with no chemical treatment exhibit a star-like structure (A). HSCs treated with ET-1 (B) become hypercontractile and change their morphology to a stretched polygon morphology compared to untreated cells (A). When pretreated with vehicle, and subsequently incubated with ET-1, HSCs again exhibited a stretched polygon structure (C); however, blebbistatin pre-treatment, inhibited ET-1 induced morphological changes in HSC structure (D).

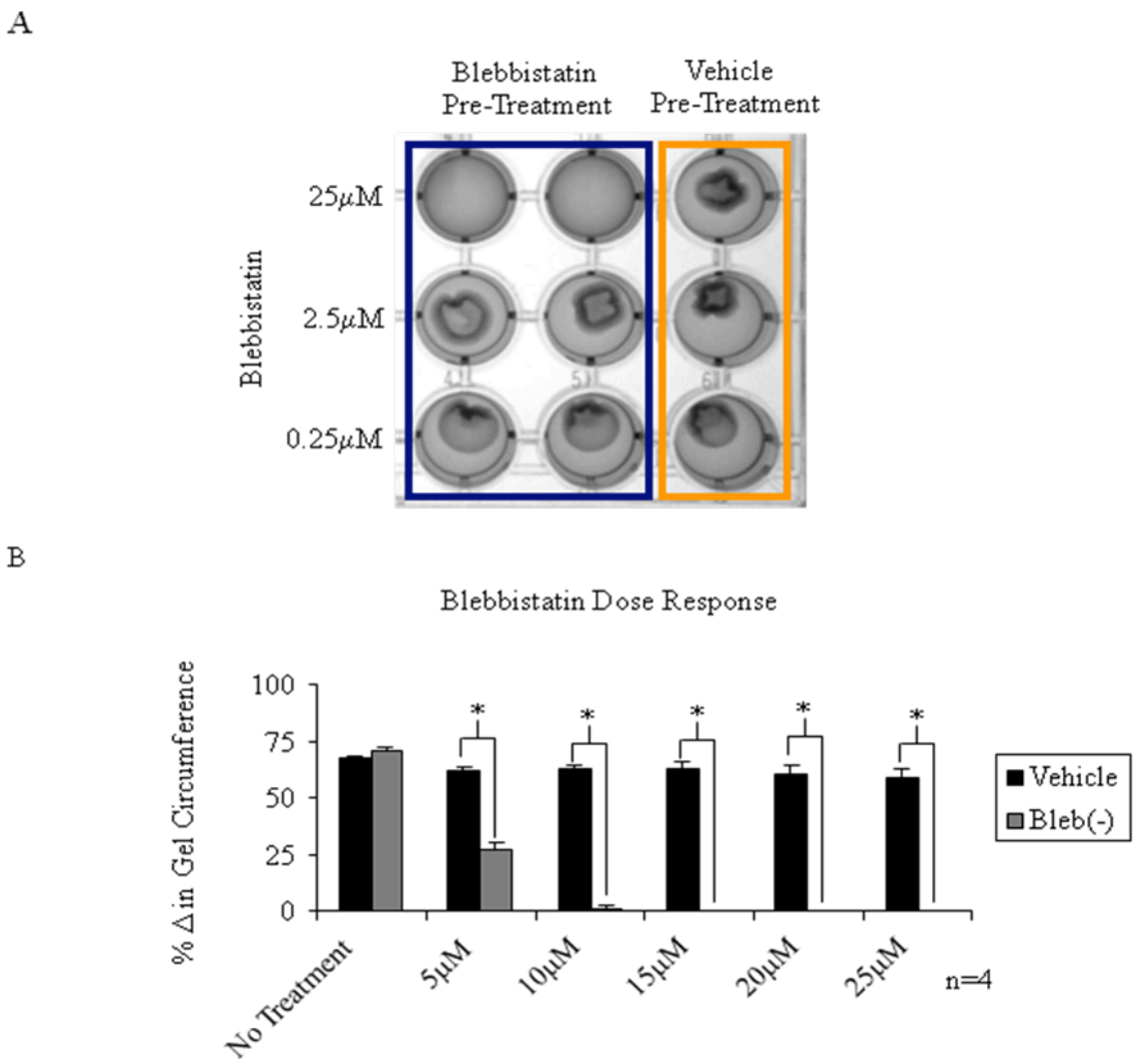

FIGURE 3.4: Blebbistatin Inhibited Basal and ET-1-Induced HSC Contraction. Optimal blebbistatin concentration was determined by inhibition of gel contraction. Day 5 culture-activated HSCs seeded onto gels were pretreated with vehicle or blebbistatin and subsequently treated with 1nM ET-1 after 30 minutes. (A) Representative image of blebbistatin inhibition of ET-1 induced contraction. (B) Blebbistatin, a myosin II inhibitor, blocked HSC contraction. Pretreatment with 5mM blebbistatin diminished ET-1 induced constriction by 54%, while 15-25mM completely abrogated ET-1 induced constriction. (*$p<0.05$ compared to the untreated sample.)

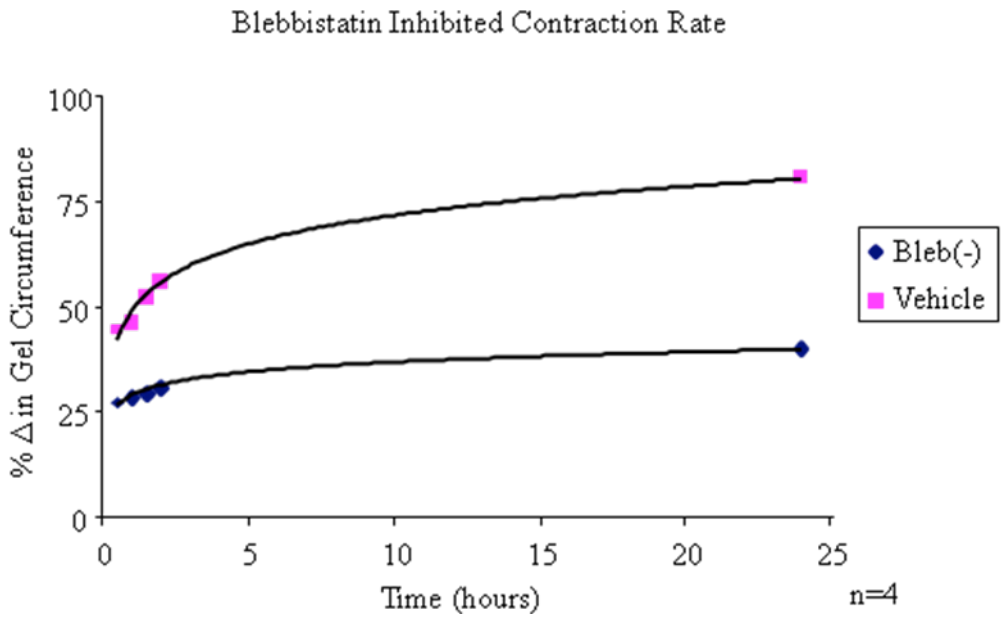

FIGURE 3.5: Blebbistatin Inhibited ET-1 Induced HSC Contraction Rate. HSCs seeded onto collagen lattices and treated with ET-1 and the vehicle, contracted maximally at 80.8%, while blebbistatin pre-treatment inhibited ET-1-induced contraction ~50% after 24 hours. Blebbistatin pre-treatment decreased the rate of HSC contraction 36% over 24 hours (vehicle=0.0577cm^2/hour; blebbistatin=0.028cm^2/hour).

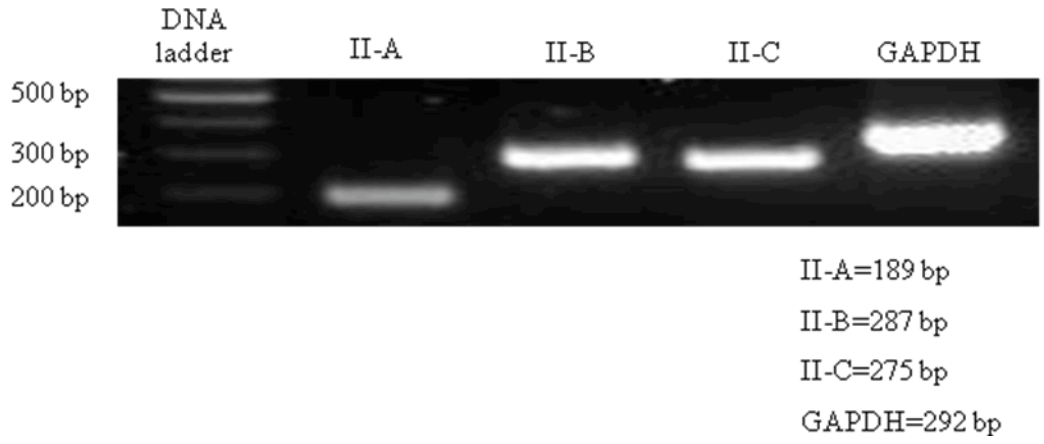

FIGURE 3.6: NMM II Isoform mRNA Expression in the Lung. Lung tissue mRNA was used to detect NMM II expression of all three isoforms by RT-PCR. Expression of all three isoforms was observed at the predicted base pair.

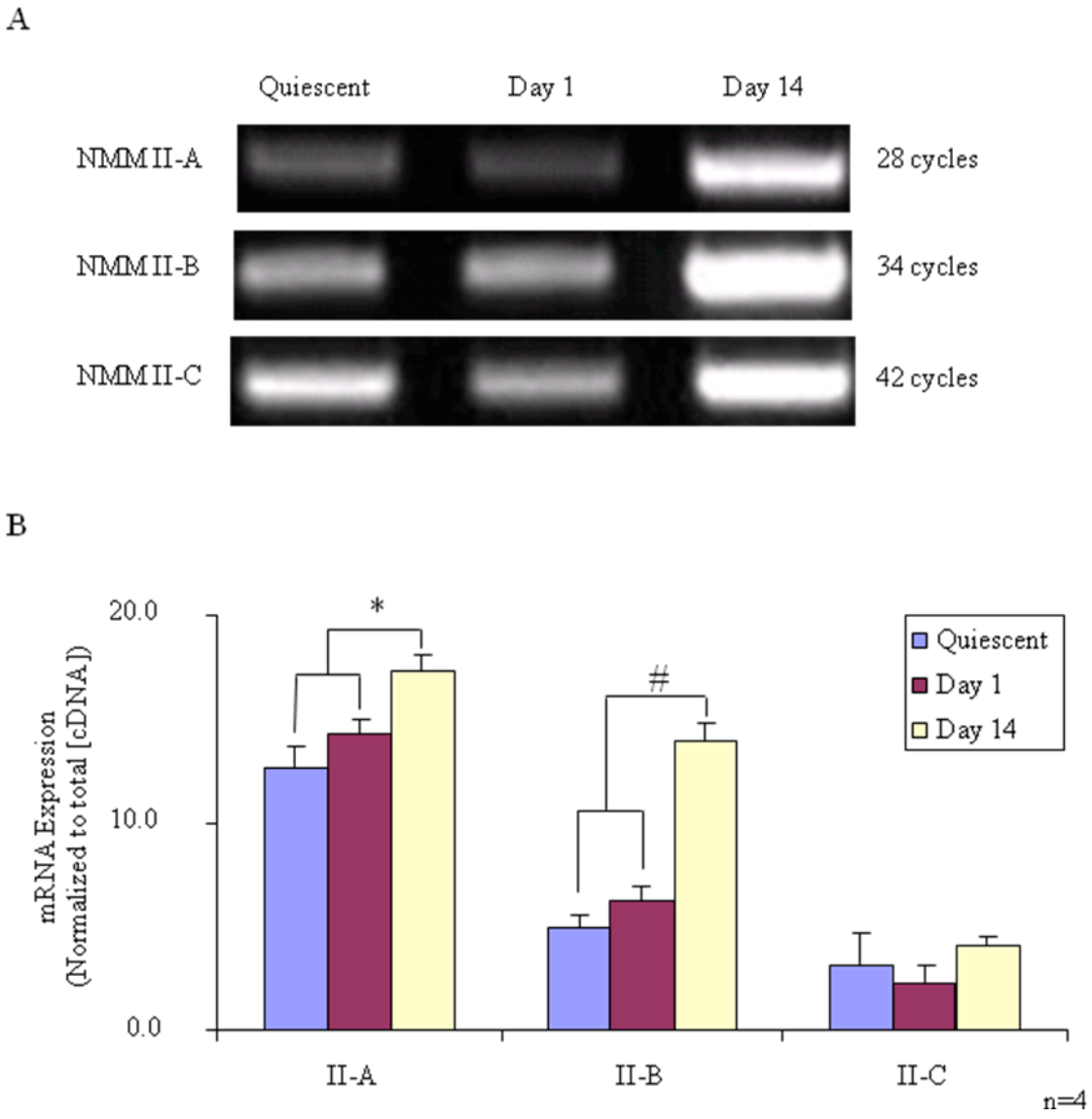

FIGURE 3.7: RT and Real-Time PCR Quantification of NMM II-A, II-B and II-C mRNA Expression in HSCs. (A) mRNA expression of all isoforms was detected in quiescent and culture-activated HSCs (day 1 and 14) by RT-PCR and visualized on an agarose gel. Strong mRNA expression of NMM II-A was detected at 28 cycles, while expression of NMM II-B and II-C was detected at 34 and 42 cycles, respectively. (B) As normalized to total cDNA concentration, mRNA expression of all isoforms was induced by culture-activation. Real-Time PCR indicated that NMM II-A mRNA expression was higher in quiescent cells compared to II-B and II-C; however, mRNA expression of II-B increased dramatically (55%) over days in culture. NMM II-C expression across culture-activation was variable. (*$p<0.05$; #$p<0.001$ as normalized to total cDNA concentration)

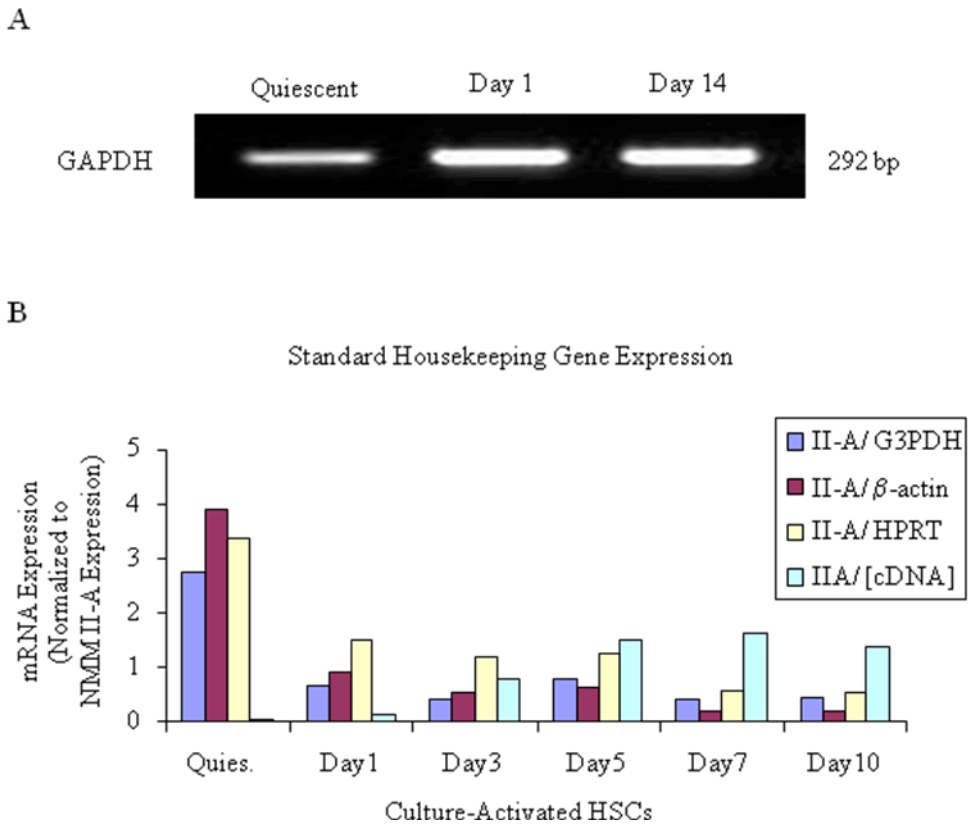

FIGURE 3.8: Housekeeping Gene mRNA Expression from Cultured HSCs. (A) mRNA expression of GAPDH was detected after 23 cycles by RT-PCR in quiescent and culture-activated HSCs (day 1 and 14). (B) As normalized to total cDNA concentration, mRNA expression of classic housekeeping genes (G3PDH, β-actin and HPRT) fluctuated over days during culture- activation, thus they served as unreliable normalization markers for NMM II isoform expression as determined by Real-Time PCR.

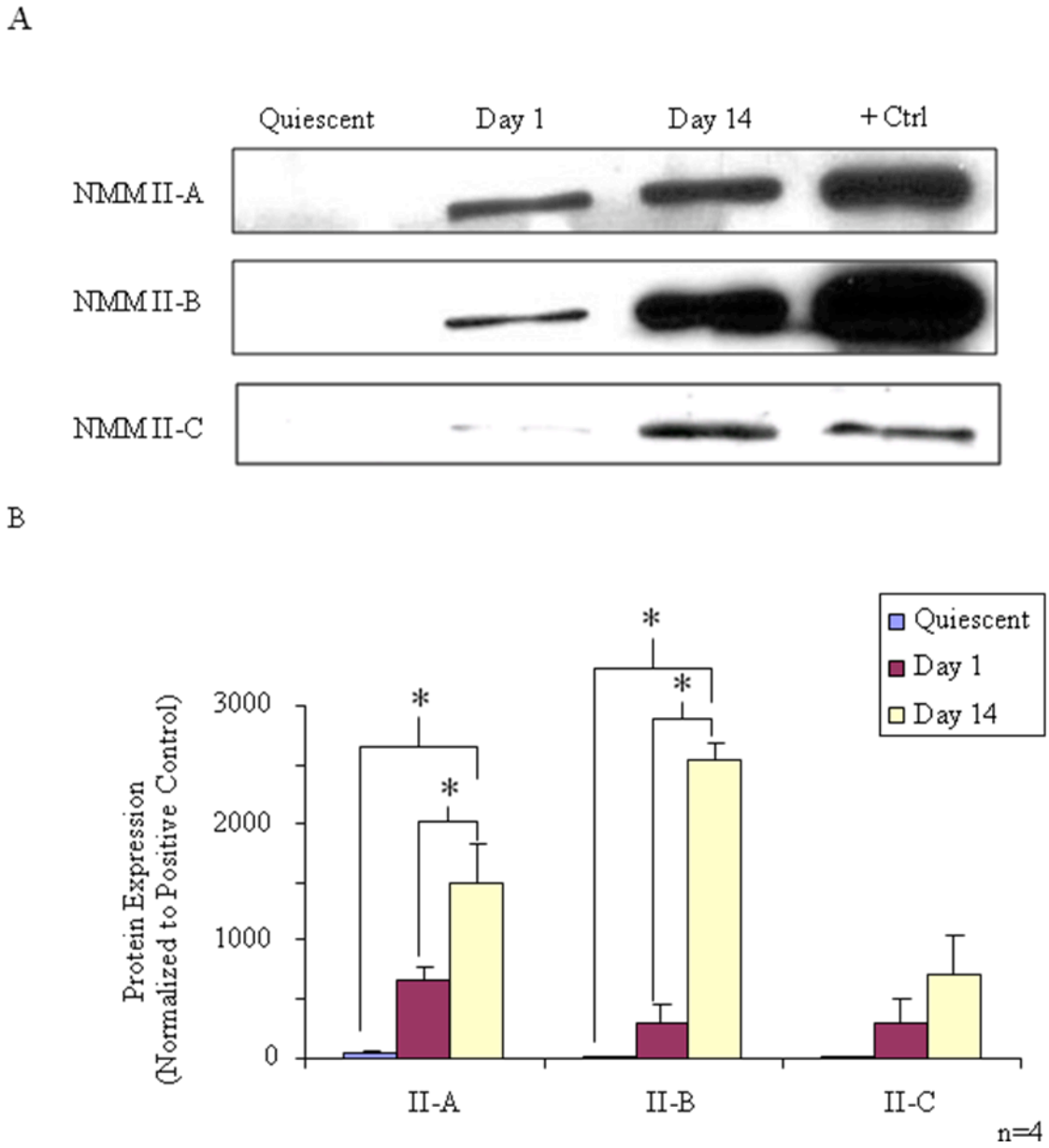

FIGURE 3.9: Quantification of NMM II-A, II-B and II-C protein expression in HSCs. (A) Protein expression of all three NMM II isoforms was undetected in quiescent HSCs by Western blot analysis. Initial activation of HSCs at day 1 produced weak NMM II isoform expression, whereas full activation at day 14 showed strong but variable expression (M.W.=200kD). (B) Quantification of Western blot. Protein expression of each isoform was normalized to protein expression of positive control (Rat-1 fibroblast cell line; *$p<0.01$).

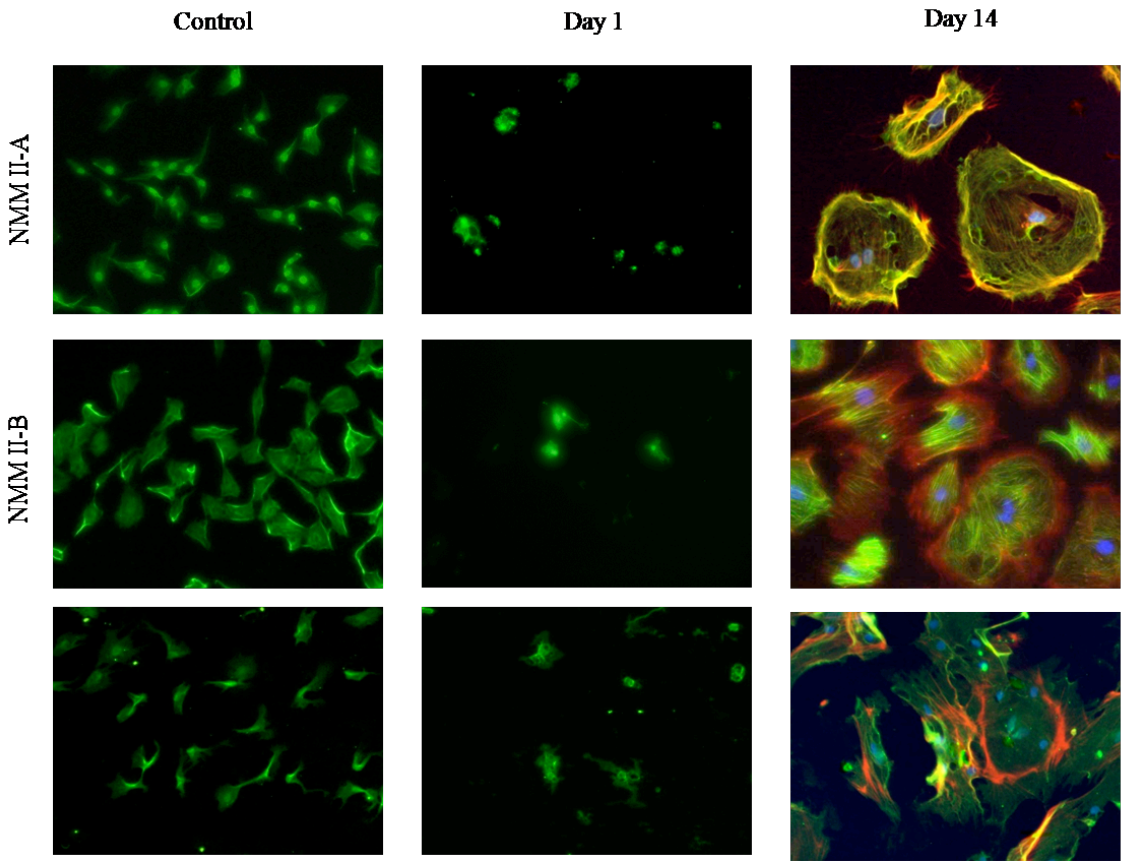

FIGURE 3.10: Immunocytochemistry: Protein Expression of NMM II-A, II-B and II-C in HSCs. Expression of all three isoforms was detected in culture-activated cells. At day 14 of culture-activation, expression of NMM II-A and II-B was co-localized (yellow) to actin stress fibers (phalloidin stain-red), while expression of NMM II-C was dispersed. Rat-1 fibroblast cell line served as a positive control.

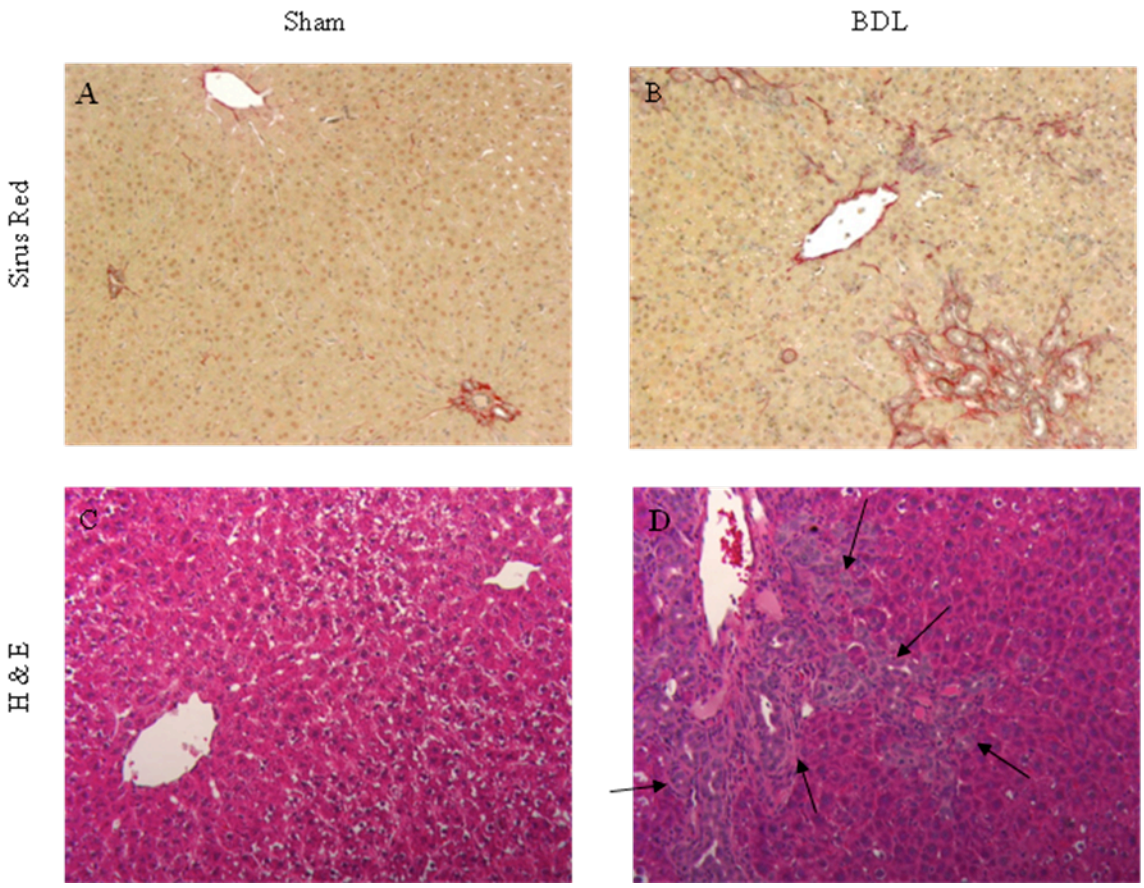

FIGURE 3.11: Bile Duct Ligation Induced Hepatic Fibrosis. BDL is a well-established model of hepatic fibrosis. The common bile duct is double-ligated and transected (right panel). Sham operation was performed in the same manner expect without BDL (left panel). Tissue was stained by Sirus red (top panel) and H&E (bottom panel) to assess liver morphology. Increased collagen deposition (red) was evident in copious amounts in BDL tissue (B), while sham tissue exhibited mild staining around the portal triad (A). An increase in cellular proliferation was evident by increased hemotoxylin staining (blue) in the portal tract (black arrows) of BDL tissue (D).

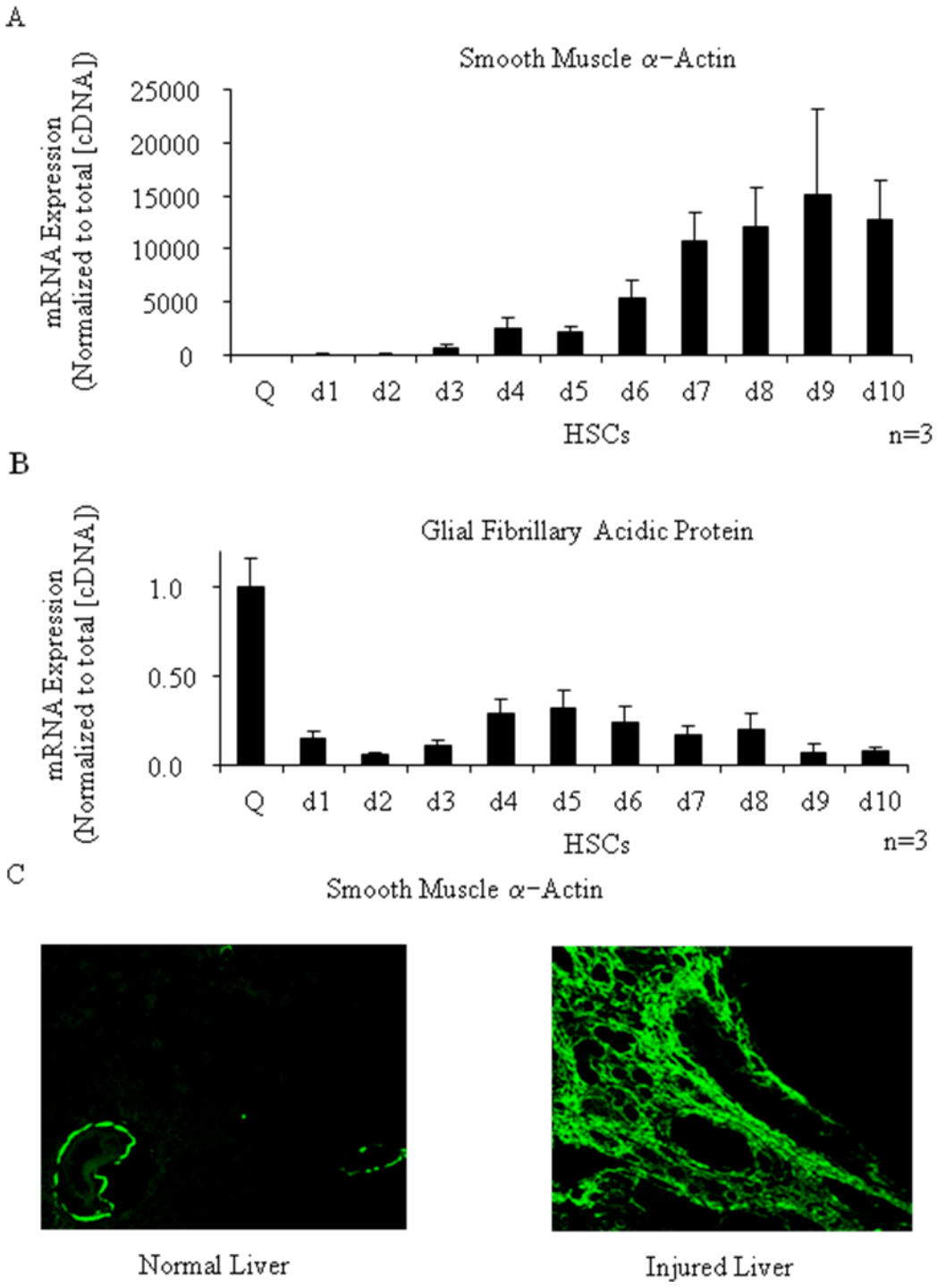

FIGURE 3.12: Classic Protein Markers of Quiescent and Activated HSCs. Culture activation of quiescent HSCs (A) up-regulated the expression of αSMA and (B) down-regulated the expression of GFAP as determined by Real-Time PCR. Protein expression of αSMA (green) was detected in normal tissue surrounding central vein, while injured liver tissue showed abundant expression as determined by fluorescent immunohistochemistry (C).

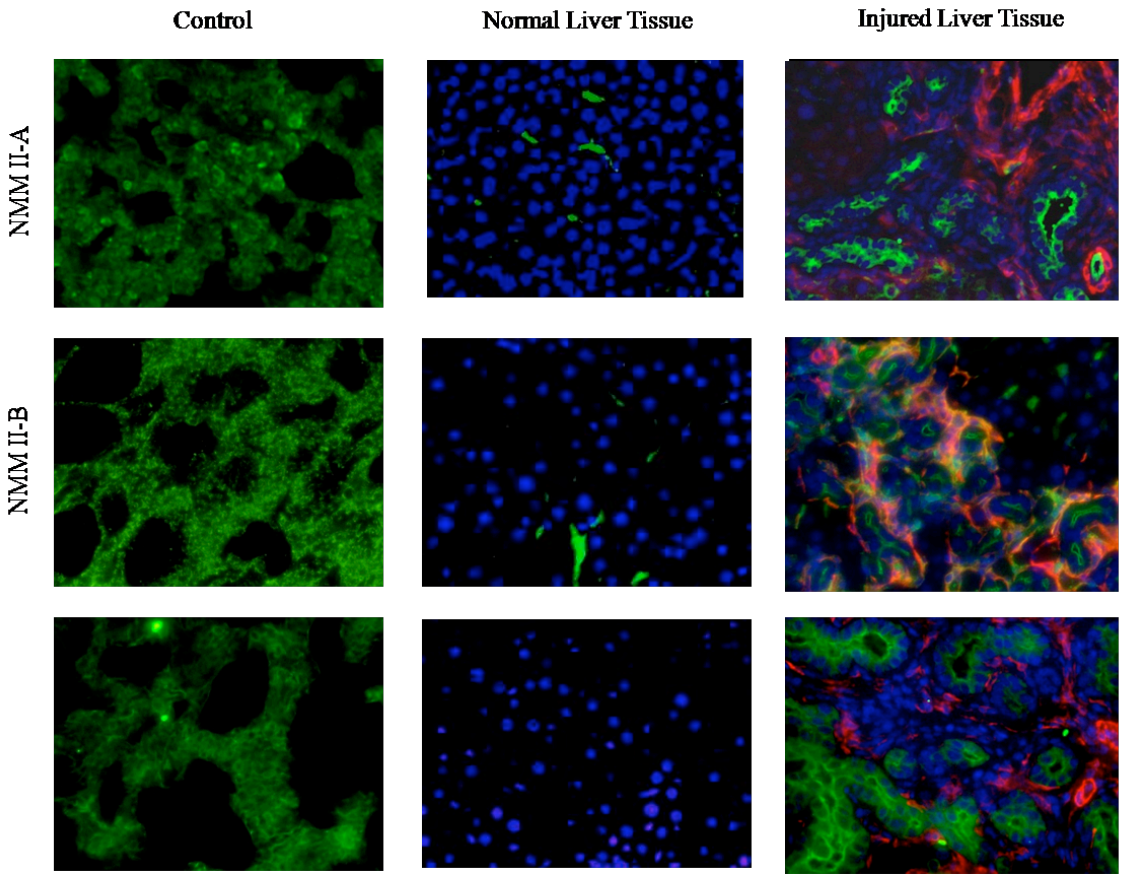

FIGURE 3.13: Immunohistochemistry: Protein Expression of NMM II-A, II-B and II-C in Normal and Injured Liver Tissue. Normal liver tissue from a sham rat demonstrated the presence of NMM II-A and II-B but not II-C. Injured liver tissue from bile duct ligated rats also demonstrated expression of NMM II-A and II-B, as well as II-C. Additionally, only II-B co-localized with activated HSCs in the injured tissue. Lung tissue served as positive control.

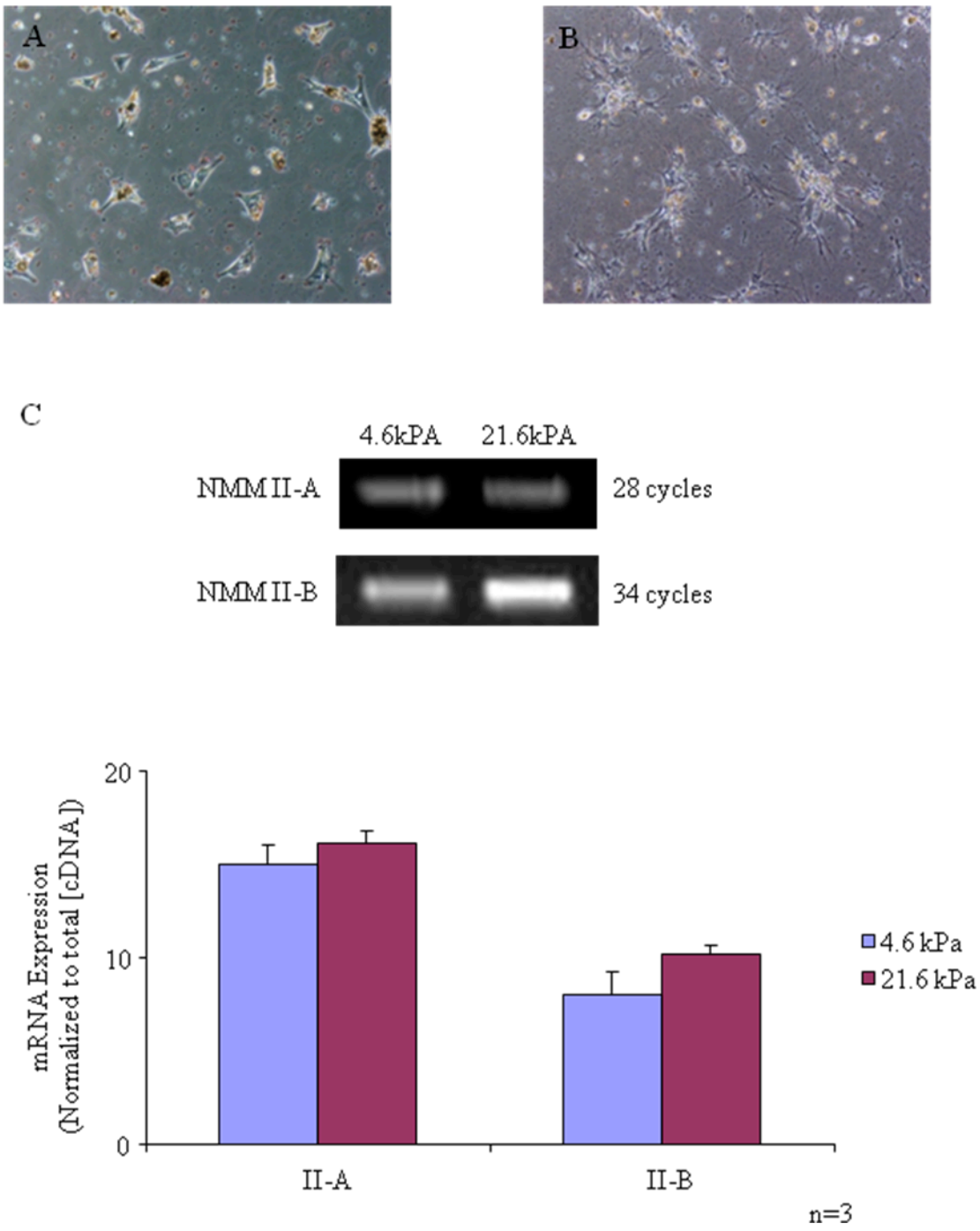

FIGURE 3.14: NMM II Isoform Expression is Regulated by Matrix Stiffness. As seen in normal liver conditions (liver stiffness ~ 4.6 kPa), day 5 culture-activated HSCs maintain quiescent phenotype (A), while cells seeded onto 'fibrotic' substrates (liver stiffness ~ 21.6 kPa) display myofibroblastic morphology (B). Cells were lysed for RT-PCR analysis; NMM II-B expression of cells seeded onto 'fibrotic' substrate was increased significantly (C).

CHAPTER 4: GENETIC INHIBITION OF NONMUSCLE II ISOFORMS IN THE HEPATIC STELLATE CELL

4.1 INTRODUCTION

Regulation of the liver microcirculation is a complex system where blood flow is under systemic and sinusoidal control. In a healthy liver, the quiescent HSC stores vitamin A, produces collagen for basement matrix remodeling and wraps around sinusoids, which regulates sinusoidal diameter, and thus blood flow, by contracting and dilating in response to local vasoactive modulators. In a damaged liver the HSC undergoes a transdifferentiation process resulting in multiple phenotypic and genotypic changes, which coordinate the contractile, migratory and proliferative phenotype of the activated HSC. Upon a fibrogenic stimulus, such as excessive alcohol intake, increased oxidative stress stimulates HSC activation. The activated HSC produces excessive collagen, loses vitamin A stores and disrupts liver microcirculation by exerting a sustained contractile force on the sinusoid, thus contributing to increased intrahepatic vascular resistance and portal hypertension. This hypercontractile phenotype of the activated HSC is associated with increased myosin II activity within the cell [32].

Myosins are a large super-family of molecular proteins that play important cellular roles in contraction, cytokinesis, motility and trafficking. Specifically, myosin II is responsible for generating contractile forces [149]. Myosin II was first identified and characterized in skeletal muscles; however, related classes of myosin II have been identified in cardiac, smooth and nonmuscle cells [149].

Three isoforms of NMM II (II-A, II-B and II-C) differ in the sequence analysis of the catalytic motor domain which allows for fine-tuning of specific cellular functions [190]. NMM II-B has a higher ADP affinity, thus spends the majority of its kinetic cycle bound to actin, while NMM II-A spends a smaller fraction of its kinetic cycle attached to actin [190]. The slower ADP release and long attachment time to actin make NMM II-B an ideal candidate for long term force maintenance, while the faster NMM II-A may be involved in the rapid tension generation [186]. In addition to variations in kinetic properties, the isoforms demonstrate varying expression levels in HSCs (FIGURES 3.7 and 3.9). While NMM II-A mRNA expression is higher in quiescent cells compared to II-B and II-C, expression of II-B increases 55% over days in culture, as compared to a 28% increase of II-A.

Genetic mutations of NMM II-A and II-B are lethal in mice due to cardiac and brain defects, indicating that these isoforms are functionally necessary [212-214]. Additionally, the cellular localization and kinetic properties of NMM II-A and II-B suggest that these isoforms are involved in specific functions, such as migration and contraction. NMM II null cells derived from embryos have impaired migratory and contractile properties [215, 216]. Additionally, siRNA-mediated knock-down of NMM II isoforms in neurons [213], cancer cells [217, 218] and fibroblast [219] modulate contraction and migration. Since the activated HSC phenotype closely resembles fibroblast cells, using siRNA-mediated knock-down of NMM II isoforms in HSCs would be a suitable approach to antagonize the contractile, migratory and proliferative activated phenotype. Therefore, the purpose of this study was to determine if hypercontraction, migration and proliferation of activated HSCs are associated with modulation of specific

NMM II isoform expression during culture-activation and whether each isoform contributes to a certain cellular function.

4.2 RESULTS

4.2.1 Human HSC cell line, LX-2, as a model of HSC contraction

One important limitation in studying cellular function in primary HSC cultures is transfection efficiency. To address this difficulty, Xu et al. established the human hepatic cell line, LX-2, which recaptures the activated phenotype of HSCs [220]. LX-2 cells retain the typical characteristics of activated HSCs such as upregulated platelet-derived growth factor, transforming growth factor (β1) and fibrogenic pro-collagen (α1) expression, making them a suitable tool for *in vitro* studies of human hepatic fibrosis. Previous studies suggest that LX-2 cells respond to fetal bovine serum-stimulated contraction of collagen lattices; however, direct measurements were not reported [120].

In order to determine if human LX-2 cells retain the hypercontractile properties of day 5 culture-activated rat HSCs, we used a collagen contraction assay (Section 2.4) to test the effects of ET-1 on LX-2 cellular contraction. LX-2 cells grown to confluency were trypsinized and seeded onto prepared collagen lattices. Cell concentrations between 2.5×10^5 and 5.0×10^5 cells were tested to determine optimal cell number (FIGURE 4.1). Cells were serum starved for 24 hours and subsequently treated with ET-1 (1nM). As compared to ET-1 induced contraction of HSCs, LX-2 cells did not induce collagen lattice contraction after 24 hours. HSCs are most responsive to ET-1 on day 5 and the contractile proteins, αSMA, myosin II and ET_A and ET_B receptors, are not expressed in abundance until day 5 [208]. Thus it may be possible that the LX-2 cell line, which most closely emulates the fully activated HSCs (day 14) phenotype may not express the

contractile proteins necessary to induce a change in collagen lattice diameter. Although transfection of small interfering RNA (siRNA) to inhibit NMM II isoform expression may be more efficient and clinically relevant in the human LX-2 cell line as compared to rat primary cell cultures, we would be unable to determine significant differences in cellular contraction attributed to isoform knock-down.

4.2.2 Transient transfection of GAPDH and NMM II isoforms in primary HSCs

To determine if we could utilize siRNA-mediated knock-down of gene expression in primary HSC cultures, we transiently transfected day 3 culture-activated HSCs with glyceraldehyde 3-phosphate dehydrogenase (GAPDH) siRNA for 48 hours. Scramble siRNA that has no significant homology to any know gene sequence was used as a negative control. Preliminary studies were carried out to determine optimal lipofectamine reagent volume and siRNA concentration (FIGURE 4.2). RT-PCR measurements indicated that HSCs incubated with 10 μl of lipofectamine and 300 nM GAPDH siRNA optimally down-regulated the expression of GAPDH mRNA expression (FIGURE 4.3).

To demonstrate that we can inhibit a specific NMM II isoform in primary rat cultures, HSCs were transiently transfected with increasing doses of NMM II isoform siRNAs. Six permutations of these genes were transfected into the cells to determine if more than one gene can be down-regulated at the same time (II-A, II-B and II-C only; II-A and II-B, II-A and II-C, II-B and II-C). Preliminary studies were carried out to identify optimal siRNA duplexes (TABLE 2.8) and concentration for each isoform.

To determine optimal duplexes and concentrations for the NMM II-A isoform, day 3 culture-activated HSCs were incubated with increasing doses (50-100 nM) of NMM II-A siRNA duplex #1 or #2 for 48 hours (Section 2.12.2). As determined by RT-

PCR, HSCs transfected with siRNA specific to NMM II-A duplex # 2 resulted in a 53% inhibition of mRNA expression using 100nM concentration compared to the cells transfected with a scramble siRNA (FIGURE 4.4A). RealTime PCR measurements also confirmed these results, as NMM II-A siRNA duplex #2 resulted in a 60 % reduction in NMM II-A mRNA expression as compared to the negative control (FIGURE 4.4B; Scramble). Additionally, specificity was shown as indicated by no reduction in NMM II-B mRNA expression in cells transfected with NMM II-A siRNA (FIGURE 4.5). Similarly, transfection with NMM II-A siRNA (100nM) showed approximately a 70% reduction in protein expression as measured by Western blot analysis (FIGURE 4.6).

Similar results were obtained for genetic inhibition of NMM II-B isoform in primary HSC cultures. RT-PCR measurements demonstrated that mRNA expression of NMM II-B in HSCs transfected with siRNA specific to NMM II-B duplex #1 was down-regulated 56% as compared to negative control and 84% as determined by quantitative RealTime PCR (FIGURE 4.7). Furthermore, knock-down was specific to the NMM II-B isoform (FIGURE 4.8), as NMM II-A mRNA expression was not inhibited by the NMM II-B siRNA duplex (FIGURE 4.9). Western blot analysis also confirmed protein expression knock-down of the NMM II-B isoform by 56% in HSCs transfected with the specific NMM II-B siRNA duplex.

As previously determined (FIGUREs 3.7 and 3.9), both the mRNA and protein expression levels of NMM II-C were undetected in quiescent and minimal in early culture-activated (day 1) HSCs. RealTime PCR results demonstrated while HSC culture-activation induced significant mRNA expression of NMM II-A and II-B, expression of NMM II-C was variable and not statistically significant. Protein expression of NMM II-C

was also minimally detected at day1 of culture activation. Therefore, it was not surprising that siRNA-mediated knock-down of the NMM II-C isoform in day 3 culture-activated HSCs was undetected (data not shown).

After determining the optimal siRNA duplexes and concentrations of NMM II-A and II-B, we were able to demonstrate the specificity of each siRNA duplex in the six permutations of these genes to determine if more than one gene can be down-regulated at the same time by RealTime PCR. As previously described, day 3 HSCs were transiently transfected with each siRNA alone or in combination with a second siRNA duplex. RealTime measurements indicate that mRNA expression down-regulation was specific in each instance as compared to the negative control (FIGURE 4.10). Successful knock-down of NMM II-A and II-B with siRNA would therefore allow us to associate NMM II isoform expression with a particular cell function, such as contraction, migration and/or proliferation.

4.2.3 Functional assays to determine NMM II isoform function

Our lab has previously shown that the myosin II inhibitor, blebbistatin, can inhibit the contractile properties of HSCs. Furthermore, Melton et al. reported that blebbistatin directly inhibits HSC migration [45]. Myosin II molecules of higher organisms can be subdivided in four categories: skeletal, cardiac, smooth and nonmuscle. Since HSCs are nonmuscle cells, we determined the functional roles these myosin isoforms play in cellular contraction, migration and proliferation.

To determine the effect of genetic inhibition of NMM II isoforms on HSC cellular function, we used contraction, migration and proliferation assays previously described (Section 2.13). For contractility assessment, HSCs were transiently transfected on day 3

of culture-activation, as shown previously, and allowed to recover overnight. Cells were subsequently treated with ET-1 for 24 hours (at this point cells were day 5 of culture-activation). The optimal concentration of ET-1 (1nM), as previously determined (FIGURE 3.2), was used to induce contraction of the collagen lattices. The effects of genetic inhibition of NMM II isoforms was determined by the changes in gel circumference after 24 hours and contraction rate, as compared to negative control (Scramble). The rate of contraction was measured by calculating changes in collagen lattice diameter at different time points (0, 0.5, 1, 1.5, 2 and 24 hours).

The motor properties of NMM II-B indicate that it is kinetically tuned to be more hypercontractile than NMM II-A [14]; therefore, we concentrated our preliminary studies on understanding the role of NMM II-B in sustained HSC contraction. However, contraction assay results indicated that siRNA-mediated knock-down of NMM II-B did not alter basal or ET-1 induced contraction of HSCs at optimally determined siRNA concentration of 100nM after 24 hours (FIGURE 4.11). In an attempt to optimize contraction assay for knock-down experiments we altered the *in vitro* assay by increasing siRNA concentration; however, this also had no effect on HSC contraction. We therefore tested selected (II-A, II-B, II-C only; II-A and II-B) permutations of the NMM II isoforms to determine if other isoforms or a combination of isoforms would have an effect. Again, siRNA-mediated knock-down of selected permutations did not have an effect on basal or ET-1 induced HSC contraction (FIGURE 4.12). Finally, we tested the effect of these knock-down permutations by altering the previously determined collagen concentration of the assay and the cell number; however, both alterations had no effect on siRNA mediated knock-down of NMM II isoform HSC contraction (FIGURE 4.13 and

4.14). We also tested the effect of longer transient transfection incubation periods (48 and 72 hours post-transfection), as previous studies have shown an increase in transfection efficiency [221]; however, these results also demonstrated no change in contraction (FIGURE 4.15).

Since kinetic evidence has suggested that NMM II-A may responsible for initial force generation of the cell rather than sustained contractile tension, we also measured the rate of basal and ET-1 induced contraction (FIGURE 4.16). Again, day 3 HSCs were transiently transfected with siRNA permutations or scramble siRNA and allowed to incubate for 24 hours. The cells were treated with ET-1 and contraction rate was measured by calculating changes in collagen lattice diameter at six different time points. All siRNA permutations tested did not alter the contraction rate of HSCs as compared to scramble.

Earlier days of culture-activation (day 5) were again used for migration and proliferation analyses since later stages of activation (day 14) result in slower migration and decreased proliferation. To determine the effect of genetic inhibition on migration, plate-scrape model of migration was performed. Cells were cultured for three days and subsequently transfected with the respected siRNA. After 48 hours, a cleared zone was created across the plate and images were immediately captured in four locations per plate. Twenty-four hours later, images were taken in the same locations and assessed for the number of cells that migrated and distance traveled into the ‘damaged area’ (cleared zone). As compared to negative control (Scramble), all isoform permutations seemed to have impaired migratory properties (FIGURE 4.17). Significant effects were seen in both II-A, II-B and II-C alone and II-A/-B, and II-B/-C combinations; indicating that all three

isoforms are necessary for HSC migration. Additionally, these results demonstrated that isoform inhibition of a single gene cannot be compensated for by another isoform for normal HSC migration.

For proliferation analysis, cells were treated as described for migration assays and direct cell counts were performed. siRNA targeted against NMM II-B in a fibroblast cell line impairs cytokinesis and thus cellular proliferation [221], siRNA-mediated knock-down of all six permutations of NMM II isoforms had no effect on proliferation as compared to the negative control (FIGURE 4.18).

Overall, our results indicate that primary HSC cultures can be successfully transfected with siRNA targeted against NMM II-A and II-B. Additionally, inhibition of these isoforms alone or in combination with other isoforms can affect HSC migration; thereby suggesting a functional role of these genes in cellular migration necessary for tissue repair during hepatic fibrosis.

4.3 DISCUSSION

Chronic liver disease is the 12th leading cause of death in the United States as it accounts for nearly 30,000 deaths per year (CDC, National Center for Health Statistics, 2005). Besides removal of insult, liver transplantation remains the only effective treatment for end-stage liver disease; however, a huge gap remains between the number of people in need of a liver transplant and the number of organs available. As the disease progresses, complications may arise such as: jaundice, hepatic encephalopathy, and/ or portal hypertension. Portal hypertension is characterized by both increased portal blood flow and augmented intrahepatic vascular resistance. It not only perpetuates insult to the hepatic tissue by depleting oxygen to the cells, but also gives rise to esophageal varicies

and ascites. If left untreated, variceal bleeding can lead to hemorrhage and death in a significant proportion of patients, as it accounts for 20-50% in-hospital mortality [28]. Treatment of cirrhosis generally focuses on preventing progression and complications of the disease to improve quality of life and prolong survival of patients awaiting transplantation by treating esophageal varicies and ascites. Therapeutics directed at restoring proper hepatic microcirculation may also provide an additive benefit.

HSCs are the main contributors of intrahepatic resistance in the liver as evidence has demonstrated that the average force generated by ET-1-induced contraction of a single HSC is 14000 dyn/cm^2 [15]. Endothelin-1 receptor antagonist (ERA) improves both collagen accumulation and portal hypertension in animal models of fibrosis. Since endothelin receptors are present on all smooth muscle cells, clinical studies have not provided statistically significant evidence to support the efficacy of ERA in the treatment of portal hypertension [222, 223]. Our previous findings have shown that three different isoforms of NMM II (II-A, II-B and II-C) are upregulated in the activated HSC, thus providing three potentially different targets for modulation. Understanding the functional roles of each NMM II isoform may be beneficial in modulating the overcompensating role HSCs play in liver fibrosis.

Genetic mutations in the NMM II-A gene coincided with the autosomal dominant giant-platelet disorders: May Hegglin anomaly, Fechtner syndrome, Epstein Syndrome and Sebastian syndrome [191]. In order to more closely examine the cellular role of each isoform, multiple genetic studies have been employed. Using targeted gene disruption to knockout NMM II-B in murine embryos, Tullio et al. showed that the majority of the homozygous embryos died in utero and the remaining pups died within 24 hours due to

cardiac and brain defects [214, 224]. Furthermore, mutations in the NMM II-C gene were linked to hearing loss as indicated by decreased auditory brainstem responses, indicating that this isoform is also functionally necessary [192].

In an attempt to identify the cellular proteins responsible for increased contraction, migration and proliferation in the activated HSC, this study examined the effects of genetic inhibition of each NMM II isoform *in vitro*. Using siRNA-mediated knock-down our results indicated that both mRNA and protein expression of NMM II-A and II-B were significantly down-regulated in day 5 culture-activated HSCs. As previously characterized (FIGURES 3.7 and 3.9), NMM II-C expression was minimally detected in early days of HSC culture-activation; therefore, it was not surprising that siRNA-mediated knock-down of this isoform was indeterminable. Additionally, inhibition of each isoform alone (II-A, II-B or II-C) or in combination with a second isoform (II-A/B, II-B/C or II-A/C) was specific to the targeted siRNA duplex (FIGURE 4.10). Successful genetic inhibition of these permutations allowed us to further investigate the role of each isoform using contraction, migration and proliferation assays.

As previously reported, day 5 culture-activated HSCs exhibited a basal contractile phenotype as measured by collagen assay. Additionally, as seen in fibrotic animal models and clinical studies, ET-1 further stimulates the contractile properties of activated HSCs [16, 17]. Therefore, we used a collagen contraction assay to determine the effects of genetic inhibition of NMM II isoforms on basal and ET-1 induced contraction (FIGURE 4.11). Our results indicated that genetic inhibition of each isoform alone or in combination with a second isoform had no effect on basal or ET-1 induced HSC contraction (FIGURE 4.13). These results indicate that although HSCs are nonmuscle

cells, NMM II isoforms may not be the molecular motor responsible for HSC contraction. As an alternative hypothesis, HSCs express a large number of early and late smooth muscle cell markers including smooth muscle (SM) α-actin, SM22α, desmin, SM myosin heavy chain, h1-calponin, h-caldesmon and myocardin; therefore, the smooth muscle myosin II proteins could regulate HSC hypercontracion associated with portal hypertension [201].

HSC proliferation is induced by platelet-derived growth factor (PDGF), which activates the FAK-PI3-K-Akt signaling cascade [132]. Similarly, this signaling pathway is also critical for HSC migration in the activated HSC; however, it has not been determined if these cellular processes are independent. Generally, mitosis is rare in migrating cells; however, specific NMM II isoforms may coordinately regulate these processes in the HSC. Based on a genetic profile of the transdifferentiation process of the HSC (i.e. freshly isolated cells through day 10 of culture-activation), our lab has previously identified days 3-6 of culture-activation to be days in which the cell has a high probability of migrating and proliferating during the activation process *in vitro* as indicated by an increase in mRNA expression of mitotic and migratory genes (Akt, cyclin D1, FAK, RhoA). Therefore, to assess the role of NMM II isoforms during migration and proliferation, we again used day 5 culture-activated HSCs. Although NMM II-A plays a role in proliferation of fibroblasts [219], our results indicated that siRNA-mediated knock-down of all six permutations of NMM II isoforms had no effect on proliferation as compared to the control. More sensitive studies to measure cellular proliferation, such as BrdU incorporation assay, may be needed to detect changes in genetic inhibition related to NMM II.

Using a plate-scrape model of migration, our results demonstrated that genetic siRNA-mediated knock-down of all six permutations of NMM II isoforms had an inhibitory effect on migration. Approximately 25% inhibition was evident for all permutations indicating that all three isoforms unexpectedly play an overlapping role in HSC migration. Previous data demonstrating localization of NMM II-A and II-B in the periphery and cortex of activated HSCs indicated that this isoform may be important for migration and contraction, respectively (FIGURE 3.10). Significant results were obtained for all permutations except II-A /-C in combination indicating that these isoforms coordinately regulate the procession of HSCs towards a chemotactic stimulus. Although we report a significant effect on HSC migration, it has yet to be determined if this would be physiologically relevant *in vivo*.

Previous data demonstrating localization of NMM II-B in the cortex of activated HSCs indicated that this isoform may be important for contraction; however, significant changes were undetected in the assays using isoform knockdown HSCs. Therefore, it may be possible that the level of genetic inhibition was not sufficient to visualize alterations in these properties and the residual NMM II content was adequate for contraction to occur. Furthermore, genetic inhibition of NMM II-C expression was undetermined; suggesting that inhibition of this isoform may be insufficient to delineate cellular function. Future studies will examine alternative strategies to knock-down NMM II isoforms in a Cre-lox recombination system and confirm or dispute these results.

Overall, these studies have begun to delineate the specific roles NMM II isoforms play in HSC contraction, migration and proliferation. These results showed that NMM II isoforms are functionally necessary for normal HSC migration on the specific day (day 5)

in which these cells are needed to contribute to the wound healing response in an injured liver; whereas, contraction and proliferation of HSCs may not be dependent on NMM II expression. While NMM II isoform inhibition may not provide an attractive therapeutic target for regulating portal hypertension, future studies will determine if complete inhibition of the NMM II isoforms or inhibition of other myosin II classes would improve the deleterious effects of HSC hypercontraction seen in hepatic fibrosis.

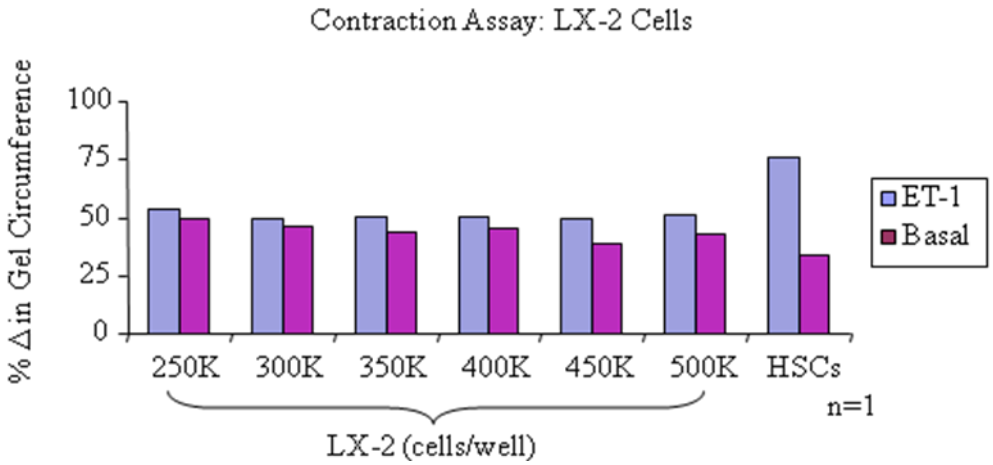

FIGURE 4.1: LX-2 Cells Do Not Respond to ET-1 Treatment. Day 5 culture-activated HSCs and increasing quantities of LX-2 cells were seeded onto collagen lattices and treated with ET-1 (1 nM). As compared HSC contraction, LX-2 cells did not respond to the vasoconstrictor, ET-1 treatment after 24 hours.

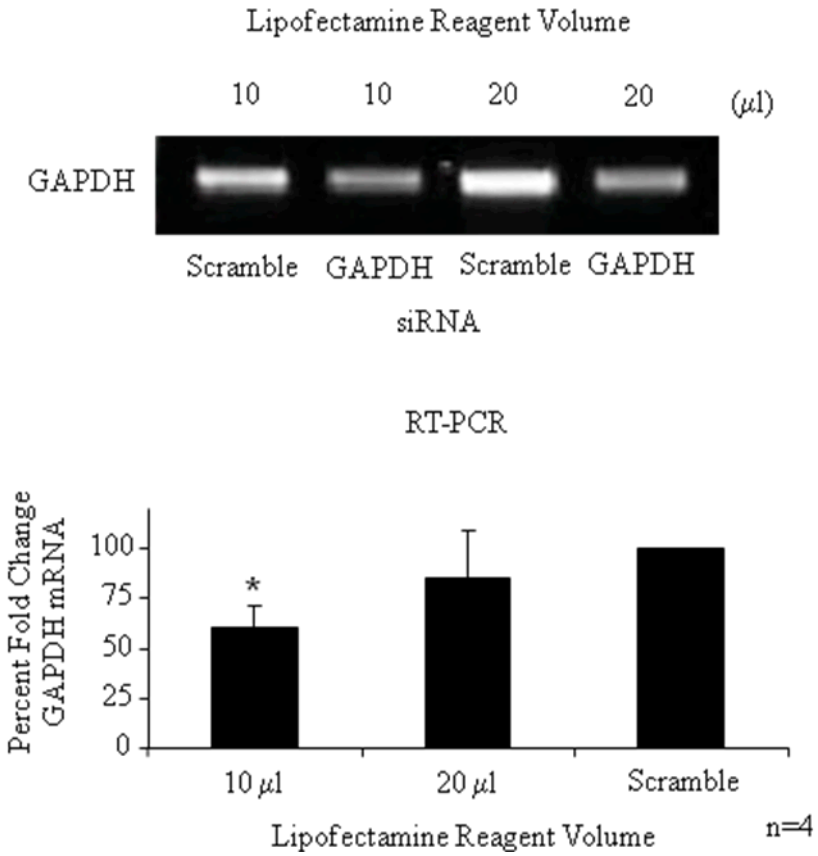

FIGURE 4.2: Lipofectamine Reagent Down Regulated GAPDH mRNA Expression. Day 3 culture-activated HSCs were incubated with GAPDH or scramble siRNA (100nM) and increasing volumes of lipofectamine reagent (10 and 20 μl) for 48 hours. As determined by RT-PCR, the expression of GAPDH mRNA was inhibited by 39% in samples incubated with 10 μl Lipofectamine and GAPDH siRNA as compared to scramble siRNA. (Top panel: representative gel; * $p<0.05$)

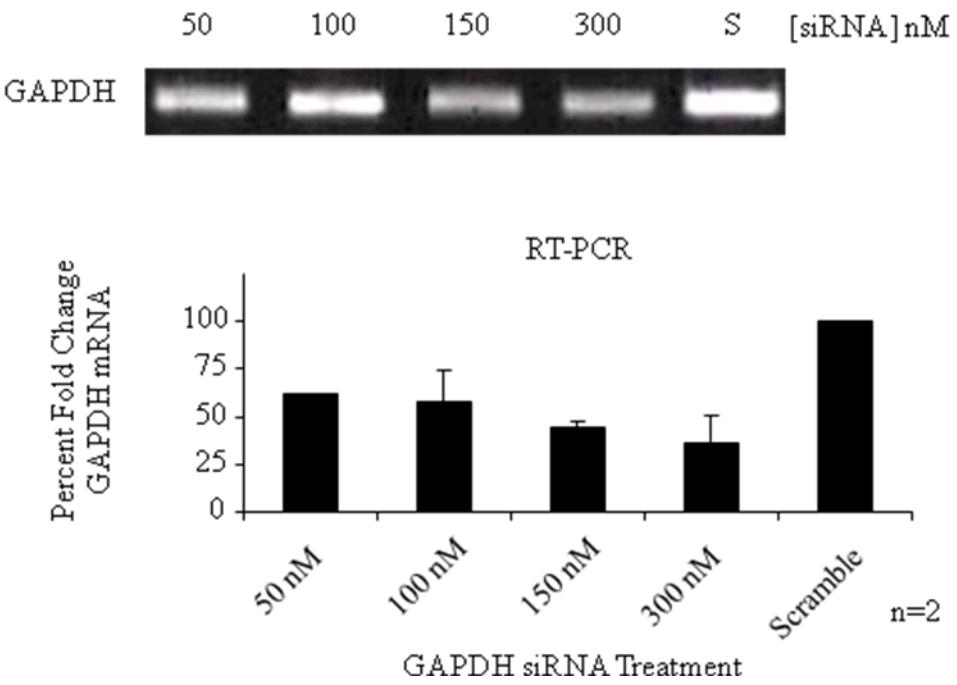

FIGURE 4.3: siRNA Inhibited GAPDH mRNA Expression in HSCs. Day 3 culture-activated HSCs were incubated with either increasing doses (50-300 nM) of GAPDH siRNA or scramble siRNA and lipofectamine reagent (10 μl) for 48 hours. RT-PCR measurements showed the greatest inhibition with 300nM siRNA of GAPDH mRNA expression as compared to scramble siRNA. (Top panel: representative gel)

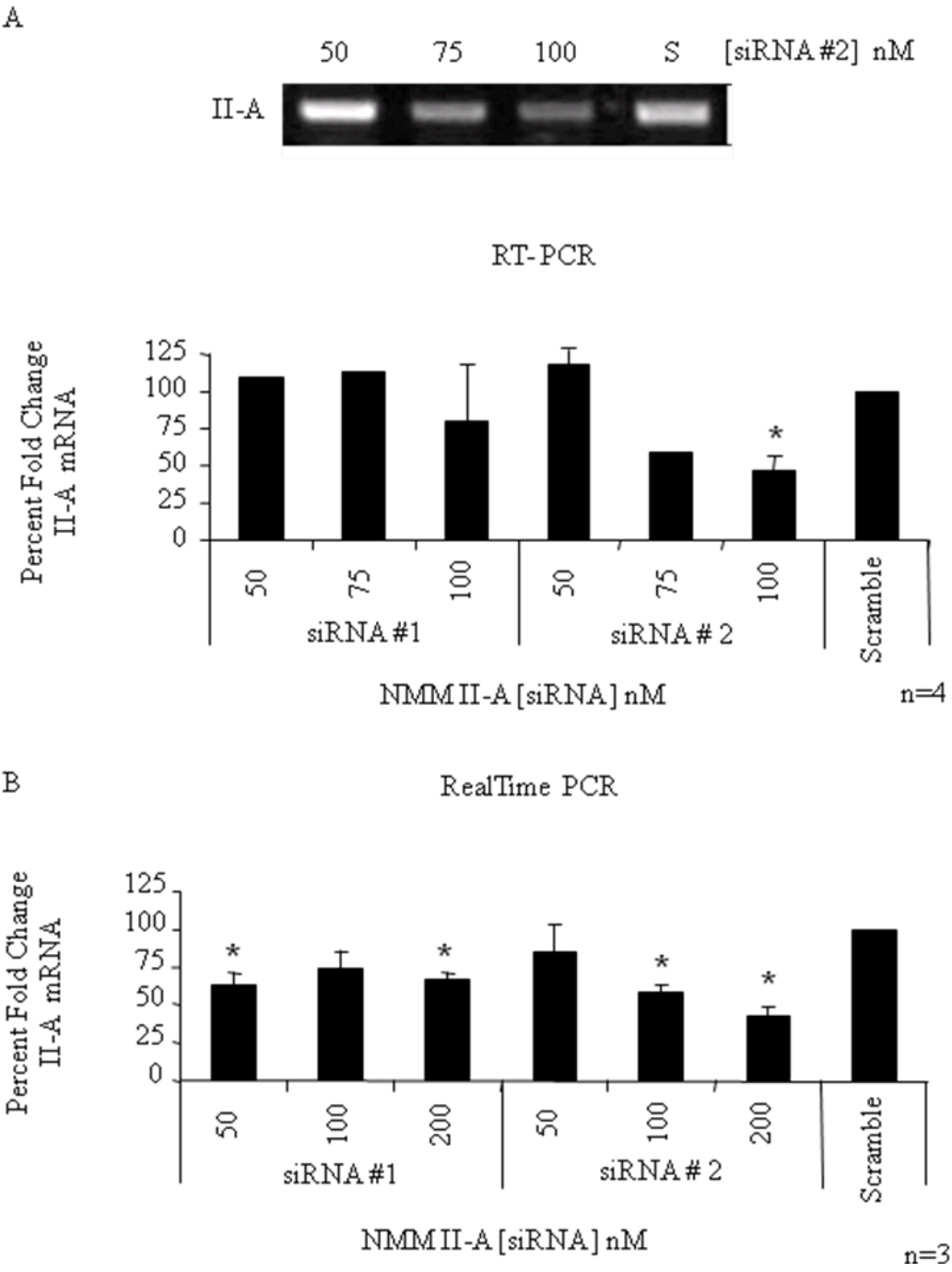

FIGURE 4.4: siRNA (#2) Successfully Down Regulated mRNA Expression of NMM II-A. Day 3 culture-activated HSCs were incubated with either increasing doses of NMM II-A siRNAs (#1 and #2; 50-100 nM) or scramble siRNA and lipofectamine reagent (10 ml) for 48 hours. As compared to the scramble siRNA, the mRNA expression of NMM II-A in samples incubated with 100 nM siRNA (#2) was significantly decreased 53% as determined by RT-PCR (A), and 60% as determined by RealTime PCR (B). (Top panel: representative gel; * $p<0.05$)

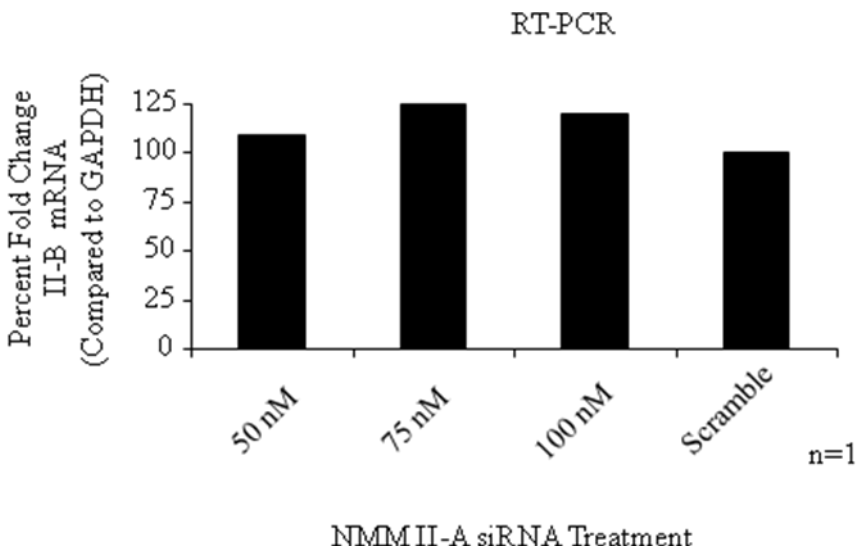

FIGURE 4.5: Specific Genetic Inhibition of NMM II-A. Day 3 culture-activated HSCs were treated with increasing doses (50-100nM) of NMM II-A siRNA or scramble siRNA and lipofectamine reagent (10 ml) for 48 hours. RT-PCR measurements indicated that NMM II-A siRNA did not inhibit NMM II-B expression as compared to the scramble.

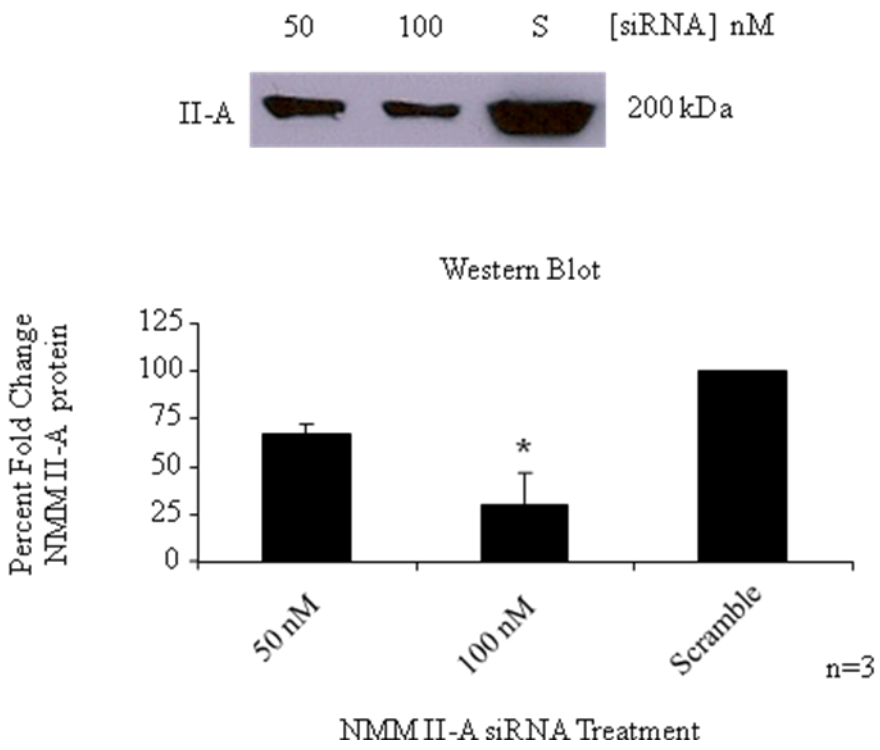

FIGURE 4.6: siRNA Inhibited NMM II-A protein expression. Day 3 culture-activated HSCs were incubated with increasing doses (50 and 100nM) of NMM II-A siRNA or scrambled siRNA and lipofectamine reagent (10 μl) for 48 hours. Whole cell extracts were isolated and subjected to actin selection. Protein complexes were run on a SDS 8% polyacrylamide gel and probed with an antibody for NMM II-A (1:1000; Covance). Western blot analysis indicated that siRNA inhibited NMM II-A expression by 70% as compared to scramble. (Top panel: representative Western blot; * $p<0.05$)

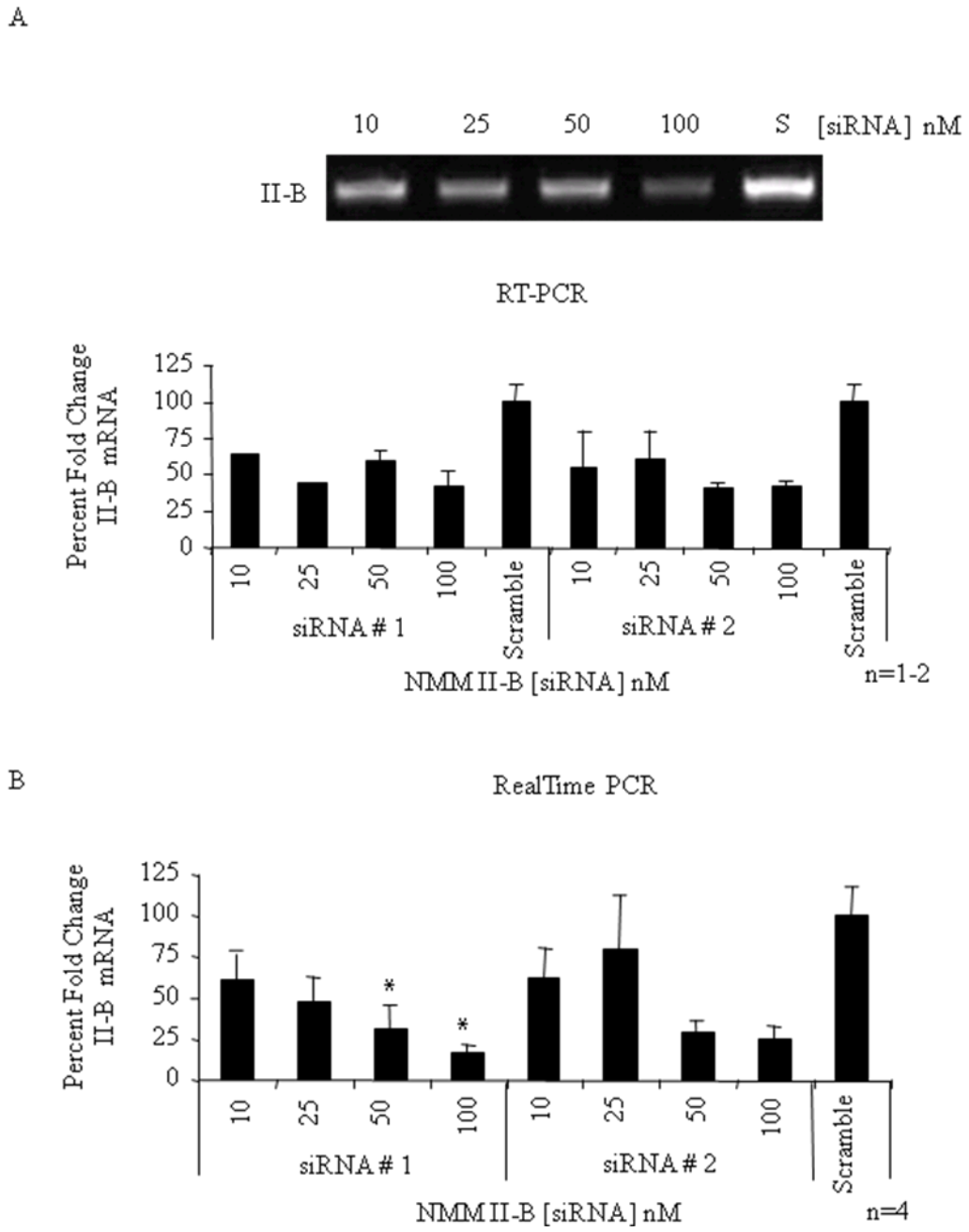

FIGURE 4.7: siRNA (#1) down regulated mRNA expression of NMM II-B. Genetic Inhibition of NMM II-B: siRNA (#1) successfully down regulated mRNA expression. Day 3 culture-activated HSCs were incubated with either increasing doses of NMM II-B siRNAs (#1 and #2; 10-100 nM) or scramble siRNA and lipofectamine reagent (10 ml) for 48 hours. As compared to the scramble siRNA, the expression of NMM II-B mRNA in samples incubated with 100 nM NMM II-B siRNA (#1) was significantly decreased 58% as determined by RT-PCR (A), and 75% as determined by RealTime PCR (B). (Top panel: representative gel; * $p<0.05$)

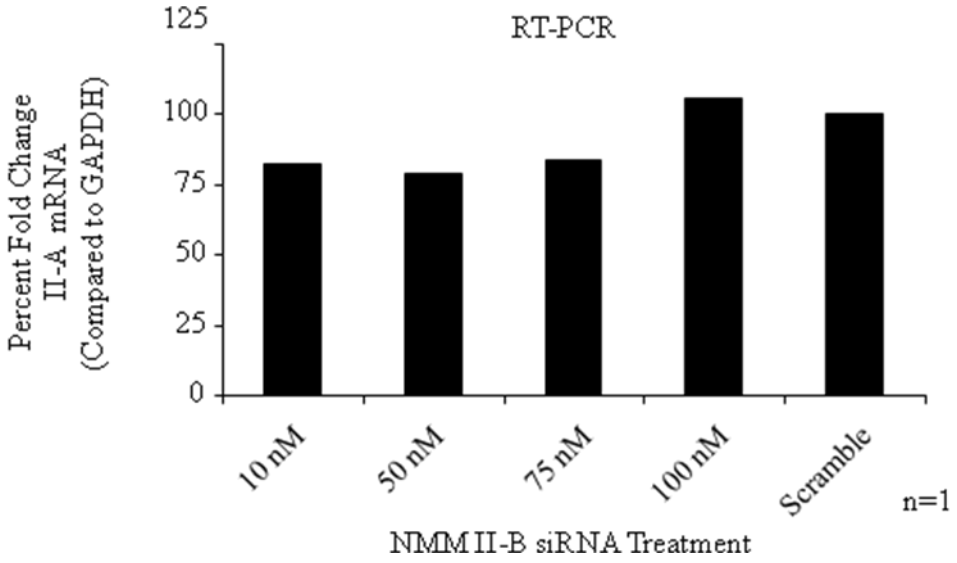

FIGURE 4.8: Specific Genetic Inhibition of NMM II-B. Day 3 culture-activated HSCs were treated with increasing doses (10-100nM) of NMM II-B or scramble siRNA for 48 hours. RT-PCR measurements indicated that siRNA did not inhibit NMM II-A expression as compared to the scramble.

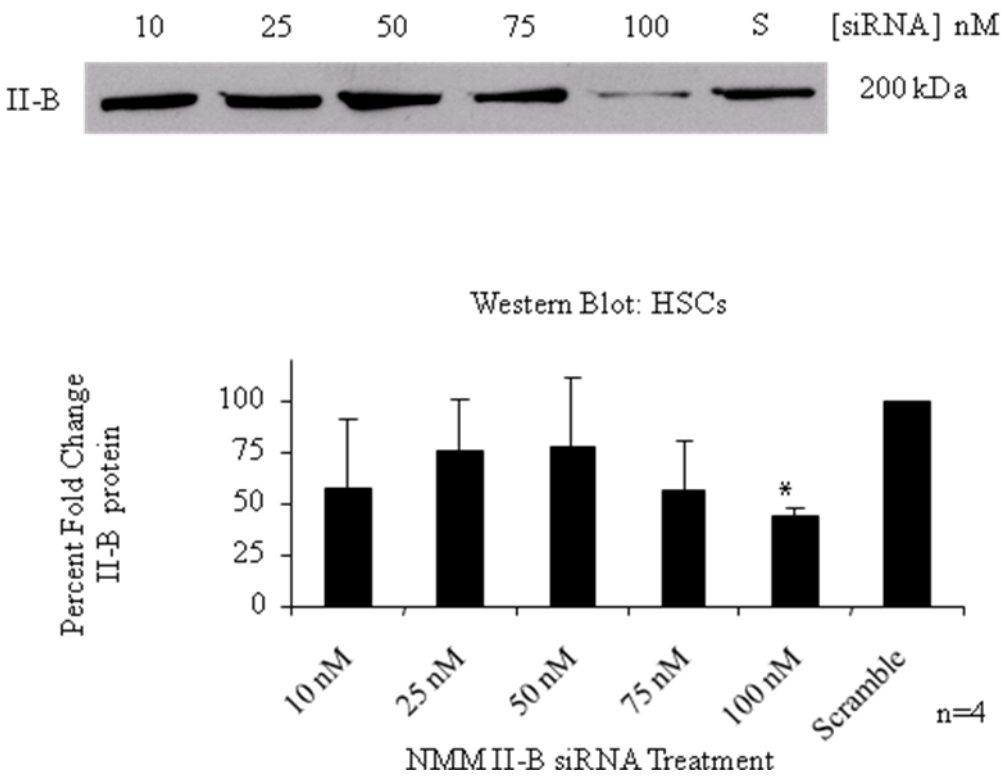

FIGURE 4.9: siRNA Inhibited NMM II-B protein expression. Day 3 culture-activated HSCs were treated with increasing doses of NMM II B (10-100 nM) siRNA or scramble siRNA for 48 hours. Whole cell extracts were isolated and subjected to actin selection. Protein complexes were run on a SDS 8% polyacrylamide gel and probed with an antibody for NMM II-B (1:1000; Covance). Western blot analyses indicate that siRNA inhibits NMM II-B expression 56% as compared to scramble. (Top panel: representative Western blot; * $p<0.05$)

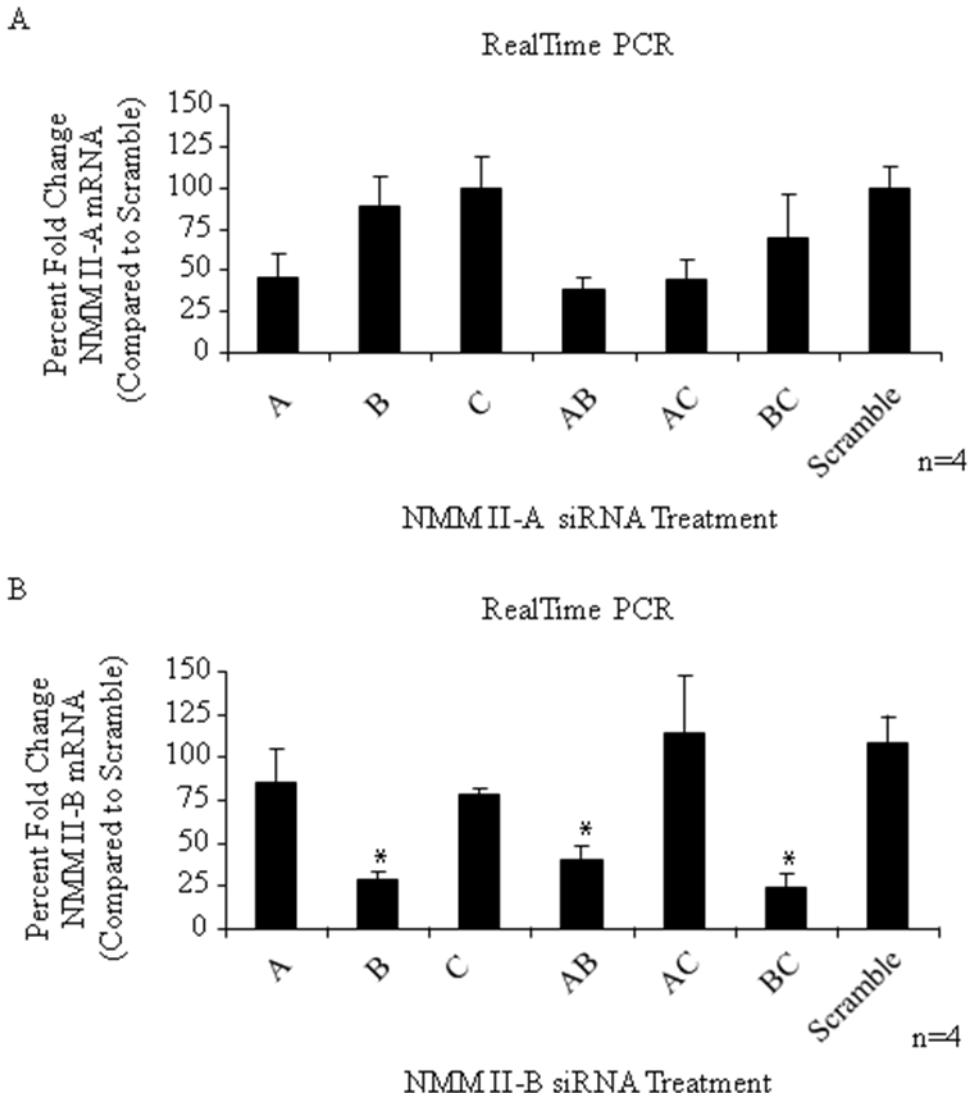

FIGURE 4.10: Specific Genetic Inhibition of NMM II Isoform Permutations. NMM II mRNA was inhibited and specific to targeted gene. Day 3 culture-activated HSCs were incubated with either permutations of siRNAs (II-A, II-B and II-C alone; II-A/-B, II-A/-C and II-B/-C) or scramble siRNA and lipofectamine reagent (10 ml) for 48 hours. (A) As compared to the scramble siRNA, the mRNA expression of NMM II-A was significantly decreased 55%, 40% and 44% in samples incubated with II-A alone, II-A/-B, II-A/ -C and II-B/C, respectively, while expression of NMM II-A remained constant in remaining samples. (B) Similar results were obtained for siRNA-mediated down-regulation of NMM II-B. Expression levels of II-B alone, II-A/-B, II-B/-C were 71%, 60% and 75% respectively, while expression of II-B in remaining samples were unchanged as compared to control. (* $p<0.05$)

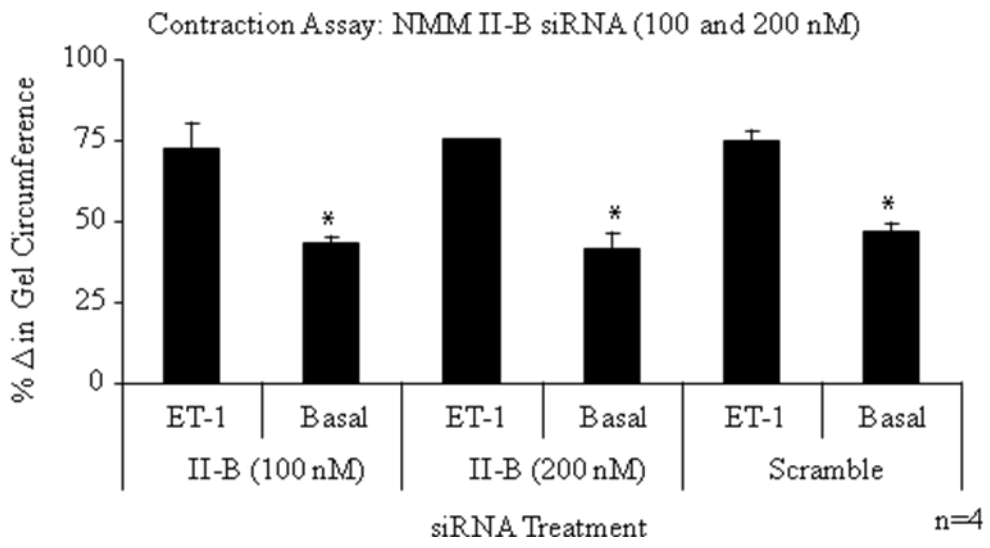

FIGURE 4.11: NMM II-B siRNA Does Alter Basal or ET-1 Induced Contraction of HSCs. Day 3 HSCs were transiently transfected with siRNA targeted to NMM II-B isoform and allowed to incubate for 24 hours. The cells were trypsinized, 100K cells seeded onto collagen lattices and serum starved for 24 hours and subsequently treated with ET-1. While expression of NMM II-B was shown to be down-regulated by II-B siRNA (100nM), it did not decrease basal or ET-1 induced contraction after 24 hours as compared to samples treated with scramble siRNA. Similar results were obtained when siRNA concentrations were increased to 200 nM. (* $p<0.05$)

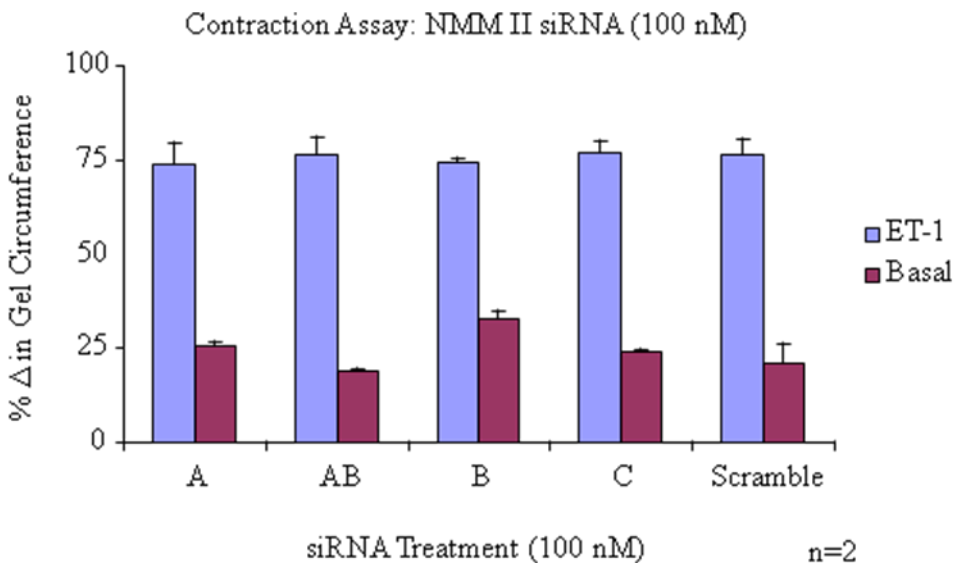

FIGURE 4.12: NMM II-A/-B/-C or II-A and -B siRNA Does Not Alter Basal or ET-1 Induced Contraction of HSCs. Day 3 HSCs were transiently transfected with siRNA targeted to NMM II-A, II-B and II-C alone, II-A/-B in combination or scramble siRNA and allowed to incubate for 24 hours. The cells were trypsinized and 100K cells seeded onto collagen lattices overnight, serum starved for 24 hours and subsequently treated with ET-1 (1nM). All siRNA permutations tested did not decrease basal or ET-1 induced contraction of HSCs as compared to scramble.

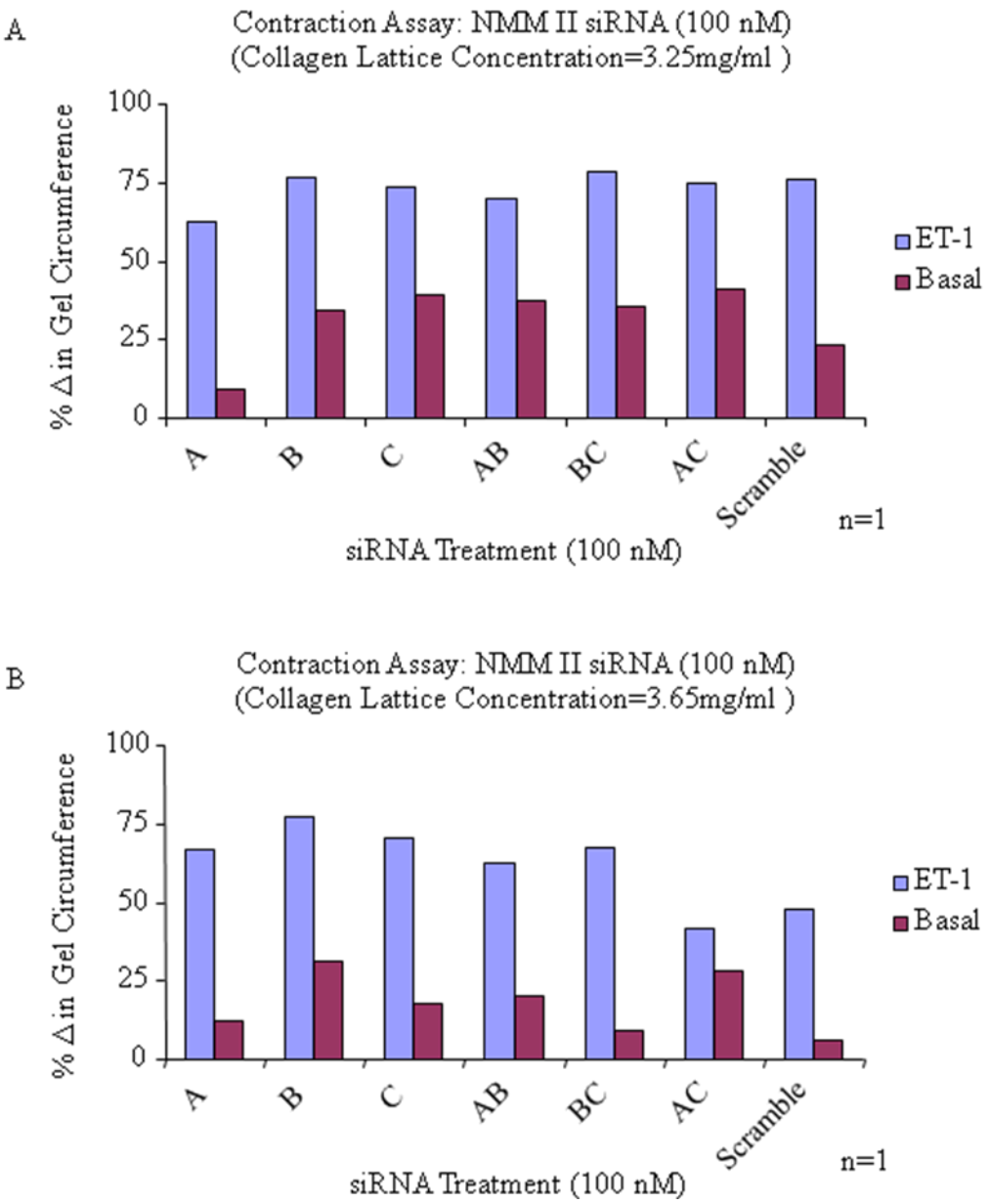

FIGURE 4.13: siRNA Treatment Does Not Alter Basal or ET-1 Induced Contraction of HSCs on Less Stiff Collagen Matrix. Day 3 HSCs were transiently transfected with siRNA targeted to NMM II-A, II-B and II-C alone, II-A/-B, II-B/-C and II-A/-C in combination or scramble siRNA and allowed to incubate for 24 hours. The cells were trypsinized and 100K cells seeded onto collagen lattices of varying concentrations (3.25 or 3.65 mg/ml) overnight, serum starved for 24 hours and subsequently treated with ET-1. All siRNA permutations tested did not decrease basal or ET-1 induced contraction of HSCs as compared to scramble.

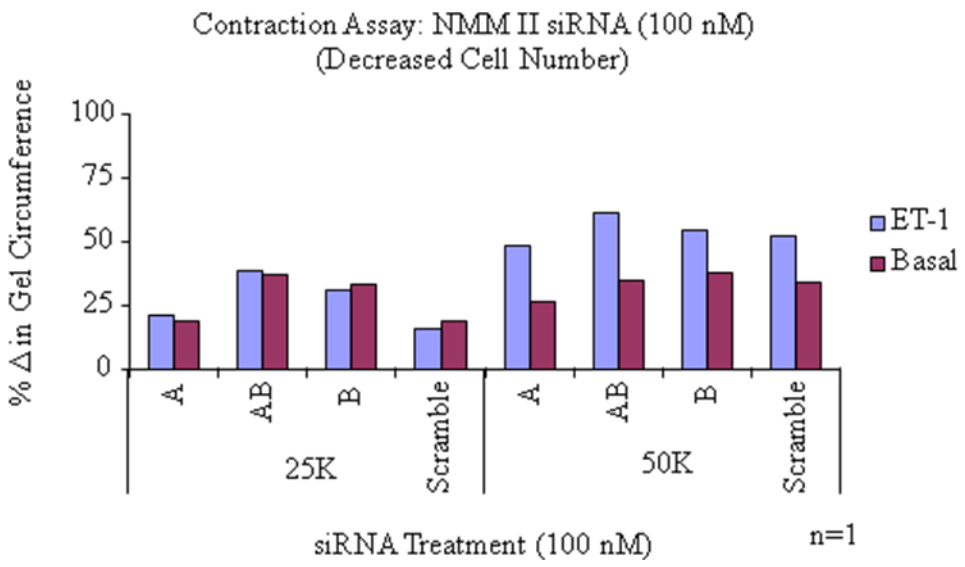

FIGURE 4.14: Decreased Cell Concentration Does Not Alter Contraction of HSCs Treated with siRNA. Day 3 HSCs were transiently transfected with siRNA targeted to NMM II-A, II-B and II-C alone, II-A/-B in combination or scramble siRNA and allowed to incubate for 24 hours. The cells were trypsinized, 100K cells seeded onto collagen lattices overnight, serum starved for 24 hours and subsequently treated with ET-1 (1nM). All siRNA permutations tested did not decrease basal or ET-1 induced contraction of HSCs.

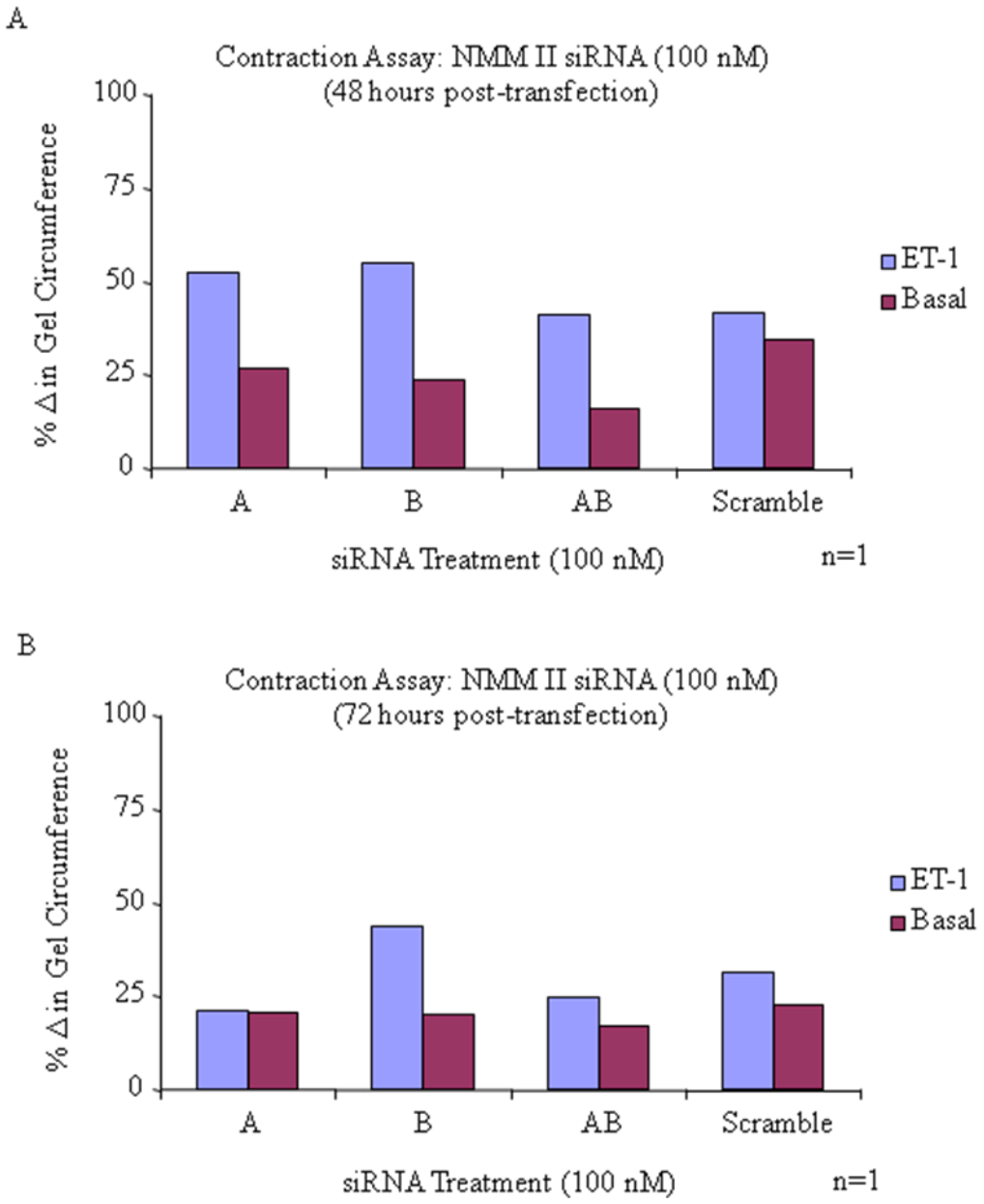

FIGURE 4.15: Increased Transfection Incubation Does Not Alter Basal or ET-1 Induced Contraction of HSCs treated with siRNA. Day 3 HSCs were transiently transfected with siRNA targeted to NMM II-A, II-B and II-C alone, II-A/-B in combination or scramble siRNA and allowed to incubate for 48 (A) or 72 (B) hours. The cells were trypsinized, 100K cells seeded onto collagen lattices overnight, serum starved for 24 hours and subsequently treated with ET-1 (1nM). All siRNA permutations tested did not decrease basal or ET-1 induced contraction of HSCs.

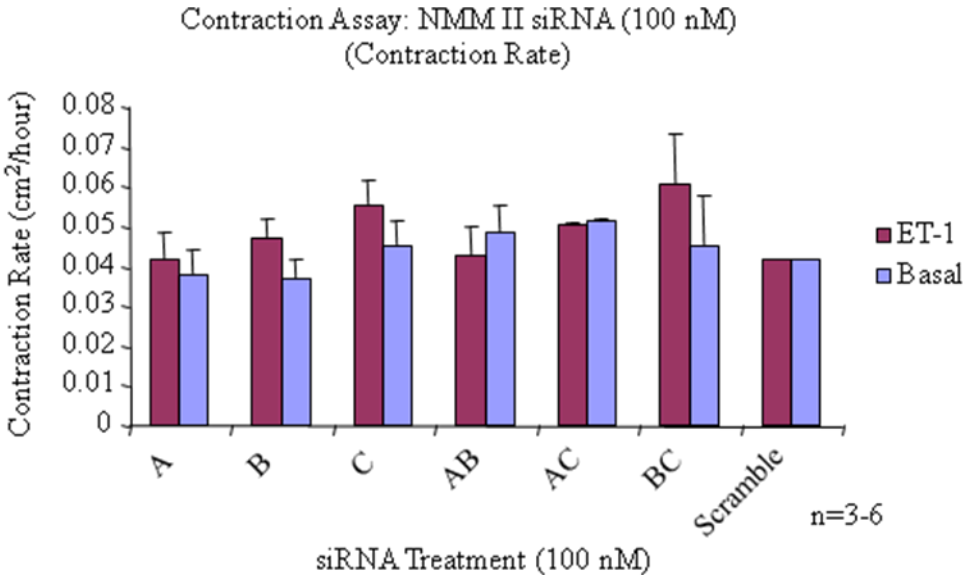

FIGURE 4.16: siRNA Treatment Does Not Alter Basal or ET-1 Induced HSC Contraction Rate. Day 3 HSCs were transiently transfected with siRNA targeted to NMM II-A, II-B and II-C alone, II-A/-B, II-B/-C and II-A/-C in combination or scramble siRNA and allowed to incubate for 24 hours. The cells were trypsinized, seeded onto collagen lattices overnight, serum starved for 24 hours and subsequently treated with ET-1. All siRNA permutations tested did not alter the contraction rate of HSCs as compared to scramble.

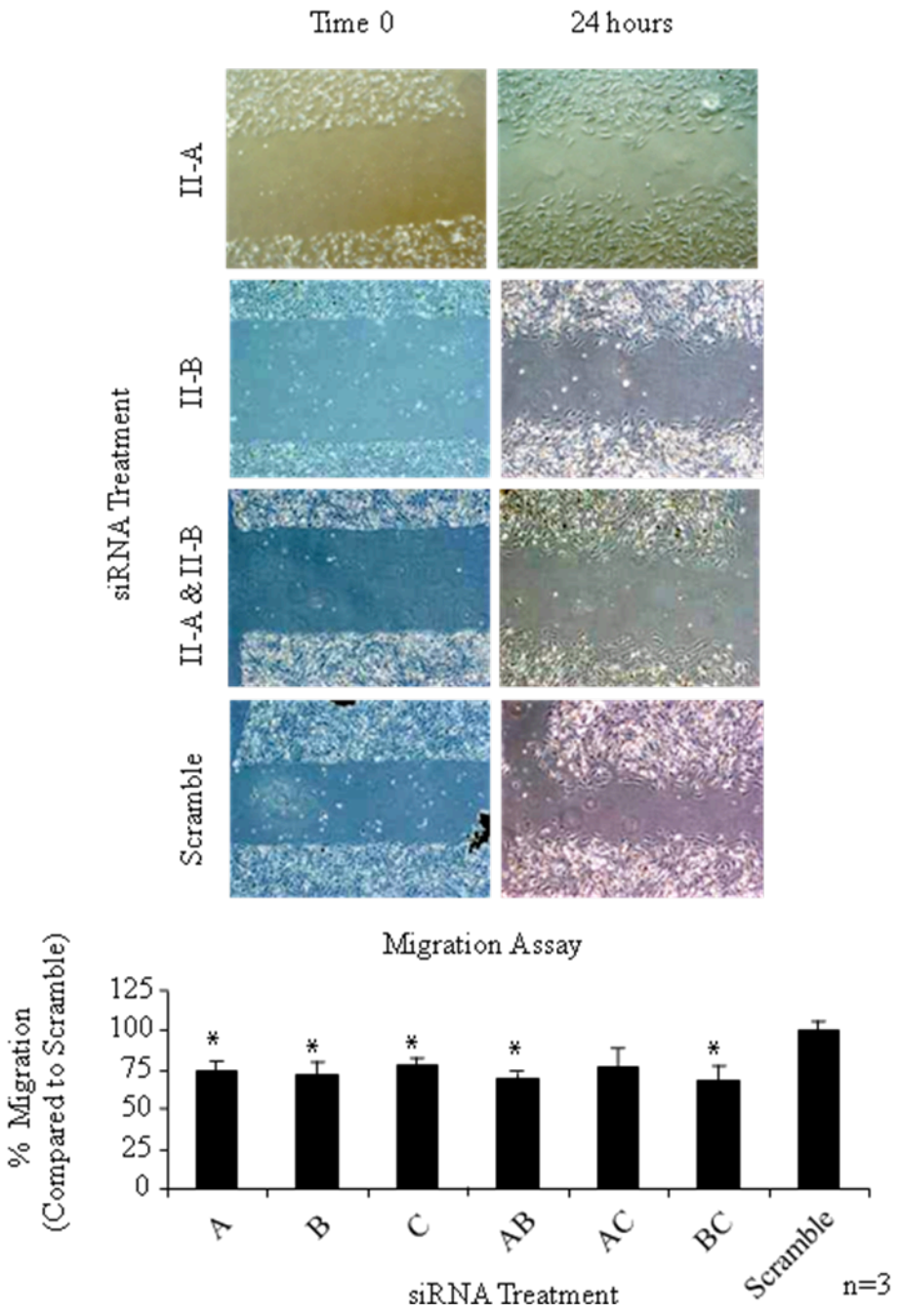

FIGURE 4.17: NMM II Modulates HSC Migration. Day 3 HSCs were transiently transfected with siRNA targeted to all NMM II permutations or scramble siRNA and allowed to incubate for 48 hours. A 10 μl pipet tip was used to create a cleared area. Images were immediately taken and the cells were incubated overnight. After 24 hours, images were again taken to determine percentage of cells migrated into the cleared area. Migration was calculated as distance travelled over time. All siRNA permutations tested except II-A/-C combination were statistically decreased as compared to scramble. (Top panel: representative micrographs; * $p<0.05$)

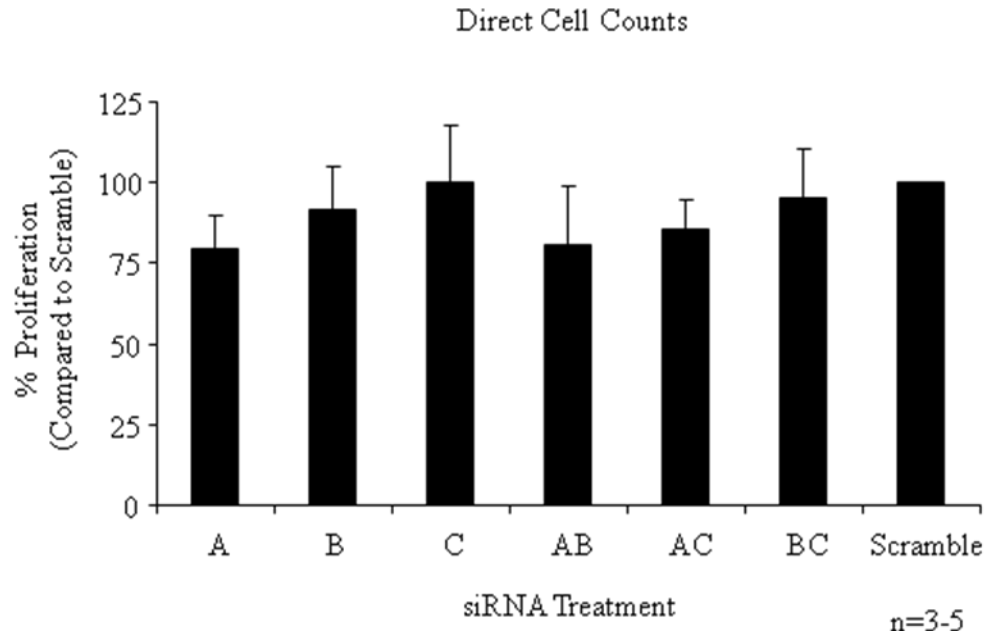

FIGURE 4.18: siRNA Treatment Does Not Modulate HSC Proliferation. Day 3 HSCs were transiently transected with siRNA targeted to NMM II-A, II-B and II-C alone, II-A/-B, II-B/-C and II-A/-C in combination or scramble siRNA and allowed to incubate for 48 hours. Direct cell counts were taken to assess HSC proliferation. All siRNA permutations tested were not statistically different from the negative control (Scramble).

CHAPTER 5: SUMMARY AND FUTURE DIRECTIONS

In non-migratory quiescent hepatic stellate cells (HSCs), cellular processes wrap around hepatic sinusoids to regulate blood flow by contracting and dilating in response to local vasoactive modulators [2, 39]. Upon a fibrogenic stimulus, HSCs activate becoming highly proliferative, hypercontractile, myofibroblast-like cells [11, 42, 43]. This transdifferentiation process facilitates wound healing, and chemotactic stimulation promotes a reorganization of cellular polarity resulting in HSC migration [70]. In order to repair the damaged area, activated HSCs increase production of fibrillar collagens replacing the low-density basement membrane with fibrous scar matrix [48]. In addition to changes in matrix stiffness, increased production of vasoconstrictors by neighboring cells induces hypercontraction of HSC protrusions decreasing toxic blood flow to the area of injury [14, 46]. Chronic injury and unresolved fibrosis perpetuates HSC activation and ultimately leads to cirrhosis and the clinical manifestation of portal hypertension [6].

Portal hypertension remains the main cause of morbidity and mortality in patients with cirrhosis. The onset of portal hypertension may be accompanied by gastrointestinal bleeding, ascites or encephalopathy [225]. Hepatic encephalopathy results from decreased liver function, which is associated with memory loss, seizures and/ or coma. Ascites is an accumulation of fluid in the peritoneal cavity, which results from an imbalance of pressure in the circulation. If a large amount of fluid accumulates, then the patient's abdomen becomes enlarged and taut. Portal hypertension is alleviated by

diverting blood flow through the systemic system, which results in varicies of the gastroesophageal blood vessels [225]. Variceal hemorrhaging occurs when sustained portal hypertension causes rupturing of these vessels. It is evident that a decrease in portal pressure is not only protective against the risks of variceal bleeding but is also associated with a lower long-term risk of gastro-esophageal varices. However, in practice, less than half the patients are protected under the current therapies [225]. Intrahepatic vasorelaxing may provide an additive benefit in patients suffering with unresolved fibrosis and cirrhosis, thus targeting all complications associated with portal hypertension.

Besides removal of insult, liver transplantation remains the only effective treatment for end-stage liver disease; however, a huge gap remains between the number of people who need a liver transplant and the number of organs available. According to the 2008 U.S. Organ Procurement and Transplantation Network and the Scientific Registry of Transplant Recipients Annual Report, the number of patients awaiting a liver transplant at year-end in 2001 was 7,084; however, over 10,000 patients were on the waiting list for a donor organ. In addition, not all patients with end-stage liver disease are suitable candidates for liver transplantation. Generally, organs are transplanted to patients with the highest degree of survival. Patients positive for AIDS or HIV, with irreversible brain damage, multi-system organ failure that are not correctable by liver transplantation, malignancy outside the liver, infections outside the hepatobiliary system, active alcohol or substance abuse are not eligible. Therefore, treatment generally focuses on preventing progression and complications of the disease. Targeting portal hypertension may improve

quality of life and prolong survival of patients awaiting transplantation by treating esophageal varicies, ascites and restoring proper hepatic microcirculation.

Modulating collagen production in the HSC is an obvious remedy to ameliorate liver fibrosis; however, targeting proliferation, migration and contraction may prove to be more beneficial in treating portal hypertension. These cellular functions are regulated by the actomyosin complex [59-61, 64]. Myosin II plays numerous roles in cellular processes such as actin-based motility, vesicle transport, endocytosis, phagocytosis, sterocilia formation, cytokinesis and contraction [149]. This molecular motor can be further subdivided into distinct classes based on motor domain amino acid sequences: the sarcomeric myosins characteristic of skeletal, cardiac and smooth muscle cells, nonmuscle myosins and myosin II from lower eukaryotic species and fungi [149]. Since the HSC is a nonmuscle cell, we focused our studies on understanding the role of three nonmuscle myosin II (NMM II) isoforms, II-A, II-B and II-C, in HSC activation. Cellular contraction, migration and proliferation are primarily regulated by dynamic remodeling of the cytoskeleton leading to changes in cellular morphology; therefore, isoform selection may serve as a plausible means to regulate these processes.

An imbalance in vasoactive modulators contributes to HSC hypercontractility in the injured liver [12, 13, 128, 226]. In addition, upregulation of the Rho signaling pathway in the activated HSC confers an increase in contractile potential; however, these findings do not distinguish between increased contraction due to myosin II inhibition or actin destabilization [132-134]. Blebbistatin is a myosin II inhibitor previously shown to block protrusion-mediated lamella formation and chemotactic migration of HSCs [45]. By using this selective inhibitor, we demonstrated that myosin II is the primary molecular

motor responsible for HSC contraction. Since myosin II controls both HSC migration and contraction, we expanded upon these studies to determine a function for each myosin II isoform. Our results indicated that the three isoforms, NMM II-A, II-B and II-C, were upregulated in culture-activated HSCs; however, only NMM II-A and II-B were significantly upregulated in activated HSCs of the injured liver. This inconsistency may be explained in part by the minimal levels of NMM II-C present in the *in vitro* cultures. An alternative justification may be attributed to the differences between *in vitro* and *in vivo* models. Expression of cellular proteins, including both myosin and actin, differed more than three-fold between *in vitro* cultures and fibrotic animal models [227]. Additionally, *in vitro* activation of a HSC monolayer on plastic tissue culture dishes does factor in the heterogeneous environment of the fibrotic liver. Multiple cell types produce cytokines and growth factors that affect chemotactic signaling of HSCs. Repeating these experiments in a co-culture system with other hepatic cell types may be beneficial to understanding the mechanisms regulating NMM II expression in the HSC.

In addition, mechanical rigidity has recently emerged as an important determinate of cellular phenotype. Culturing HSCs on plastic is a widely accepted model to mimic the fibrotic environment; however, the stiffness of the culture dish may not accurately reflect the stiffness of the fibrotic matrix. Therefore, matrix stiffness assays were employed to alter in vitro conditions to more accurately reflect the *in vivo* environment. In the current study we demonstrated that NMM II expression is matrix-stiffness dependent, further validating a role for NMM II in fibrosis. Since the fibrotic liver is a heterogeneous substrate, future studies may be employed to confirm these results by gradually varying the matrix stiffness.

By characterizing the expression profile of the specific isoforms NMM II-A, II-B and II-C, we were able to identify isoforms that may be responsible for the fibrogenic response of activated HSC contraction, migration and proliferation. As previously verified, myosin II is the molecular motor responsible for HSC contraction and migration. Typically, contraction, migration and proliferation contribute to wound repair but appear to be controlled by independent mechanisms that are mutually exclusive. Endothelin-1 is the primary vasoconstrictor responsible for HSC contraction, which is modulated by the upstream Rho signaling pathway [132-134]. HSC proliferation is induced by platelet-derived growth factor (PDGF) subsequently activating the FAK-PI3k -Akt signaling cascade [70]. This signaling pathway is also critical for HSC migration in the activated HSC; however, it has not been determined which myosin II classes regulate these cellular processes. Generally, mitosis rarely occurs in migrating cells [228, 229]; however, specific NMM II isoforms may coordinately regulate these processes in the HSC. siRNA-mediated knock-downs of each isoform alone or in combination demonstrated that HSC migration was inhibited by approximately 25% as compared to cells treated with scramble siRNA indicating a functional role of these isoforms. Future studies will be needed to validate these results as the experimental method employed does not account for the proliferating compartment of the assay. To assess three-dimensional constraints on cellular behavior, the Boyden chamber model and suspension gels of varying matrix compositions and rigidity would be beneficial.

HSC contraction and proliferation were not statistically altered by the genetic inhibition, further suggesting certain functions for each isoform during different cellular activities. Although siRNA-mediated knockdown did not significantly alter contraction

and proliferation; the expression levels may be sufficient to support these cellular processes and future studies should be carried out to completely obliterate these isoforms using a Cre-lox recombination system to confirm these preliminary results.

Although HSCs are nonmuscle cells, they express a large number of early and late smooth muscle cell markers including smooth muscle (SM) α-actin, SM22α, desmin, SM myosin heavy chain, h1-calponin, h-caldesmon and myocardin; therefore, future studies will examine the role smooth muscle myosin II isoforms play in HSC contraction and proliferation. To confirm that *in vitro* results correlate with *in vivo* models, adenoviral constructs expressing siRNA under promoter specific regulation will need to be generated to confirm if down-regulation of specific myosin II classes in activated HSCs contribute to changes in HSC contraction, migration and proliferation.

Future biophysical studies should also examine the contractile, migratory and proliferative properties of HSCs in more detail. Specifically, using genetic inhibition of specific isoforms, a force transducer could be used to examine the rate of force development, maximum force, and contractile velocity of each isoform in the HSCs. Additionally, a novel live cell imaging method is being developed in which fluorescence resonance energy transfer (FRET) could be changed between a fluorescent probe on myosin II and a probe on actin to estimate the number of myosin heads interacting with actin during HSC contraction. These measurements would allow us to estimate the force per cross-bridge and begin to extract force-velocity and work velocity curves of HSC contraction. Biophysical measurements would facilitate understanding the role of myosin II isoforms in the progression of hepatic fibrosis and portal hypertension. Complete eradication of HSCs would be detrimental to normal liver function and ultimately fibrotic

resolution; therefore, it is imperative to develop treatment regimes that target specific myosin II isoforms.

REFERENCES

1. Higuchi, H. and G.J. Gores, *Mechanisms of liver injury: an overview.* Curr Mol Med, 2003. 3(6): p. 483-90.

2. Bedossa, P. and V. Paradis, *Liver extracellular matrix in health and disease.* J Pathol, 2003. 200(4): p. 504-15.

3. Gaudio, E., et al., *Microcorrosion casting in normal and pathological biliary tree morphology.* Scanning Microsc, 1988. 2(1): p. 471-5.

4. Bataller, R. and D.A. Brenner, *Liver fibrosis.* J Clin Invest, 2005. 115(2): p. 209-18.

5. Sato, M., S. Suzuki, and H. Senoo, *Hepatic stellate cells: unique characteristics in cell biology and phenotype.* Cell Struct Funct, 2003. 28(2): p. 105-12.

6. Friedman, S.L., *Mechanisms of hepatic fibrogenesis.* Gastroenterology, 2008. 134(6): p. 1655-69.

7. Friedman, S.L., *Liver fibrosis -- from bench to bedside.* J Hepatol, 2003. 38 Suppl 1: p. S38-53.

8. Friedman, S.L., *Cellular sources of collagen and regulation of collagen production in liver.* Semin Liver Dis, 1990. 10(1): p. 20-9.

9. Gupta, T.K., L. Chen, and R.J. Groszmann, *Pathophysiology of portal hypertension.* Clin Liver Dis, 1997. 1(1): p. 1-12.

10. Pinzani, M., *Hepatic stellate (ITO) cells: expanding roles for a liver-specific pericyte.* J Hepatol, 1995. 22(6): p. 700-6.

11. Ramadori, G., *The stellate cell (Ito-cell, fat-storing cell, lipocyte, perisinusoidal cell) of the liver. New insights into pathophysiology of an intriguing cell.* Virchows Arch B Cell Pathol Incl Mol Pathol, 1991. 61(3): p. 147-58.

12. Zhang, J.X., W. Pegoli, Jr., and M.G. Clemens, *Endothelin-1 induces direct constriction of hepatic sinusoids.* Am J Physiol, 1994. 266(4 Pt 1): p. G624-32.

13. Bauer, M., et al., *ET-1 induced alterations of hepatic microcirculation: sinusoidal and extrasinusoidal sites of action.* Am J Physiol, 1994. 267(1 Pt 1): p. G143-9.

14. Kawada, N., et al., *Action of endothelins on hepatic stellate cells.* J Gastroenterol, 1995. 30(6): p. 731-8.

15. Thimgan, M.S. and H.F. Yee, Jr., *Quantitation of rat hepatic stellate cell contraction: stellate cells' contribution to sinusoidal resistance.* Am J Physiol, 1999. 277(1 Pt 1): p. G137-43.

16. Leivas, A., et al., *Gene expression of endothelin-1 and ET(A) and ET(B) receptors in human cirrhosis: relationship with hepatic hemodynamics.* J Vasc Res, 1998. 35(3): p. 186-93.

17. Li, D. and S.L. Friedman, *Liver fibrogenesis and the role of hepatic stellate cells: new insights and prospects for therapy.* J Gastroenterol Hepatol, 1999. 14(7): p. 618-33.

18. Bellentani, S., et al., *Drinking habits as cofactors of risk for alcohol induced liver damage. The Dionysos Study Group.* Gut, 1997. 41(6): p. 845-50.

19. Rockey, D.C., *Hepatic fibrosis, stellate cells, and portal hypertension.* Clin Liver Dis, 2006. 10(3): p. 459-79, vii-viii.

20. Zekry, A., et al., *A prospective cross-over study comparing the effect of mycophenolate versus azathioprine on allograft function and viral load in liver transplant recipients with recurrent chronic HCV infection.* Liver Transpl, 2004. 10(1): p. 52-7.

21. Hoofnagle, J.H., *Course and outcome of hepatitis C.* Hepatology, 2002. 36(5 Suppl 1): p. S21-9.

22. Wiley, T.E., et al., *Impact of alcohol on the histological and clinical progression of hepatitis C infection.* Hepatology, 1998. 28(3): p. 805-9.

23. Talwalkar, J.A. and K.D. Lindor, *Primary biliary cirrhosis.* Lancet, 2003. 362(9377): p. 53-61.

24. Tsukamoto, H., M. Matsuoka, and S.W. French, *Experimental models of hepatic fibrosis: a review.* Semin Liver Dis, 1990. 10(1): p. 56-65.

25. Kershenobich Stalnikowitz, D. and A.B. Weissbrod, *Liver fibrosis and inflammation. A review.* Ann Hepatol, 2003. 2(4): p. 159-63.

26. Pinzani, M., *Liver fibrosis.* Springer Semin Immunopathol, 1999. 21(4): p. 475-90.

27. Friedman, S.L., *Mechanisms of disease: Mechanisms of hepatic fibrosis and therapeutic implications.* Nat Clin Pract Gastroenterol Hepatol, 2004. 1(2): p. 98-105.

28. Burroughs, A.K., *Pharmacological treatment of acute variceal bleeding.* Digestion, 1998. 59 Suppl 2: p. 28-36.

29. Rockey, D.C., *Pharmacologic therapy for gastrointestinal bleeding due to portal hypertension and esophageal varices.* Curr Gastroenterol Rep, 2006. 8(1): p. 7-13.

30. Lai, H.S., et al., *Effects of octreotide on epidermal growth factor receptor, tissue plasminogen activator, and plasminogen activator inhibitor during intraperitoneal adhesion formation.* J Gastroenterol, 2003. 38(6): p. 555-60.

31. Villanueva, C., et al., *Current endoscopic therapy of variceal bleeding.* Best Pract Res Clin Gastroenterol, 2008. 22(2): p. 261-78.

32. Rockey, D.C., C.N. Housset, and S.L. Friedman, *Activation-dependent contractility of rat hepatic lipocytes in culture and in vivo.* J Clin Invest, 1993. 92(4): p. 1795-804.

33. Kalinichenko, V.V., et al., *Foxf1 +/- mice exhibit defective stellate cell activation and abnormal liver regeneration following CCl4 injury.* Hepatology, 2003. 37(1): p. 107-17.

34. Gualdi, R., et al., *Hepatic specification of the gut endoderm in vitro: cell signaling and transcriptional control.* Genes Dev, 1996. 10(13): p. 1670-82.

35. Vassy, J., et al., *Confocal microscopy immunofluorescence localization of desmin and other intermediate filament proteins in fetal rat livers.* Hepatology, 1993. 17(2): p. 293-300.

36. Weiss, M.C. and H. Strick-Marchand, *Isolation and characterization of mouse hepatic stem cells in vitro.* Semin Liver Dis, 2003. 23(4): p. 313-24.

37. Geerts, A., *On the origin of stellate cells: mesodermal, endodermal or neuro-ectodermal?* J Hepatol, 2004. 40(2): p. 331-4.

38. Cassiman, D., et al., *Hepatic stellate cells do not derive from the neural crest.* J Hepatol, 2006. 44(6): p. 1098-104.

39. Wake, K., *[One hundred years of sinusoidal cells in the liver].* Kaibogaku Zasshi, 1997. 72(5): p. 407-23.

40. Blomhoff, R., et al., *Transport and storage of vitamin A.* Science, 1990. 250(4979): p. 399-404.

41. Tsukamoto, H., *Adipogenic phenotype of hepatic stellate cells.* Alcohol Clin Exp Res, 2005. 29(11 Suppl): p. 132S-133S.

42. Rippe, R.A., et al., *NF-kappaB inhibits expression of the alpha1(I) collagen gene.* DNA Cell Biol, 1999. 18(10): p. 751-61.

43. Eng, F.J. and S.L. Friedman, *Fibrogenesis I. New insights into hepatic stellate cell activation: the simple becomes complex.* Am J Physiol Gastrointest Liver Physiol, 2000. 279(1): p. G7-G11.

44. Ramadori, G., et al., *Expression of the gene of the alpha-smooth muscle-actin isoform in rat liver and in rat fat-storing (ITO) cells.* Virchows Arch B Cell Pathol Incl Mol Pathol, 1990. 59(6): p. 349-57.

45. Melton, A.C. and H.F. Yee, *Hepatic stellate cell protrusions couple platelet-derived growth factor-BB to chemotaxis.* Hepatology, 2007. 45(6): p. 1446-53.

46. Rockey, D.C. and R.A. Weisiger, *Endothelin induced contractility of stellate cells from normal and cirrhotic rat liver: implications for regulation of portal pressure and resistance.* Hepatology, 1996. 24(1): p. 233-40.

47. Rojkind, M., M.H. Rojkind, and J. Cordero-Hernandez, *In vivo collagen synthesis and deposition in fibrotic and regenerating rat livers.* Coll Relat Res, 1983. 3(4): p. 335-47.

48. Martinez-Hernandez, A., *The hepatic extracellular matrix. II. Electron immunohistochemical studies in rats with CCl4-induced cirrhosis.* Lab Invest, 1985. 53(2): p. 166-86.

49. Arthur, M.J., et al., *Secretion of 72 kDa type IV collagenase/gelatinase by cultured human lipocytes. Analysis of gene expression, protein synthesis and proteinase activity.* Biochem J, 1992. 287 (Pt 3): p. 701-7.

50. Milani, S., et al., *Differential expression of matrix-metalloproteinase-1 and -2 genes in normal and fibrotic human liver.* Am J Pathol, 1994. 144(3): p. 528-37.

51. Han, Y.P., et al., *A matrix metalloproteinase-9 activation cascade by hepatic stellate cells in trans-differentiation in the three-dimensional extracellular matrix.* J Biol Chem, 2007. 282(17): p. 12928-39.

52. Vyas, S.K., et al., *Rat hepatic lipocytes synthesize and secrete transin (stromelysin) in early primary culture.* Gastroenterology, 1995. 109(3): p. 889-98.

53. Benyon, R.C. and M.J. Arthur, *Extracellular matrix degradation and the role of hepatic stellate cells.* Semin Liver Dis, 2001. 21(3): p. 373-84.

54. Han, Y.P., *Matrix metalloproteinases, the pros and cons, in liver fibrosis.* J Gastroenterol Hepatol, 2006. 21 Suppl 3: p. S88-91.

55. Arthur, M.J., *Fibrogenesis II. Metalloproteinases and their inhibitors in liver fibrosis.* Am J Physiol Gastrointest Liver Physiol, 2000. 279(2): p. G245-9.

56. Ramadori, G. and B. Saile, *Portal tract fibrogenesis in the liver.* Lab Invest, 2004. 84(2): p. 153-9.

57. Forbes, S.J., et al., *A significant proportion of myofibroblasts are of bone marrow origin in human liver fibrosis.* Gastroenterology, 2004. 126(4): p. 955-63.

58. Gressner, A.M., *Hepatic fibrogenesis: the puzzle of interacting cells, fibrogenic cytokines, regulatory loops, and extracellular matrix molecules.* Z Gastroenterol, 1992. 30 Suppl 1: p. 5-16.

59. Ivarsson, M., et al., *Type I collagen synthesis in cultured human fibroblasts: regulation by cell spreading, platelet-derived growth factor and interactions with collagen fibers.* Matrix Biol, 1998. 16(7): p. 409-25.

60. Ghosh, A.K., *Factors involved in the regulation of type I collagen gene expression: implication in fibrosis.* Exp Biol Med (Maywood), 2002. 227(5): p. 301-14.

61. Lindquist, J.N., B. Stefanovic, and D.A. Brenner, *Regulation of collagen alpha1(I) expression in hepatic stellate cells.* J Gastroenterol, 2000. 35 Suppl 12: p. 80-3.

62. Bornstein, P., *Regulation of expression of the alpha 1 (I) collagen gene: a critical appraisal of the role of the first intron.* Matrix Biol, 1996. 15(1): p. 3-10.

63. Rossouw, C.M., et al., *DNA sequences in the first intron of the human pro-alpha 1(I) collagen gene enhance transcription.* J Biol Chem, 1987. 262(31): p. 15151-7.

64. Sherwood, A.L., et al., *Structural and functional analysis of the first intron of the human alpha 2(I) collagen-encoding gene.* Gene, 1990. 89(2): p. 239-44.

65. Stefanovic, B., et al., *Posttranscriptional regulation of collagen alpha1(I) mRNA in hepatic stellate cells.* Mol Cell Biol, 1997. 17(9): p. 5201-9.

66. Bedossa, P., et al., *Dystroglycan expression in hepatic stellate cells: role in liver fibrosis.* Lab Invest, 2002. 82(8): p. 1053-61.

67. Carloni, V., et al., *Expression and function of integrin receptors for collagen and laminin in cultured human hepatic stellate cells.* Gastroenterology, 1996. 110(4): p. 1127-36.

68. Olaso, E., et al., *DDR2 receptor promotes MMP-2-mediated proliferation and invasion by hepatic stellate cells.* J Clin Invest, 2001. 108(9): p. 1369-78.

69. Gentilini, A., et al., *Phosphatidylinositol-3 kinase and extracellular signal-regulated kinase mediate the chemotactic and mitogenic effects of insulin-like growth factor-I in human hepatic stellate cells.* J Hepatol, 2000. 32(2): p. 227-34.

70. Reif, S., et al., *The role of focal adhesion kinase-phosphatidylinositol 3-kinase-akt signaling in hepatic stellate cell proliferation and type I collagen expression.* J Biol Chem, 2003. 278(10): p. 8083-90.

71. Lichtinghagen, R., et al., *Matrix metalloproteinase (MMP)-2, MMP-7, and tissue inhibitor of metalloproteinase-1 are closely related to the fibroproliferative process in the liver during chronic hepatitis C.* J Hepatol, 2001. 34(2): p. 239-47.

72. Wells, R.G., *The role of matrix stiffness in hepatic stellate cell activation and liver fibrosis.* J Clin Gastroenterol, 2005. 39(4 Suppl 2): p. S158-61.

73. Li, Z., et al., *Transforming growth factor-beta and substrate stiffness regulate portal fibroblast activation in culture.* Hepatology, 2007. 46(4): p. 1246-56.

74. Davis, B.H., *Transforming growth factor beta responsiveness is modulated by the extracellular collagen matrix during hepatic ito cell culture.* J Cell Physiol, 1988. 136(3): p. 547-53.

75. Friedman, S.L., et al., *Maintenance of differentiated phenotype of cultured rat hepatic lipocytes by basement membrane matrix.* J Biol Chem, 1989. 264(18): p. 10756-62.

76. Foucher, J., et al., *Diagnosis of cirrhosis by transient elastography (FibroScan): a prospective study.* Gut, 2006. 55(3): p. 403-8.

77. Hendriks, H.F., et al., *Distributions of retinoids, retinoid-binding proteins and related parameters in different types of liver cells isolated from young and old rats.* Eur J Biochem, 1988. 171(1-2): p. 237-44.

78. Senoo, H., et al., *Transfer of retinol-binding protein from HepG2 human hepatoma cells to cocultured rat stellate cells.* Proc Natl Acad Sci U S A, 1993. 90(8): p. 3616-20.

79. Popper, H., *Distribution of vitamin A in tissue as visualized by flurescence microscopy.* Physiological Review, 1944. 24: p. 205-224.

80. Bonacchi, A., et al., *The chemokine CCL21 modulates lymphocyte recruitment and fibrosis in chronic hepatitis C.* Gastroenterology, 2003. 125(4): p. 1060-76.

81. Marra, F., et al., *Monocyte chemotactic protein-1 as a chemoattractant for human hepatic stellate cells.* Hepatology, 1999. 29(1): p. 140-8.

82. Schwabe, R.F., R. Bataller, and D.A. Brenner, *Human hepatic stellate cells express CCR5 and RANTES to induce proliferation and migration.* Am J Physiol Gastrointest Liver Physiol, 2003. 285(5): p. G949-58.

83. Paik, Y.H., et al., *Hepatic stellate cells primed with cytokines upregulate inflammation in response to peptidoglycan or lipoteichoic acid.* Lab Invest, 2006. 86(7): p. 676-86.

84. Paik, Y.H., et al., *Toll-like receptor 4 mediates inflammatory signaling by bacterial lipopolysaccharide in human hepatic stellate cells.* Hepatology, 2003. 37(5): p. 1043-55.

85. Schwabe, R.F., et al., *CD40 activates NF-kappa B and c-Jun N-terminal kinase and enhances chemokine secretion on activated human hepatic stellate cells.* J Immunol, 2001. 166(11): p. 6812-9.

86. March, S., et al., *Identification and functional characterization of the hepatic stellate cell CD38 cell surface molecule.* Am J Pathol, 2007. 170(1): p. 176-87.

87. Debonera, F., et al., *Activation of interleukin-6/STAT3 and liver regeneration following transplantation.* J Surg Res, 2001. 96(2): p. 289-95.

88. Kovalovich, K., et al., *Increased toxin-induced liver injury and fibrosis in interleukin-6-deficient mice.* Hepatology, 2000. 31(1): p. 149-59.

89. Jin, X., et al., *Paradoxical effects of short- and long-term interleukin-6 exposure on liver injury and repair.* Hepatology, 2006. 43(3): p. 474-84.

90. Li, W., et al., *Global changes in interleukin-6-dependent gene expression patterns in mouse livers after partial hepatectomy.* Hepatology, 2001. 33(6): p. 1377-86.

91. Choi, I., et al., *IL-6 induces hepatic inflammation and collagen synthesis in vivo.* Clin Exp Immunol, 1994. 95(3): p. 530-5.

92. Natsume, M., et al., *Attenuated liver fibrosis and depressed serum albumin levels in carbon tetrachloride-treated IL-6-deficient mice.* J Leukoc Biol, 1999. 66(4): p. 601-8.

93. Greenwel, P., et al., *Liver fat-storing cell clones obtained from a CCl4-cirrhotic rat are heterogeneous with regard to proliferation, expression of extracellular matrix components, interleukin-6, and connexin 43.* Lab Invest, 1993. 69(2): p. 210-6.

94. Tsukamoto, H., *Cytokine regulation of hepatic stellate cells in liver fibrosis.* Alcohol Clin Exp Res, 1999. 23(5): p. 911-6.

95. Nieto, N., *Oxidative-stress and IL-6 mediate the fibrogenic effects of Kupffer cells on stellate cells.* Hepatology, 2006. 44(6): p. 1487-501.

96. Friedman, S.L., *Molecular mechanisms of hepatic fibrosis and principles of therapy.* J Gastroenterol, 1997. 32(3): p. 424-30.

97. Tiggelman, A.M., et al., *Interleukin-6 production by human liver (myo)fibroblasts in culture. Evidence for a regulatory role of LPS, IL-1 beta and TNF alpha.* J Hepatol, 1995. 23(3): p. 295-306.

98. Toda, K., et al., *Induction of hepatic stellate cell proliferation by LPS-stimulated peripheral blood mononuclear cells from patients with liver cirrhosis.* J Gastroenterol, 2000. 35(3): p. 214-20.

99. Friedman, S.L., *Molecular regulation of hepatic fibrosis, an integrated cellular response to tissue injury.* J Biol Chem, 2000. 275(4): p. 2247-50.

100. Armendariz-Borunda, J., K. Katayama, and J.M. Seyer, *Transcriptional mechanisms of type I collagen gene expression are differentially regulated by*

interleukin-1 beta, tumor necrosis factor alpha, and transforming growth factor beta in Ito cells. J Biol Chem, 1992. 267(20): p. 14316-21.

101. Bachem, M.G., et al., *Tumor necrosis factor alpha (TNF alpha) and transforming growth factor beta 1 (TGF beta 1) stimulate fibronectin synthesis and the transdifferentiation of fat-storing cells in the rat liver into myofibroblasts.* Virchows Arch B Cell Pathol Incl Mol Pathol, 1993. 63(2): p. 123-30.

102. Friedman, S.L., S. Wei, and W.S. Blaner, *Retinol release by activated rat hepatic lipocytes: regulation by Kupffer cell-conditioned medium and PDGF.* Am J Physiol, 1993. 264(5 Pt 1): p. G947-52.

103. Kim, Y., et al., *Transcriptional activation of transforming growth factor beta1 and its receptors by the Kruppel-like factor Zf9/core promoter-binding protein and Sp1. Potential mechanisms for autocrine fibrogenesis in response to injury.* J Biol Chem, 1998. 273(50): p. 33750-8.

104. Matsuoka, M., N.T. Pham, and H. Tsukamoto, *Differential effects of interleukin-1 alpha, tumor necrosis factor alpha, and transforming growth factor beta 1 on cell proliferation and collagen formation by cultured fat-storing cells.* Liver, 1989. 9(2): p. 71-8.

105. Weiner, F.R., et al., *Ito-cell gene expression and collagen regulation.* Hepatology, 1990. 11(1): p. 111-7.

106. Meyer, D.H., M.G. Bachem, and A.M. Gressner, *Modulation of hepatic lipocyte proteoglycan synthesis and proliferation by Kupffer cell-derived transforming growth factors type beta 1 and type alpha.* Biochem Biophys Res Commun, 1990. 171(3): p. 1122-9.

107. Mullhaupt, B., et al., *Liver expression of epidermal growth factor RNA. Rapid increases in immediate-early phase of liver regeneration.* J Biol Chem, 1994. 269(31): p. 19667-70.

108. Win, K.M., et al., *Mitogenic effect of transforming growth factor-beta 1 on human Ito cells in culture: evidence for mediation by endogenous platelet-derived growth factor.* Hepatology, 1993. 18(1): p. 137-45.

109. Friedman, S.L. and M.J. Arthur, *Activation of cultured rat hepatic lipocytes by Kupffer cell conditioned medium. Direct enhancement of matrix synthesis and stimulation of cell proliferation via induction of platelet-derived growth factor receptors.* J Clin Invest, 1989. 84(6): p. 1780-5.

110. Slack, J.L., D.J. Liska, and P. Bornstein, *Regulation of expression of the type I collagen genes.* Am J Med Genet, 1993. 45(2): p. 140-51.

111. Wang, S.C., et al., *Expression of interleukin-10 by in vitro and in vivo activated hepatic stellate cells.* J Biol Chem, 1998. 273(1): p. 302-8.

112. Rosenbloom, J., et al., *Transcriptional control of human diploid fibroblast collagen synthesis by gamma-interferon.* Biochem Biophys Res Commun, 1984. 123(1): p. 365-72.

113. Stephenson, M.L., et al., *Immune interferon inhibits collagen synthesis by rheumatoid synovial cells associated with decreased levels of the procollagen mRNAs.* FEBS Lett, 1985. 180(1): p. 43-50.

114. Kawada, N., et al., *The contraction of hepatic stellate (Ito) cells stimulated with vasoactive substances. Possible involvement of endothelin 1 and nitric oxide in the regulation of the sinusoidal tonus.* Eur J Biochem, 1993. 213(2): p. 815-23.

115. Pinzani, M., et al., *Endothelin 1 is overexpressed in human cirrhotic liver and exerts multiple effects on activated hepatic stellate cells.* Gastroenterology, 1996. 110(2): p. 534-48.

116. Schrader, J., et al., *[Plasma endothelin in normal probands and patients with nephrologic-rheumatologic and cardiovascular diseases].* Klin Wochenschr, 1990. 68(15): p. 774-9.

117. Rockey, D.C. and J.J. Chung, *Inducible nitric oxide synthase in rat hepatic lipocytes and the effect of nitric oxide on lipocyte contractility.* J Clin Invest, 1995. 95(3): p. 1199-206.

118. Browner, N.C., et al., *Regulation of cGMP-dependent protein kinase expression by soluble guanylyl cyclase in vascular smooth muscle cells.* J Biol Chem, 2004. 279(45): p. 46631-6.

119. Khatri, J.J., et al., *Role of myosin phosphatase isoforms in cGMP-mediated smooth muscle relaxation.* J Biol Chem, 2001. 276(40): p. 37250-7.

120. Perri, R.E., et al., *Defects in cGMP-PKG pathway contribute to impaired NO-dependent responses in hepatic stellate cells upon activation.* Am J Physiol Gastrointest Liver Physiol, 2006. 290(3): p. G535-42.

121. Fukushige, H., et al., *Synthesis and receptor sites of endothelin-1 in the rat liver vasculature.* Anat Rec, 2000. 259(4): p. 437-45.

122. Rockey, D., *The cellular pathogenesis of portal hypertension: stellate cell contractility, endothelin, and nitric oxide.* Hepatology, 1997. 25(1): p. 2-5.

123. Xu, D., et al., *ECE-1: a membrane-bound metalloprotease that catalyzes the proteolytic activation of big endothelin-1.* Cell, 1994. 78(3): p. 473-85.

124. Yanagisawa, M., et al., *A novel peptide vasoconstrictor, endothelin, is produced by vascular endothelium and modulates smooth muscle Ca2+ channels.* J Hypertens Suppl, 1988. 6(4): p. S188-91.

125. Housset, C., D.C. Rockey, and D.M. Bissell, *Endothelin receptors in rat liver: lipocytes as a contractile target for endothelin 1.* Proc Natl Acad Sci U S A, 1993. 90(20): p. 9266-70.

126. Rockey, D.C., *Characterization of endothelin receptors mediating rat hepatic stellate cell contraction.* Biochem Biophys Res Commun, 1995. 207(2): p. 725-31.

127. Laleman, W., et al., *Both Ca2+ -dependent and -independent pathways are involved in rat hepatic stellate cell contraction and intrahepatic hyperresponsiveness to methoxamine.* Am J Physiol Gastrointest Liver Physiol, 2007. 292(2): p. G556-64.

128. Zhang, J.X., M. Bauer, and M.G. Clemens, *Vessel- and target cell-specific actions of endothelin-1 and endothelin-3 in rat liver.* Am J Physiol, 1995. 269(2 Pt 1): p. G269-77.

129. Gandhi, C.R., L.A. Sproat, and V.M. Subbotin, *Increased hepatic endothelin-1 levels and endothelin receptor density in cirrhotic rats.* Life Sci, 1996. 58(1): p. 55-62.

130. Eguchi, S., et al., *Endothelin receptor subtypes are coupled to adenylate cyclase via different guanyl nucleotide-binding proteins in vasculature.* Endocrinology, 1993. 132(2): p. 524-9.

131. Rockey, D.C., *Vascular mediators in the injured liver.* Hepatology, 2003. 37(1): p. 4-12.

132. Katoh, K., et al., *Rho-kinase--mediated contraction of isolated stress fibers.* J Cell Biol, 2001. 153(3): p. 569-84.

133. Dudek, S.M. and J.G. Garcia, *Rho family of guanine exchange factors (GEFs) in cellular activation: who's dancing? And with whom?* Circ Res, 2003. 93(9): p. 794-5.

134. Kawada, N., et al., *ROCK inhibitor Y-27632 attenuates stellate cell contraction and portal pressure increase induced by endothelin-1.* Biochem Biophys Res Commun, 1999. 266(2): p. 296-300.

135. Kitamura, K., et al., *Rho/Rho kinase is a key enzyme system involved in the angiotensin II signaling pathway of liver fibrosis and steatosis.* J Gastroenterol Hepatol, 2007. 22(11): p. 2022-33.

136. Yanase, M., et al., *Functional diversity between Rho-kinase- and MLCK-mediated cytoskeletal actions in a myofibroblast-like hepatic stellate cell line.* Biochem Biophys Res Commun, 2003. 305(2): p. 223-8.

137. Pinzani, M., *PDGF and signal transduction in hepatic stellate cells.* Front Biosci, 2002. 7: p. d1720-6.

138. Pinzani, M., et al., *Regulation of macrophage colony-stimulating factor in liver fat-storing cells by peptide growth factors.* Am J Physiol, 1992. 262(4 Pt 1): p. C876-81.

139. Gabele, E., et al., *The role of p70S6K in hepatic stellate cell collagen gene expression and cell proliferation.* J Biol Chem, 2005. 280(14): p. 13374-82.

140. Marra, F., et al., *Involvement of phosphatidylinositol 3-kinase in the activation of extracellular signal-regulated kinase by PDGF in hepatic stellate cells.* FEBS Lett, 1995. 376(3): p. 141-5.

141. Pinzani, M., *Platelet-derived growth factor receptor expression in hepatic stellate cells: how too much of a good thing can be bad.* Hepatology, 1995. 22(3): p. 997-9.

142. Schnabl, B., et al., *TAK1/JNK and p38 have opposite effects on rat hepatic stellate cells.* Hepatology, 2001. 34(5): p. 953-63.

143. Datta, S.R., A. Brunet, and M.E. Greenberg, *Cellular survival: a play in three Akts.* Genes Dev, 1999. 13(22): p. 2905-27.

144. Carloni, V., et al., *Tyrosine phosphorylation of focal adhesion kinase by PDGF is dependent on ras in human hepatic stellate cells.* Hepatology, 2000. 31(1): p. 131-40.

145. Pinzani, M., et al., *Expression of platelet-derived growth factor in a model of acute liver injury.* Hepatology, 1994. 19(3): p. 701-7.

146. Wong, L., et al., *Induction of beta-platelet-derived growth factor receptor in rat hepatic lipocytes during cellular activation in vivo and in culture.* J Clin Invest, 1994. 94(4): p. 1563-9.

147. Yang, C.Q., et al., *[Mechanism of hepatic stellate cell migration during liver fibrosis].* Zhonghua Yi Xue Za Zhi, 2008. 88(2): p. 119-22.

148. Tangkijvanich, P., S.P. Tam, and H.F. Yee, Jr., *Wound-induced migration of rat hepatic stellate cells is modulated by endothelin-1 through rho-kinase-mediated alterations in the acto-myosin cytoskeleton.* Hepatology, 2001. 33(1): p. 74-80.

149. Sellers, J.R., *Myosins: a diverse superfamily.* Biochim Biophys Acta, 2000. 1496(1): p. 3-22.

150. Cheney, R.E. and M.S. Mooseker, *Unconventional myosins.* Curr Opin Cell Biol, 1992. 4(1): p. 27-35.

151. Bresnick, A.R., *Molecular mechanisms of nonmuscle myosin-II regulation.* Curr Opin Cell Biol, 1999. 11(1): p. 26-33.

152. Saez, C.G., et al., *Human nonmuscle myosin heavy chain mRNA: generation of diversity through alternative polyadenylylation.* Proc Natl Acad Sci U S A, 1990. 87(3): p. 1164-8.

153. Zeng, W., et al., *Dynamics of actomyosin interactions in relation to the cross-bridge cycle.* Philos Trans R Soc Lond B Biol Sci, 2004. 359(1452): p. 1843-55.

154. Rosenfeld, S.S., et al., *Myosin IIb is unconventionally conventional.* J Biol Chem, 2003. 278(30): p. 27449-55.

155. Adelstein, R.S. and M.A. Conti, *Phosphorylation of platelet myosin increases actin-activated myosin ATPase activity.* Nature, 1975. 256(5518): p. 597-8.

156. Amano, M., et al., *Phosphorylation and activation of myosin by Rho-associated kinase (Rho-kinase).* J Biol Chem, 1996. 271(34): p. 20246-9.

157. Kelley, C.A. and R.S. Adelstein, *The 204-kDa smooth muscle myosin heavy chain is phosphorylated in intact cells by casein kinase II on a serine near the carboxyl terminus.* J Biol Chem, 1990. 265(29): p. 17876-82.

158. van Leeuwen, F.N., et al., *Rac regulates phosphorylation of the myosin-II heavy chain, actinomyosin disassembly and cell spreading.* Nat Cell Biol, 1999. 1(4): p. 242-8.

159. Wilson, J.R., T.J. Biden, and R.I. Ludowyke, *Increases in phosphorylation of the myosin II heavy chain, but not regulatory light chains, correlate with insulin secretion in rat pancreatic islets and RINm5F cells.* Diabetes, 1999. 48(12): p. 2383-9.

160. Moussavi, R.S., C.A. Kelley, and R.S. Adelstein, *Phosphorylation of vertebrate nonmuscle and smooth muscle myosin heavy chains and light chains.* Mol Cell Biochem, 1993. 127-128: p. 219-27.

161. Calle, R., et al., *Glucose-induced phosphorylation of myristoylated alanine-rich C kinase substrate (MARCKS) in isolated rat pancreatic islets.* J Biol Chem, 1992. 267(26): p. 18723-7.

162. Shaw, M.A., E.M. Ostap, and Y.E. Goldman, *Mechanism of inhibition of skeletal muscle actomyosin by N-benzyl-p-toluenesulfonamide.* Biochemistry, 2003. 42(20): p. 6128-35.

163. Narumiya, S., *[Cellular functions & pharmacological manipulations of the small GTPase Rho & Rho effectors].* Nippon Yakurigaku Zasshi, 1999. 114 Suppl 1: p. 1P-5P.

164. Limouze, J., et al., *Specificity of blebbistatin, an inhibitor of myosin II.* J Muscle Res Cell Motil, 2004. 25(4-5): p. 337-41.

165. Higuchi, H., S. Takemori, and Y. Umazume, *Suppressing effect of 2,3-butanedione monoxime on contraction and ATPase activity of rabbit skeletal muscle.* Prog Clin Biol Res, 1989. 315: p. 225-6.

166. Cheung, A., et al., *A small-molecule inhibitor of skeletal muscle myosin II.* Nat Cell Biol, 2002. 4(1): p. 83-8.

167. Loirand, G., P. Guerin, and P. Pacaud, *Rho kinases in cardiovascular physiology and pathophysiology.* Circ Res, 2006. 98(3): p. 322-34.

168. Zhang, M. and P.V. Rao, *Blebbistatin, a novel inhibitor of myosin II ATPase activity, increases aqueous humor outflow facility in perfused enucleated porcine eyes.* Invest Ophthalmol Vis Sci, 2005. 46(11): p. 4130-8.

169. Eddinger, T.J., et al., *Potent inhibition of arterial smooth muscle tonic contractions by the selective myosin II inhibitor, blebbistatin.* J Pharmacol Exp Ther, 2007. 320(2): p. 865-70.

170. Kovacs, M., et al., *Mechanism of blebbistatin inhibition of myosin II.* J Biol Chem, 2004. 279(34): p. 35557-63.

171. Straight, A.F., et al., *Dissecting temporal and spatial control of cytokinesis with a myosin II Inhibitor.* Science, 2003. 299(5613): p. 1743-7.

172. D'Apolito, M., et al., *Cloning of the murine non-muscle myosin heavy chain IIA gene ortholog of human MYH9 responsible for May-Hegglin, Sebastian, Fechtner, and Epstein syndromes.* Gene, 2002. 286(2): p. 215-22.

173. Somlyo, A.P. and A.V. Somlyo, *Vascular smooth muscle. I. Normal structure, pathology, biochemistry, and biophysics.* Pharmacol Rev, 1968. 20(4): p. 197-272.

174. Dillon, P.F., et al., *Myosin phosphorylation and the cross-bridge cycle in arterial smooth muscle.* Science, 1981. 211(4481): p. 495-7.

175. Rembold, C.M. and R.A. Murphy, *Myoplasmic calcium, myosin phosphorylation, and regulation of the crossbridge cycle in swine arterial smooth muscle.* Circ Res, 1986. 58(6): p. 803-15.

176. Hai, C.M. and H.R. Kim, *An expanded latch-bridge model of protein kinase C-mediated smooth muscle contraction.* J Appl Physiol, 2005. 98(4): p. 1356-65.

177. Pavalko, F.M., et al., *Phosphorylation of dense-plaque proteins talin and paxillin during tracheal smooth muscle contraction.* Am J Physiol, 1995. 268(3 Pt 1): p. C563-71.

178. Veigel, C., et al., *Load-dependent kinetics of force production by smooth muscle myosin measured with optical tweezers.* Nat Cell Biol, 2003. 5(11): p. 980-6.

179. Babij, P., C. Kelly, and M. Periasamy, *Characterization of a mammalian smooth muscle myosin heavy-chain gene: complete nucleotide and protein coding sequence and analysis of the 5′ end of the gene.* Proc Natl Acad Sci U S A, 1991. 88(23): p. 10676-80.

180. Hamada, Y., et al., *Distinct vascular and intestinal smooth muscle myosin heavy chain mRNAs are encoded by a single-copy gene in the chicken.* Biochem Biophys Res Commun, 1990. 170(1): p. 53-8.

181. Kelley, C.A., et al., *An insert of seven amino acids confers functional differences between smooth muscle myosins from the intestines and vasculature.* J Biol Chem, 1993. 268(17): p. 12848-54.

182. White, S., A.F. Martin, and M. Periasamy, *Identification of a novel smooth muscle myosin heavy chain cDNA: isoform diversity in the S1 head region.* Am J Physiol, 1993. 264(5 Pt 1): p. C1252-8.

183. Sweeney, H.L., et al., *Kinetic tuning of myosin via a flexible loop adjacent to the nucleotide binding pocket.* J Biol Chem, 1998. 273(11): p. 6262-70.

184. Babu, G.J., et al., *Loss of SM-B myosin affects muscle shortening velocity and maximal force development.* Nat Cell Biol, 2001. 3(11): p. 1025-9.

185. Nabeshima, Y., et al., *Nonmuscle and smooth muscle myosin light chain mRNAs are generated from a single gene by the tissue-specific alternative RNA splicing.* J Biol Chem, 1987. 262(22): p. 10608-12.

186. Golomb, E., et al., *Identification and characterization of nonmuscle myosin II-C, a new member of the myosin II family.* J Biol Chem, 2004. 279(4): p. 2800-8.

187. Simons, M., et al., *Human nonmuscle myosin heavy chains are encoded by two genes located on different chromosomes.* Circ Res, 1991. 69(2): p. 530-9.

188. Katsuragawa, Y., et al., *Two distinct nonmuscle myosin-heavy-chain mRNAs are differentially expressed in various chicken tissues. Identification of a novel gene family of vertebrate non-sarcomeric myosin heavy chains.* Eur J Biochem, 1989. 184(3): p. 611-6.

189. Leal, A., et al., *A novel myosin heavy chain gene in human chromosome 19q13.3.* Gene, 2003. 312: p. 165-71.

190. Kovacs, M., et al., *Functional divergence of human cytoplasmic myosin II: kinetic characterization of the non-muscle IIA isoform.* J Biol Chem, 2003. 278(40): p. 38132-40.

191. Seri, M., et al., *Mutations in MYH9 result in the May-Hegglin anomaly, and Fechtner and Sebastian syndromes. The May-Heggllin/Fechtner Syndrome Consortium.* Nat Genet, 2000. 26(1): p. 103-5.

192. Matsushita, T., et al., *Targeted disruption of mouse ortholog of the human MYH9 responsible for macrothrombocytopenia with different organ involvement:*

hematological, nephrological, and otological studies of heterozygous KO mice. Biochem Biophys Res Commun, 2004. 325(4): p. 1163-71.

193. Kawamoto, S. and R.S. Adelstein, *Chicken nonmuscle myosin heavy chains: differential expression of two mRNAs and evidence for two different polypeptides.* J Cell Biol, 1991. 112(5): p. 915-24.

194. Conrad, A.H., T. Jaffredo, and G.W. Conrad, *Differential localization of cytoplasmic myosin II isoforms A and B in avian interphase and dividing embryonic and immortalized cardiomyocytes and other cell types in vitro.* Cell Motil Cytoskeleton, 1995. 31(2): p. 93-112.

195. Kolega, J., *Cytoplasmic dynamics of myosin IIA and IIB: spatial 'sorting' of isoforms in locomoting cells.* J Cell Sci, 1998. 111 (Pt 15): p. 2085-95.

196. Wang, F., et al., *Kinetic mechanism of non-muscle myosin IIB: functional adaptations for tension generation and maintenance.* J Biol Chem, 2003. 278(30): p. 27439-48.

197. Kato, M., et al., *Role of Rho small GTP binding protein in the regulation of actin cytoskeleton in hepatic stellate cells.* J Hepatol, 1999. 31(1): p. 91-9.

198. Melton, A.C., A. Datta, and H.F. Yee, Jr., *[Ca2+]i-independent contractile force generation by rat hepatic stellate cells in response to endothelin-1.* Am J Physiol Gastrointest Liver Physiol, 2006. 290(1): p. G7-13.

199. Saab, S., et al., *Myosin mediates contractile force generation by hepatic stellate cells in response to endothelin-1.* J Biomed Sci, 2002. 9(6 Pt 2): p. 607-12.

200. Yanase, M., et al., *Lysophosphatidic acid enhances collagen gel contraction by hepatic stellate cells: association with rho-kinase.* Biochem Biophys Res Commun, 2000. 277(1): p. 72-8.

201. Wirz, W., et al., *Hepatic stellate cells display a functional vascular smooth muscle cell phenotype in a three-dimensional co-culture model with endothelial cells.* Differentiation, 2008. 76(7): p. 784-94.

202. Pfaffl, M.W., *A new mathematical model for relative quantification in real-time RT-PCR.* Nucleic Acids Res, 2001. 29(9): p. e45.

203. Pelham, R.J., Jr. and Y. Wang, *Cell locomotion and focal adhesions are regulated by substrate flexibility.* Proc Natl Acad Sci U S A, 1997. 94(25): p. 13661-5.

204. Maher, J.J. and R.F. McGuire, *Extracellular matrix gene expression increases preferentially in rat lipocytes and sinusoidal endothelial cells during hepatic fibrosis in vivo.* J Clin Invest, 1990. 86(5): p. 1641-8.

205. Wake, K., *Perisinusoidal stellate cells (fat-storing cells, interstitial cells, lipocytes), their related structure in and around the liver sinusoids, and vitamin A-storing cells in extrahepatic organs.* Int Rev Cytol, 1980. 66: p. 303-53.

206. Bauer, M., et al., *Chronic ethanol consumption increases hepatic sinusoidal contractile response to endothelin-1 in the rat.* Hepatology, 1995. 22(5): p. 1565-76.

207. De la Roche, M.A., et al., *Signaling pathways regulating Dictyostelium myosin II.* J Muscle Res Cell Motil, 2002. 23(7-8): p. 703-18.

208. Rockey, D.C., et al., *Rat hepatic lipocytes express smooth muscle actin upon activation in vivo and in culture.* J Submicrosc Cytol Pathol, 1992. 24(2): p. 193-203.

209. Matsui, H. and N. Kawada, *Effect of S-adenosyl-L-methionine on the activation, proliferation and contraction of hepatic stellate cells.* Eur J Pharmacol, 2005. 509(1): p. 31-6.

210. Ramamurthy, B., et al., *Kinetic mechanism of blebbistatin inhibition of nonmuscle myosin IIb.* Biochemistry, 2004. 43(46): p. 14832-9.

211. Okada, Y., et al., *Pressure loading and ethanol exposure differentially modulate rat hepatic stellate cell activation.* J Cell Physiol, 2008. 215(2): p. 472-80.

212. Conti, M.A., et al., *Defects in cell adhesion and the visceral endoderm following ablation of nonmuscle myosin heavy chain II-A in mice.* J Biol Chem, 2004. 279(40): p. 41263-6.

213. Ma, X., et al., *A point mutation in the motor domain of nonmuscle myosin II-B impairs migration of distinct groups of neurons.* Mol Biol Cell, 2004. 15(6): p. 2568-79.

214. Takeda, K., et al., *Ablation and mutation of nonmuscle myosin heavy chain II-B results in a defect in cardiac myocyte cytokinesis.* Circ Res, 2003. 93(4): p. 330-7.

215. Lo, C.M., et al., *Nonmuscle myosin IIb is involved in the guidance of fibroblast migration.* Mol Biol Cell, 2004. 15(3): p. 982-9.

216. Meshel, A.S., et al., *Basic mechanism of three-dimensional collagen fibre transport by fibroblasts.* Nat Cell Biol, 2005. 7(2): p. 157-64.

217. Betapudi, V., L.S. Licate, and T.T. Egelhoff, *Distinct roles of nonmuscle myosin II isoforms in the regulation of MDA-MB-231 breast cancer cell spreading and migration.* Cancer Res, 2006. 66(9): p. 4725-33.

218. Sandquist, J.C., et al., *Rho kinase differentially regulates phosphorylation of nonmuscle myosin II isoforms A and B during cell rounding and migration.* J Biol Chem, 2006. 281(47): p. 35873-83.

219. Even-Ram, S., et al., *Myosin IIA regulates cell motility and actomyosin-microtubule crosstalk.* Nat Cell Biol, 2007. 9(3): p. 299-309.

220. Xu, L., et al., *Human hepatic stellate cell lines, LX-1 and LX-2: new tools for analysis of hepatic fibrosis.* Gut, 2005. 54(1): p. 142-51.

221. Bao, J., et al., *Replacement of nonmuscle myosin II-B with II-A rescues brain but not cardiac defects in mice.* J Biol Chem, 2007. 282(30): p. 22102-11.

222. Cho, J.J., et al., *An oral endothelin-A receptor antagonist blocks collagen synthesis and deposition in advanced rat liver fibrosis.* Gastroenterology, 2000. 118(6): p. 1169-78.

223. Laleman, W., R. Bisschops, and S. Vermeire, *Electronic clinical challenges and images in GI. Colocolonic intussusception of pediculated lipoma.* Gastroenterology, 2009. 136(1): p. e5-6.

224. Tullio, A.N., et al., *Nonmuscle myosin II-B is required for normal development of the mouse heart.* Proc Natl Acad Sci U S A, 1997. 94(23): p. 12407-12.

225. Villanueva, C. and J. Balanzo, *Variceal bleeding : pharmacological treatment and prophylactic strategies.* Drugs, 2008. 68(16): p. 2303-24.

226. Bauer, M., et al., *Endothelin-1 as a regulator of hepatic microcirculation: sublobular distribution of effects and impact on hepatocellular secretory function.* Shock, 1994. 1(6): p. 457-65.

227. Kristensen, D.B., et al., *Proteome analysis of rat hepatic stellate cells.* Hepatology, 2000. 32(2): p. 268-77.

228. Savagner, P., *Leaving the neighborhood: molecular mechanisms involved during epithelial-mesenchymal transition.* Bioessays, 2001. 23(10): p. 912-23.

229. Zagon, I.S., J.W. Sassani, and P.J. McLaughlin, *Cellular dynamics of corneal wound re-epithelialization in the rat. I. Fate of ocular surface epithelial cells synthesizing DNA prior to wounding.* Brain Res, 1999. 822(1-2): p. 149-63.